CRANFIELD UNIVERSITY
SCHOOL OF ENGINEERING

Development of a Preliminary Weight Estimation Method for Advanced Turbofan Engines

Periklis Lolis

Ph.D. Thesis

July 2014

CRANFIELD UNIVERSITY
SCHOOL OF ENGINEERING
DEPARTMENT OF POWER AND PROPULSION

Ph.D. Thesis

2014

Periklis Lolis

Development of a Preliminary Weight Estimation Method for Advanced Turbofan Engines

Supervisors: Dr. V. Sethi - Prof. P. Pilidis

This thesis is submitted in partial fullfillment of the requirements for the degree of Doctor of Philosophy

We know nothing for sure: the truth is hidden at the bottom of a well

DIOGENES LEARTIUS

Abstract

The present work focuses on preliminary weight estimation methods that enable the feasibility studies of novel aero engines. The key contributions can be found in the analysis of the existing preliminary weight estimation methods, the development of a new preliminary weight estimation method and the study on the feasibility of a Geared Turbofan (GTF) engine.

In more detail, the existing preliminary weight estimation methods are examined in the first part of the thesis, aiming to define their suitability for current turbofan engines, but also for future engine arrangements. For this purpose, they are examined not only quantitatively, to verify their accuracy, but also qualitatively to figure out if they are able to reflect the key thermodynamic and design parameter variations on weight. Apart from NASA WATE no method achieves either the required accuracy, or simulates the weight trends.

Realising the need for a more accurate, robust, flexible and extensible method, a new "component based" method that performs basic component design to estimate engine weight, is devised. Its accuracy is verified by comparing the whole engine weight prediction and estimated component design against the publicly available data of two major turbofan engines and the weight predictions of existing weight estimation methods.

ATLAS, the tool based on the above method was used to estimate weight over a range of Bypass Ratio (BPR) and Turbine Entry Temperature (TET) values for a Direct Drive Turbofan (DDTF) and a GTF two spool arrangement, reaching the following conclusions:

- The adjustments of Low Pressure Turbine (LPT) number of stages or geometry are not sufficient, if high stage isentropic efficiency values are targeted at high BPR values

- For the examined engine model, with the given weight estimation methodology, the weight reduction, when a gearbox is introduced at a DDTF, depends on the reduction of LPT stages, with the other components having negligible impact. However, it should be noted that a constant fan diameter was assumed for both configurations. A fan loss model and more detailed weight estimation of frames, shafts and control and accessories is required to verify this conclusion.

- The comparison of a DDTF and a GTF engine is representative only if the cycles corresponding to the installed performance optima are considered.

Engines with the same thermodynamic cycle could only be compared when the optima cannot be reached, due to geometry restrictions

Acknowledgements

I am not particular good at thanking people with words, but I will try my best for the ones that contributed towards the completion of this work.

First of all, I would like to thank my supervisor and friend Dr. Bobby Sethi for his useful advice and above all for his invaluable guidance. He was always there for me in every step of the way.

A big "thank you" goes to Prof. Pericles Pilidis for giving me the opportunity to work on this project and for being a great mentor. Also, I am grateful for the help and support of the staff of the Department of Power and Propulsion and its successor, the Center for Propulsion.

This thesis would not have been possible without the help and support of a special friend and great scientist, that provided the performance calculations and helped me fully understand the potential of weight estimation. A simple "thank you" is not enough for Dr Panagiotis Giannakakis.

Dr Pavlos Zachos deserves a special acknowledgement. A friend for the biggest part of my life, helped me with his advice and support, always being there for me.

I would like also to thank Balasubramaniam Arumugam Shanmugasundaram and Hussain Bajwa, the two master students I had the chance to work with and gain valuable knowledge and experience.

My fullest gratitude goes to my roomates Pavlos, Panos, George, Fanis and Marie for being a family to me and providing a pleasant living environment. Also, a big "thank you" to the friends in Cranfield, Asteris, Elias, Kostis, Dimitra, Avgoustinos, Nikos, George and to the friends all over the world, Dimitris, Marios, Popi, Ilias, Fotini, Tasos, Maria, Xristina, Afroditi and Marina, that filled these years for the countless moments and everlasting memories. I would also like to acknowledge my "psychologist" and officemate Eduardo that always lifted my spirits when I was down.

My parents George and Athina, and my brother Paschalis deserve a very big "thank you" for their love and support. An even bigger one has to go to my other half, Dora for the same reasons and above all for her patience.

Finally, I would like to acknowledge Mr. Michael Tong of NASA and Prof, Peter Spelluci of Darmstadt Technical University for providing their tools, without which this thesis would not have been possible.

Contents

List of Figures

List of Tables

Nomenclature

$\dot{W}$	Power
A	Area
AFR	Combustor fuel atomising flow ratio
AR	Aspect ratio
C	Velocity
C_D	Drag coefficient
Co	Constant
D	Diameter
$DCFR$	Combustor dome cooling flow rate
DF	Diffusion factor
DGR	Combustor dome gap ratio
DH	DeHaller number
Dr	Drag
E	Modulus of elasticity
E_{kin}	Kinetic energy
F	Force
FN	Thrust
K	Gearbox weight correction factor
K_B	Blockage factor
K_{range}	Range factor
Ma	Mach number
N	Rotational speed

Nr Number

P Pressure

PCN Non dimensional rotational speed

PR Pressure ratio

R Stage reaction

R_{air} Gas constant

$Range$ Aircraft range

S_f Safety factor

SFN Specific fuel consumption

T Temperature

To Torsion

TR Taper ratio

TR Temperature ratio

U Blade speed

V Relative velocity

V_{cr} Aircraft cruise velocity

Vol Volume

WT Weight

$\dot{m}$ Mass flow

a Angle

c Chord

c_p Specific heat at constant pressure

h Height

k_i Drag interference factor

l Length

m Mass

p_{st} Static pressure

r Radius

s	Space
sol	Solidity
t_{st}	Static temperature
u	Displacement
x	x or axial direction
z	Gear ratio
α	Absolute velocity angle or coefficient of thermal expansion
β	Relative velocity angle
η	Efficiency
γ	Specific heat ratio
ν	Poisson ratio
ω	Rotational velocity
ϕ	Flow coefficient or combustor primary zone equivalence ratio
ψ	Loading coefficient
ρ	Density
σ	Stress
σ_e	von Mises stress
σ_h	Hoop stress
σ_{UTS}	Ultimate tensile stress
σ_y	Yield stress
θ	Angle

Subscripts

0	Free stream
θ	Tangential direction
a	Atomiser air
abs	Absolute
af	Afterbody
avg	Average

ax	Axial
bl	Blade
bo	Body
bp	Bypass
$C\&A$	Controls and accessories
c	Cooling
ca	Casing or cowl
CHW	Connecting hardware
co	Core
cob	Combustor
cog	Center of gravity
con	Containment
cr	Cruise
d	Combustor dome
des	Desing
eng	Engine
f	Fuel
fan	Fan
fnz	Fuel nozzle
gg	Gas generator
h	Hub
i	Inner
in	Inlet
ise	Isentropic
m	Mean
nac	Nacelle
o	Outer
out	Outlet

p	Combustor passage
pl	Gearbox planets
$poly$	Polytropic
pr	Pressure
R	Rotor
r	Radial direction
rel	Relative
rim	Rim
row	Row
S	Stator
s	Gearbox sun
sg	Stage
sh	Shaft
sl	Slope
st	Static
$stoi$	Stoichiometric
t	Tip
to	Take off
tot	Total
w	Swirl

Abbreviations

ACARE Advisory Council for Aeronautics Research in Europe

ANN Artificial Neural Network

AR Aspect Ratio

BPR Bypass Ratio

CU Cranfield University

DDTF Direct Drive Turbofan

EIS Entry Into Service

EU EUEuropean Union

FAR Fuel to Air Ratio

FPR Fan Pressure Ratio

GTF Geared Turbofan

HPC High Pressure Compressor

HPT High Pressure Turbine

IPC Intermediate Pressure Compressor

IPT Intermediate Pressure Turbine

IGV Inlet Guide Vane

LP Low Pressure

LPT Low Pressure Turbine

NGV Nozzle Guide Vane

OEM Original Equipment Manufacturer

OGV Outlet Guide Vane

OPR Overall Pressure Ratio

SFC Specific Fuel Consumption

STOL Short Take Off and Landing

TBC Thermal Barrier Coating

TERA Techno-economic Environmental Risk Analysis

TET Turbine Entry Temperature

TO Take Off

TOC Top of Climb

VIGV Variable Inlet Guide Vane

VGV Variable Guide Vane

VTOL Vertical Take Off and Landing

Chapter 1

Introduction

1.1 Project scope

Lately there has been an increasing concern about the effect of human activities on the environment[1], resulting in strict policies by international organisations[2] in an effort to reduce emissions and noise produced by gas turbines used in aero applications. These trends are also evident in the targets set by Advisory Council for Aeronautics Research in Europe (ACARE) for year 2020, dictating a reduction in NO_x emissions by 80% and in CO_2 emissions, aircraft fuel consumption and noise by 50%[3;4].

In addition, the increasing oil price and the current economic situation are driving the need for more efficient engines that will promote fuel savings, but will also achieve low acquisition and maintenance cost, providing, this way, financially appealing solutions[5]. These concerns combined with the introduction of new technologies and the complexity of applications, have made the selection of the suitable gas turbine for a given utilisation, a challenging task[6].

The increased complexity of the current situation has led to the development of multi-disciplinary tools that can model and connect effectively all the aspects of engine, aircraft and mission, by performing design space exploration, parametric analysis and trade-off studies. In that context, Cranfield University, in collaboration with Original Equipment Manufacturers (OEMs) and universities,

developed a Techno-economic Environmental Risk Analysis (TERA)[7] framework.

The TERA framework integrates a series of modules, each one modelling a different aspect of the engine, mission or aircraft, which are used to produce a detailed analysis of the gas turbine behaviour in a specific application[8]. Coupled with appropriate methods, it can define the engine characteristics that satisfy the design requirements and restrictions, thus identifying the potential power plant candidates for a given application.

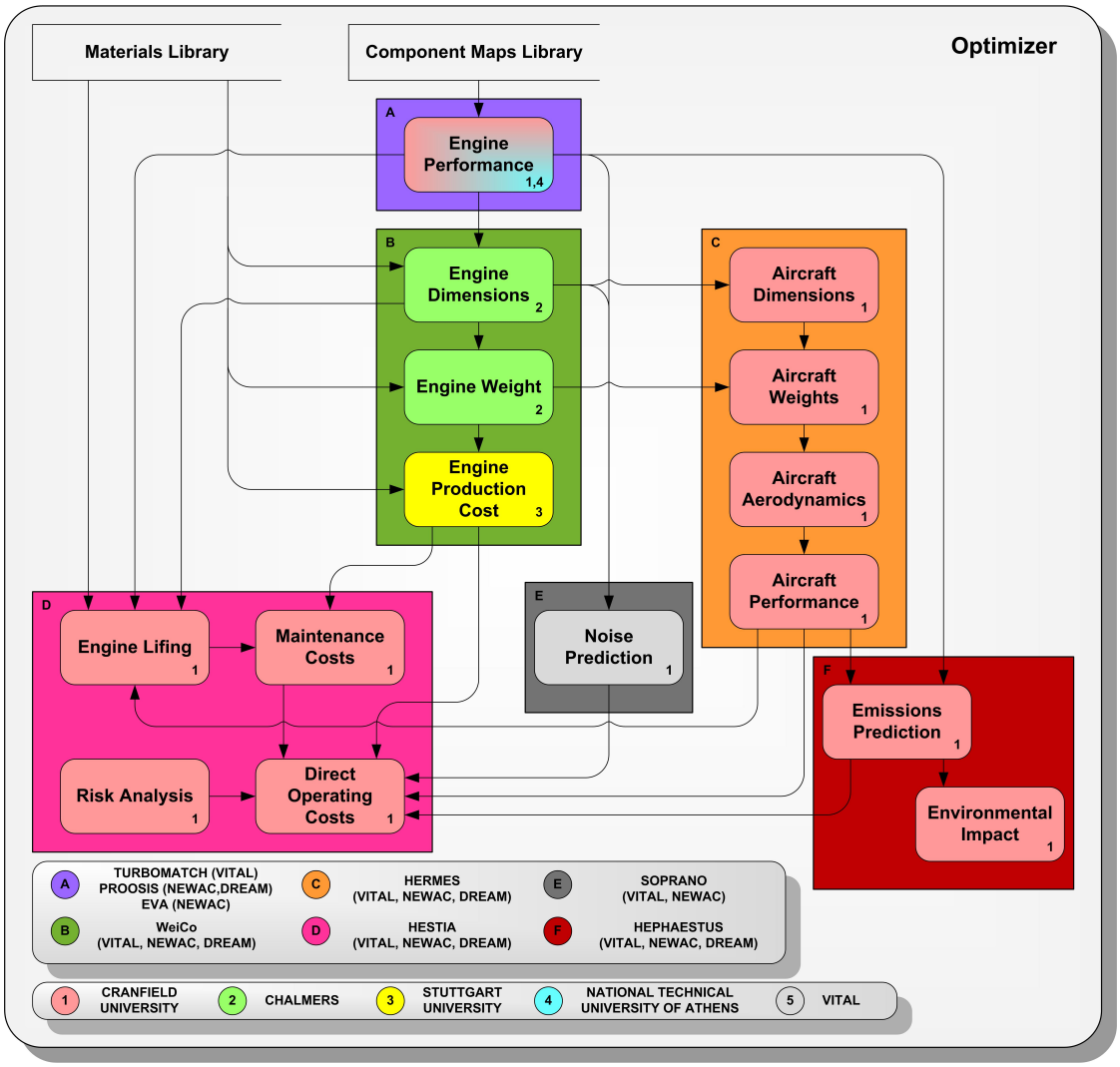

Figure 1.1: TERA2020 conceptual design process[9]

A typical structure of a TERA framework, used in the VITAL[10], NEWAC[11] and DREAM[12] EU (EU) projects, is presented in figure 1.1[9]. Performing a brief overview of the available modules, TURBOMATCH[13], PROOSIS[14] and EVA[15]

are the three performance codes, WeiCo[9] handles the powerplant weight and cost estimation and HERMES[16] estimates the aircraft performance. HESTIA estimates the engine life and the operating and maintenance cost, HEPHAESTUS[17] performs an evaluation of the emissions and environmetal impact and finally SOPRANO[18] is responsible for noise predictions. All the above modules are integrated in a commercial multidisciplinary optimiser called iSIGHT[19].

One of the modules included in a TERA framework is the aero preliminary weight estimation module, which not only provides a weight estimate, but also the layout and dimensions of the whole engine. It holds a key role in the TERA context, with the weight values having a significant effect on many of the output parameters.

The weight prediction methods available within the public domain are numerous and vary significantly, as far as accuracy and complexity are concerned. Single equation models, based usually on empirical or statistical data, are very simple and easily employed, but lack the necessary accuracy. On the contrary, more detailed approaches tend to rely on physical models, achieving the desired accuracy, but significantly increasing the complexity of the method and the calculation time that is required. The former, are in most cases part of the "whole engine based" methods group that estimate the weight of the whole engine, whereas the latter usually belong in the "component based" methods that estimate the weight of each component separately and sum them to provide the engine weight.

Due to the multi-disciplinary approach of a TERA framework, it is ideal for assessing the design envelope and feasibility of novel engine configurations. The ones that have emerged as potential candidates for future aero engines include the GTF, the open rotor, usually with a contra rotating turbine and the intercooled and/or recuperated engines.

The feasibility of the GTF arrangement will be examined, but only based on the influence of design and weight on engine performance. It should be noted that even though the introduction of a gearbox is also associated with a larger and heavier fan to achieve improved SFC, this was not included in the present study, due to lack of appropriate tools.

1.2 Project objectives

The main objective of this project was to analyse and evaluate existing preliminary weight estimation methods for turbofan engines and develop a new "component based" method, suitable for use in engine optimisation studies at the conceptual and preliminary design phases. It's target was to estimate the weight of novel engine architectures in order to evaluate their potential, identify their limitations and define their design space.

Based on the above, the following individual project objectives were set:

- Analyse and evaluate the existing aero preliminary weight estimation methods. In particular, assess their ability to accurately predict the weight of recent turbofan engines, along with the physics that govern them. Crucially, for use in engine optimisation studies, study the ability of existing aero preliminary weight estimation methods to reflect changes in performance and design parameters on engine weight.

- Develop a new "component based" aero preliminary weight estimation method, able to provide weight estimates for components included in a turbofan engine, but also for novel ones, enabling the study of innovative engine layouts. The use of component design methods was preferred, since they don't rely on existing engine data, thus providing more accurate weight predictions for future engines for aero applications.

- Build a tool based on the new "component based" aero preliminary weight estimation method for use in engine optimisation studies within a TERA framework. This tool achieves the target accuracy, provides low calculation time and increased flexibility and extensibility, in order to allow for the easy integration of additional components.

- Investigate the influence of key performance and design parameters on engine weight, in order to identify the ones to use in a simplified aero preliminary weight estimation method.

- Provide insight on the feasibility and design space of novel engine configurations. In this context, the GTF configuration was assessed, since there is only limited information on its influence on engine and component weight and its installed performance.

1.3 Project contribution

The present work contribution can be detected in the analysis of the existing preliminary weight estimation methods, the development of a new preliminary weight estimation method and the investigation on the feasibility of a GTF arrangement. In detail, the project contributes to the following areas, which to the author's knowledge are not addressed in the literature:

- This work is the first to provide an extensive literature survey of the existing preliminary weight estimation methods, which were thoroughly analysed quantitatively and qualitatively, in order evaluate their accuracy and their ability to follow variations of the major engine parameters.

- The new "component based" preliminary weight estimation method (ATLAS) that was developed as part of this work is a valuable contribution to the Center for Propulsion. Even though it follows the principles of NASA WATE, it employs more robust component design methods and can be expanded to allow for the weight estimation of novel engines.

- Very high BPR values were considered for DDTF configurations, revealing that the adjustments of LPT number of stages or LPT diameter are not sufficient, if high stage isentropic efficiency values are targeted. On the other hand, this is possible if the LPT rotational speed is modified, with the GTF configuration being a possible design solution.

- The introduction of a gearbox in a DDTF engine results in overall weight reduction, for a fixed fan geometry, since the smaller number of LPT stages,

outweighs the heavier components due to increased stresses. For the examined case study, this is true even after introducing the weight of the gearbox, but the feasibility of the GTF arragement is dependent on the trade-off between the total estimated weight decrease and the gearbox accessories weight that is not estimated. However, a larger fan, associated with the GTF configuration imposes a weight penalty, but also a performance benefit and should be evaluated based on the installed performance.

- For a given thrust requirement, the comparison of DDTF and GTF engines is not realistic considering the same thermodynamic cycle, but in order to realise the full potential of the GTF their installed performance optima should be compared. The same cycle is only considered if the optimum cycle cannot be utilised due to restrictions on design parameters, with the aircraft ground clearance being a typical case.

1.4 Publications

The author has contributed the following publications, related to the present work:

1. P. Lolis, P. Giannakakis, Sethi V., A. J. B. Jackson, and P. Pilidis. Evaluation of aero gas turbine preliminary weight estimation methods. *The Aeronautical Journal*, 118(1204), June 2014

2. P. Lolis, B. Arumungam Shanmugasundaram, Sethi V., and P. Pilidis. An empirical aero gas turbine preliminary weight estimation method based on artificial neural networks. In *Proceedings of the 71st SAWE Conference*. Society of allied weight engineers (SAWE), 2012
   Winner of UK chapter student paper award.

3. P. Lolis, V. Sethi, A.J.B. Jackson, and P. Pilidis. Analysis of aero engine preliminary weight estimation methods used within a Techno-economic and

Environmental Risk Analysis framework. In *Proccedings of the 24th International Cogress On Condition Monitoring and Diagnostics Engineering Management (COMADEM)*. COMADEM International, 2011

1.5 Thesis structure

Chapter 2 provides a comprehensive literature review of the existing aero preliminary weight estimation methods, categorising them into "whole engine based" and "component based", according to the weight estimation method used. Furthermore, their limitations and accuracy, as quoted by their authors, are highlighted. A quantitative and qualitative analysis based on existing turbofan engines is also performed, aiming to identify the physics behind them and their ability to provide accurate weight predictions.

Realising the need for a new "component based" aero preliminary weight estimation method, chapter 3 presents the design and weight prediction methodology for components that can be combined to provide a turbofan weight estimate. Furthermore, a methodology to estimate the weight of a gearbox is presented, enabling thus the modelling of a GTF engine. Finally, suggestions for improvement of the used design and weight methods are provided.

Chapter 4 aims to verify the new aero preliminary weight estimation method, by comparing the estimated engine design and weight against two major existing turbofans. Furthermore, it is also compared quantitatively and qualitatively against the NASA WATE method, in order to verify its accuracy and the weight trends followed.

Chapter 5 explores the feasibility of a GTF configuration by looking into the performance and mechanical integrity aspects of this modification and their influence on engine weight. Moreover, the installed performance, which is dependent on fuel consumption and engine weight, is taken into account to reach the conclusions.

Finally, the last chapter (Chapter 6) summarises the present work and conclusions, but also provides suggestions for future work.

Chapter 2

Existing preliminary weight estimation methods

2.1 Introduction

Due to the significance of engine weight to the performance and design of the aircraft, attempts to predict accurately the weight of aero gas turbines were made since the design of the very first. However, due to the complexity and diversity of the engine designs, the determination of the parameters that affect the engine weight and their correlation was no trivial task. This had as a result the development of several preliminary weight estimation methods throughout the years, using different parameters and physics.

For simplicity reasons, in the present analysis the available methods will be qualified into two major categories. The first one consists of "whole engine based" methods that predict the weight of the whole engine, or just separate the core from the fan structure. On the other hand, there are "component based" methods that attempt to estimate weight by dividing the engine into components and calculate the weight of each one separately.

The development of methods with different philosophy and the subsequent distinction was mainly a result of three major parameters.

- **Different levels of fidelity required.** An accurate estimate of the engine

weight is required at almost all stages of the engine development and design. However, during the conceptual design stage, there are a lot of assumptions and uncertainties regarding the engine and aircraft, that will be clarified later in the design process. Therefore, a very accurate weight estimation is not desired for the selection of concept, but as the design process progresses, more accurate gas turbine weight predictions are required to optimise the performance and ensure the mechanical integrity of the engine and aircraft.

Regarding accuracy, a $\pm 10\%$ error target limit was adopted in this study, following what has been used in all existing preliminary weight estimation methods, aiming for minimal error, but also taking into account the difficulty in producing accurate weight estimations[23]. The required accuracy for a preliminary weight estimation method, however, should be a result of a sensitivity study considering the effect of engine weight on the installed performance. This task was not performed in this project, but it is proposed as future work.

- **Complexity and calculation time.** The weight of a gas turbine, as will be shown in the following sections, can be easily calculated if the volume of the engine parts and the corresponding material properties are known. However, the final shapes of the engine components, and therefore their volumes, are not known until the final design stages. If a weight estimation is required at an earlier stage, a preliminary design has to be performed first to estimate the missing component volume. Due to the fact that there are several preliminary design methods available, their accuracy, complexity and calculation time vary significantly.

  The complexity and calculation time can be also greatly decrease with a penalty in accuracy. This is achievable by linking a limited number of engine performance and design parameters with engine weight, usually through use of existing data. This results in most cases to a single equation, categorised in the "whole engine based" methods group.

- **Availability of component weight data.** Due to confidentiality rea-

sons, the OEMs provide only the weight of the whole turbofan engine, in most cases excluding the nacelle and thrust reverser, and don't disclose the weight of each component. This prohibits not only the development of empirical "component based" methods, but also the validation of analytical approaches, encouraging the creation of "whole engine based" methods.

During the conceptual design phase, the engine weight estimation is challenging even for the OEMs, since only limited design parameters are fixed. Therefore, there is a rationale for the development of empirical "whole engine based" methods that require only few input variables available at the early design stages.

2.2 "Whole engine based" approaches

The need for fast engine weight prediction and the lack of data during the conceptual design stage, have set the ground for the development of many simple correlations. These choose to estimate the weight of the whole engine, rather than add complexity with component weight calculations and thus are classified as "whole engine based" approaches. All of the available methods can be characterised as empirical, since they make use of an engine database and correlate the parameters of interest to the real engine weight. These approaches are therefore limited to weight predictions on engines similar to the database cases and don't capture the full range of weight influencing parameters. As a result, they are unable to provide weight predictions for future engines and novel arrangements. On the upside, they achieve fast calculation times with just few inputs, but can also capture characteristics that are challenging to calculate analytically.

2.2.1 Single equation methods

A subgroup of the "whole engine based" approaches is the single equation methods. As their name implies, they consist of only one equation that connects engine weight with no more than four variables.

2.2.1.1 Simple weight correlations

One of the first attempts to provide a rough correlation of the engine weight was developed by Whitehead and Brown[24] in 1953, linking the weight of a gas turbine with the design mass flow for lightweight and orthodox turbojet designs (Eq. 2.1, Eq. 2.2), for design mass flow up to 200 lbs/s (90.72 kg/s).

$$WT \propto (\dot{m}_{des})^{1.45} \text{ , for lightweight design} \tag{2.1}$$

$$WT \propto (\dot{m}_{des})^{1.36} \text{ , for "orthodox" design} \tag{2.2}$$

In a similar way, a few years later, Pennington[25] in 1959, provided only a rough estimation of the thrusts influence on the weight of turbojet gas turbines (Eq. 2.3).

$$WT \propto FN^{1.5} \tag{2.3}$$

These first attempts to link engine weight with engine parameters were mainly focused on turbojets or low bypass ratio turbofans intended for military applications, where just the thrust or mass flow can provide a rough estimation of engine weight. They have no practical value for absolute weight predictions, but can provide some insight into the parameters that influence engine weight.

2.2.1.2 Guha et al. method

The need for an absolute weight prediction has led to the development of methods that use a single equation to estimate engine weight in the preliminary design stage. The most recent method by Guha et al.[26] was created by using data from 30 engines by four manufacturers to correlate fan diameter with engine weight, producing equation 2.4 for use with imperial units.

$$WT(lbs) = 2.65 \cdot \left(1.81 \cdot D_{fan}(in)^3 - 19.8 \cdot D_{fan}(in)^3\right)^{0.5833} \tag{2.4}$$

The authors don't mention the accuracy of the method, but the use of only a single variable is expected to fail to capture all the synergies that influence engine weight. However, as will be shown in later sections, fan diameter is the most suitable parameter for a single variable weight estimation equation.

2.2.1.3 Svoboda method

Svoboda[27] in 2000, collected publicly available data of 68 gas turbines with by-pass ratio greater than two. Through simple two dimension plots (Fig. 2.1) he attempted to link thrust with several parameters, including engine weight. The result was a very simple correlation, connecting take-off thrust with engine weight (Eq. 2.5).

$$WT(lbs) = 250 + 0.175 \cdot FN_{to}(lbf) \tag{2.5}$$

Even though the method error for most of the tested engines is quoted to be below ±10%, but similarly to method by Guha et al., it employs only one variable, which is only sufficient for a very crude preliminary estimation of engine weight.

2.2.1.4 Raymer - Jenkinson et al. methods

About a decade earlier, Raymer[28] in 1989, used apart from take-off thrust, the BPR of the engine at take-off to form his equation. The same two variables were used by Jenkinson et al.[29] in 1999 in their equation (Eq. 2.7). Both these equations work with the take-off thrust expressed in kN.

$$WT = 14.7 \cdot FN_{to}^{1.1} \cdot e^{-0.045 \cdot BPR} \tag{2.6}$$

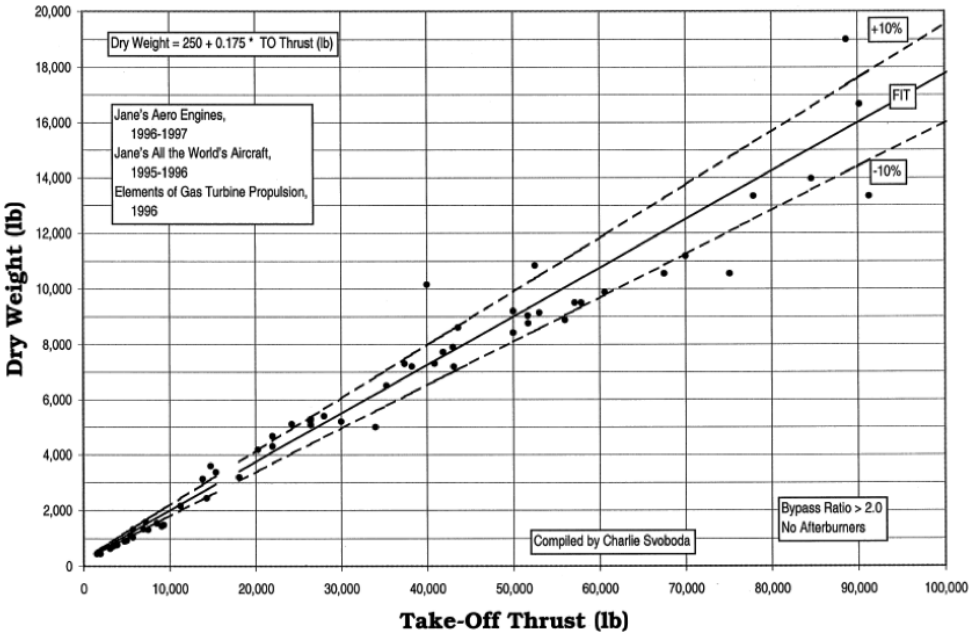

Figure 2.1: Svoboda weight correlation[27]

$$\frac{WT}{FN_{to}} = 8.7 + 1.14 \cdot BPR \tag{2.7}$$

In order to define the correction factors in his equation, Raymer used statistical methods on data derived from the public domain[30]. As the author suggests, it is only valid for subsonic engines with BPR less than six, making it unsuitable for the latest high BPR engines. A version of the equation is also available for supersonic engines, but its analysis is beyond the scope of the present work.

Jenkinson et al., on the other hand, used not only existing, but also projected high BPR $(5 - 14)$ engine data to define the correction factors for his equation. However, no information on the engines that were used or the extrapolation method is provided. Furthermore, the correlation plot (Fig. 2.2) is based on only a few engines, including also some outliers.

2.2.1.5 Torenbeek method

Torenbeek[31], following a physics based path, produced a weight estimating correlation with the rationale that engine weight is a combination of the gas generator

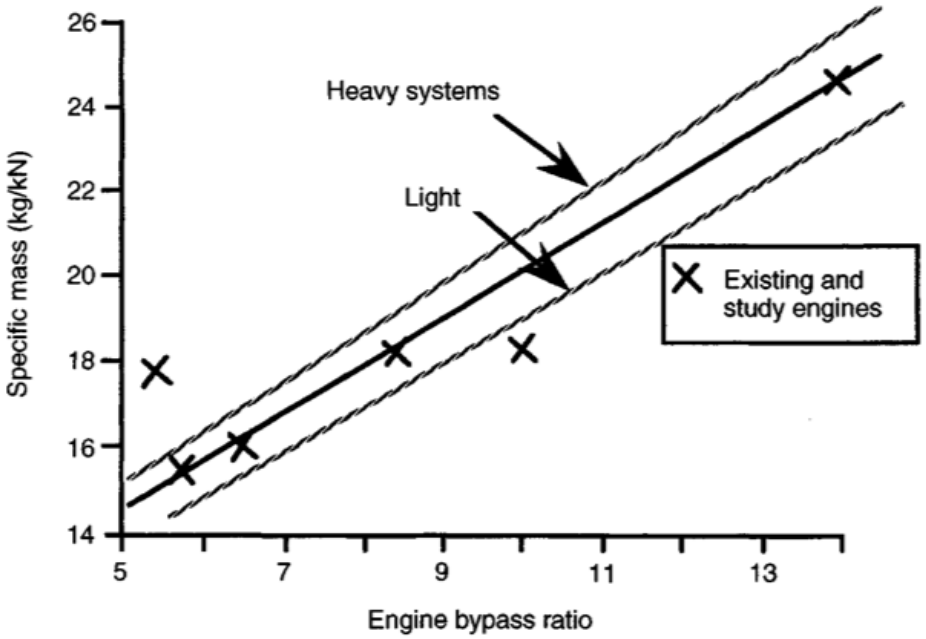

Figure 2.2: Jenkinson et al. weight correlation[29]

weight and the weight of the propulsive device, which includes the fan, low pressure turbine and nozzle. He then produced a correlation (Eq. 2.8) by assuming that the gas generator weight is linearly linked with the core mass flow, whereas the propulsive device weight is proportional to the fan thrust at take-off.

$$WT = Co_1 \cdot \dot{m}_{gg} + Co_2 \cdot FN_{fan,to} \tag{2.8}$$

In order to present the correlation in a more applicable form, Torenbeek used a series of engine performance based transformations for the gas generator mass flow and the fan thrust. The core mass flow was expressed as a function of the specific thrust (i.e. thrust divided by mass flow) and BPR at take-off, while the fan thrust as function of the BPR only. Furthermore, he determined the values of the two correction factors, Co_1 and Co_2, based on engine data, with the core correction factor coming out as a function of the Overall Pressure Ratio (OPR), instead of a constant value. These steps resulted in the final form of the equation (Eq. 2.9), which can only be used with imperial units and not for high BPR engines (up to 8). It included not only the take-off thrust and BPR as variables,

as was the case in the previously examined single equation methods, but also the OPR and specific thrust at take-off, raising the number of inputs to four. Torenbeek had also considered geared turbofan configurations and variable pitch fan blades, suggesting that the weight of the propulsive device is 20% higher in each case respectively.

$$\frac{WT}{FN_{to}} = \frac{10 \cdot OPR^{1/4}}{\left(\frac{FN}{\dot{m}}\right)_{to} \cdot (1 + BPR)} \tag{2.9}$$

2.2.1.6 Single equation methods summary

In summary, single correlation or equation methods give immediate results and can be used for almost every engine, because they require only few publicly available variables. However, since these methods have been derived from existing engine data, it is advisable to use them only for engines similar to the ones used for their development, and respect the restrictions set by their authors. Furthermore, most of them do not quote the expected error, which is expected to fall above the desired 10% value, as only a few aspects of the gas turbines are captured. Table 2.1 provides an overview of the available single equation methods and the input variables required by each one of them.

Table 2.1: Single equation methods

Method	**Year**	**Weight Correlation**
Whitehead and Brown	1953	$WT = f(\dot{m}_{des})$
Pennington	1959	$WT = f(FN)$
Torenbeek	1975	$WT = f(FN_{to}, \dot{m}_{to}, BPR, OPR)$
Raymer	1989	$WT = f(FN_{to}, BPR)$
Jenkinson et al.	1999	$WT = f(FN, BPR)$
Svoboda	2000	$WT = f(FN_{to})$
Guha et al.	2012	$WT = f(D_{fan})$

2.2.2 Clavier method

Another study that was conducted at Cranfield University in 2008 by Clavier[32] can be classified in the "whole engine based" group as well. The method was developed based on a database of more than 150 turbofan engines, as is the case with all the other "whole engine based" approaches. Failing to successfully correlate a single variable with engine weight, Clavier constructed a parameter that included OPR, BPR and mass flow (Eq. 2.10). This parameter was plotted against real engine weight (Fig. 2.3) and a three part quadratic equation was produced (Eq. 2.11) having the engine weight as a function of the parameter only.

$$parameter = OPR^2 \cdot BPR \cdot \dot{m} \cdot 10^{-6} \tag{2.10}$$

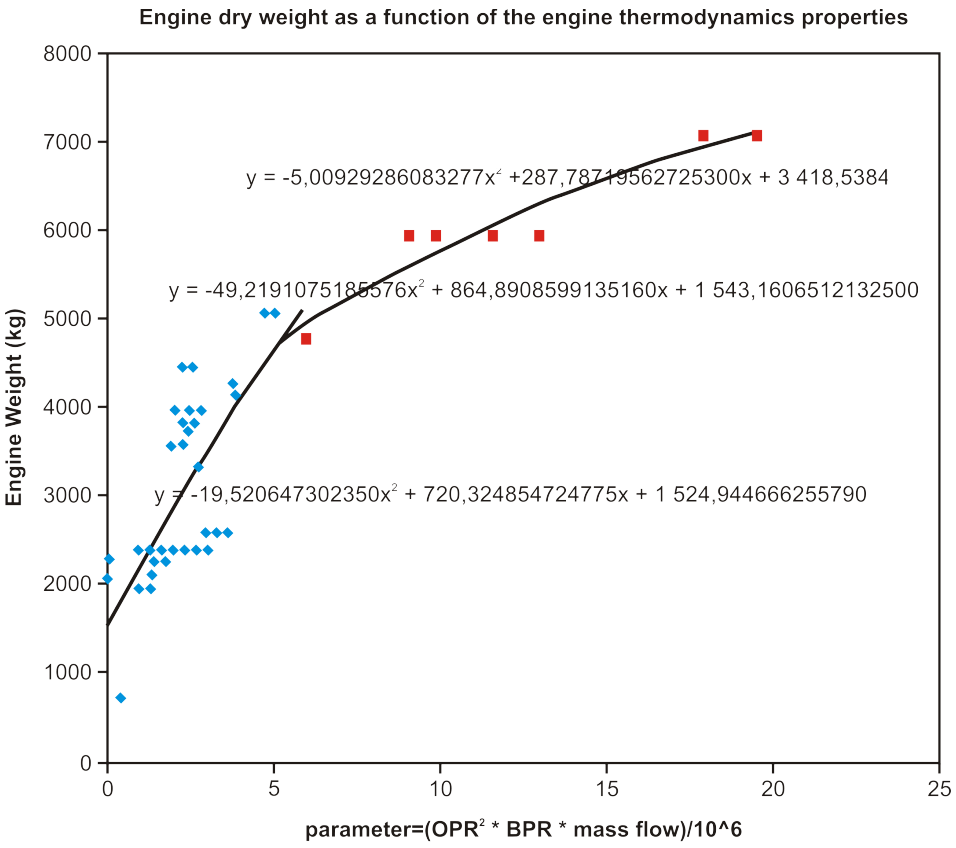

Figure 2.3: Clavier weight correlation[32]

This equation, contrary to the simpler equations that were examined, features a non-linear relation between weight and its variables. More specifically, mass flow and BPR correlate with a quadratic function, while OPR has a fourth order relation with weight, as was also the case in Torenbeek's approach. However, it should be noted that the first term of the equation, which is also the dominant term, is negative, resulting in negative engine weight for large values of the parameter. This is most likely to happen for high OPR values, since this is the most influential variable within the parameter. Futhermore, even though this method includes three major variables for the weight estimation, to define fully a turbofan engine a fourth variable is required as well. This could be either the TET, as suggested by Clavier, or the thrust that is publicly available for all the engines.

$$\begin{gathered} WT = -19.821 \cdot parameter^2 + 720.325 \cdot parameter + 1524.945 \\ \text{if } \; parameter < 5 \\ \\ WT = -49.219 \cdot parameter^2 + 864.891 \cdot parameter + 1543.161 \\ \text{if } \; 5 < parameter < 7 \\ \\ WT = -5.009 \cdot parameter^2 + 287.787 \cdot parameter + 3418.538 \\ \text{if } \; parameter > 7 \end{gathered} \tag{2.11}$$

2.2.3 Gerend and Roundhill method

The method developed by Gerend and Rounhill[33] in 1970 was one of the first complete and detailed studies on the preliminary estimation of a gas turbine weight and dimensions. The method is again following the "whole engine based" approach, using data from over 350 engines available in the public domain, manufactured or at the design stage, dated between 1940 and 1980. The diameter, length and weight of the engines were studied in relation with various parameters,

trying to include not only thermodynamic aspects, but other factors as well. In other words, apart from OPR, BPR, Fan Pressure Ratio (FPR), mass flow and TET, parameters such as the manufacturer, noise, life and entry into service date were taken into account.

Nonetheless, the plots that were used to produce the correction factors reflect only the influence of one input variable on engine weight and fail to capture the connections and interactions between them. Furthermore, the data on some plots have considerable scatter, compromising the accuracy of the final correlations. The authors state that the method achieves ±10% error, but also advise that the results are only valid for comparative conceptual studies for engines developed prior to 1980. Moreover, they set certain limits to the input variables, which are considered outdated for the current and future turbofan engines (Table 2.2).

Table 2.2: Gerend and Roundhill method limitations

Variable	**Min Limit**	**Max Limit**
Year of First Flight	1940	1980
Bypass Ratio (BPR)	0	10
Core Mass Flow	9 kg/s	362 kg/s
Max Flight Mach Nr.	0	3

This method, being very simple and with acceptable accuracy, was used in Cranfield University in various projects. Whellens[34] in 2003 used the original method to predict the weight of turbofan engines and more recently, Colmenares Quintero[35] in 2009 modified the method by extrapolating the data to cover a wider range of OPR and BPR.

2.3 "Component based" approaches

The second category of preliminary weight estimation methods contains the "component based" approaches. As the name implies, the weight of each component is estimated separately and are summed to provide the total engine weight. However, the complexity of the engine components, combined with the lack of extensive component weight data, have made imperative the need for a preliminary

design method prior to the weight estimation. Thus, higher levels of accuracy are achieved, but with higher complexity and increased input variables and calculation time. Based on these characteristics, these methods are not ideal during the conceptual design phase, but they are highly recommended at the preliminary design stage. Finally, the preliminary design of the engine components, enables the simulation of novel engine design concepts, but also captures the weight variations associated with different design philosophies and technology levels.

2.3.1 Sagerser et al method

One of the first methods that tried to estimate each components weight and dimensions separately was developed by Sagerser et al.[36]. Even though the method was initially conceived for Vertical Take Off and Landing (VTOL)/Short Take Off and Landing (STOL) aircraft, it can also be used for cruise engines, since the appropriate correlating factors are estimated as well. The component equations were structured initially by following physical rules, but their final form was deduced by correlating them with the available engine data. The variables used are primarily geometrical characteristics of the components, that are available only after a basic preliminary design is performed.

Table 2.3: Range of correlating data for the Sagerser et al. method

Component	**Variable**	**Min Limit**	**Max Limit**
Fan	Tip diameter [m]	0.73	2.6
	Rotor aspect ratio	2.5	7.7
	Number of stages	1	2
Compressor	Mean diameter [m]	0.34	0.98
	Number of stages	2	14
	Length/ Mean D at inlet	0.29	1.4
Combustor	Mean diameter [m]	0.40	0.91
Turbine	Mean diameter [m]	0.43	1.2
	Number of stages	2	6
	Mean speed [m/sec]	120	510
Controls & Accessories	Thrust [kN]	18	170
Frames	Estimated weight [kg]	100	2000

The authors of the method, bearing in mind the variability of the data avail-

able at the time, advise to use the method only as a comparative and not an absolute weight prediction tool. Despite these considerations, they state that it manages to achieve an acceptable level of accuracy (±10% error, as stated by the authors) for most of the examined cases. However, the error should be considerably large for recent engines since the original method was developed in 1971 and thus does not capture the present technology level. This is more evident regarding the correlating database range, which includes variable limits that are exceeded when engines currently in production are considered (Table 2.3). Furthermore, since the method was developed and intended for VTOL/STOL engines, their unique characteristics also influence the method accuracy, when the weight of a turbofan engine is estimated.

2.3.2 NASA WATE method

A different "component based" appoach was initially developed within NASA, in collaboration with Boeing, by Pera et al.[37] in 1977. This method, named WATE predicts the weight and dimensions of the gas turbine's components by performing a rough preliminary design and sizing of the engine.

Despite that, the weight and dimensions prediction equations were further corrected with the help of a gas turbine database. This includes 29 engines, military and commercial, turbofan and turbojet, in production and in development. However, the database consists almost entirely of engines from two manufactures, with only 12 of them in production, restricting thus the accuracy and generalisation of the method. Furthermore, only eight engines, seven of which were manufactured by the two major manufacturers in the database, were used for validation purposes.

The sizing method is analytical and uses a detailed calculation procedure that models every part in each component. For instance, for the compressor calculation, as presented in figure 2.4, the component is split into blades and vanes, discs, cases and connecting hardware, resulting in weight calculation of each one separately. This approach claims to provide results with error within ±5%, sur-

passing the initial target of ±10% set by the authors. The main disadvantage, however, can be found in the requirement for many input variables, even though many of them can be estimated or calculated at the preliminary design stage. Furthermore, the complexity of the method, along with the increased calculation time arise extra difficulties when it is used within optimisation studies.

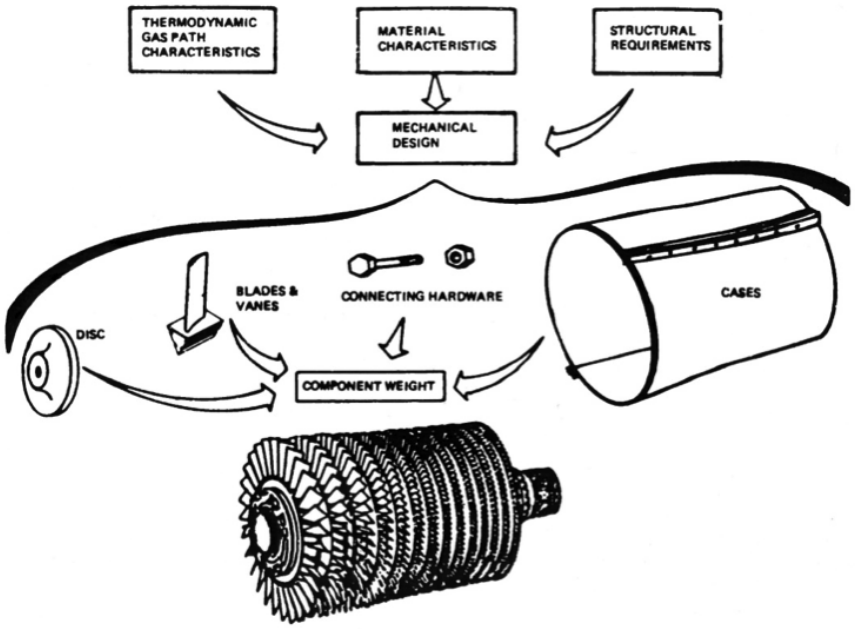

Figure 2.4: Compressor weight calculation with Pera et al. method[37]

After the implementation of the initial code, a series of modifications, expansions and improvements have been published for WATE. Shortly after the publication of the original method, Klees and Fishbach[38] provided a simplified version with calculation examples. Following their steps, Onat and Klees[39], who were among the authors of the original method by Pera et al., made several corrections and improvements on the WATE approach. The revised method, named WATE-2, even though it achieved a slightly higher level of accuracy, required even more input variables, increasing the complexity as well. Apart from the above, WATE-2 introduced a new methodology for predicting the weight and dimensions of small gas turbines, based mainly on the approach for large gas turbines. Based on this, Hale[40] in 1982 compiled a new code, named WATE-S. The new code introduced corrected calculation methods, suited for small gas turbines

and components more common to these engines, such as radial compressors and turbines. After more than two decades without major publicly available improvements, Tong et al.[41], in 2004, devised a method to improve the calculation of the disk weight and life, which was included in the WATE codes. More recently, Tong and Naylor[42] modified the existing WATE-2 code into an object-oriented code, named WATE++. Despite its complexity, the Pera et al. method is the most accurate preliminary estimation method of weight and dimensions available and was used in several studies. Sanghi et al.[43] used and adjusted the original Pera et al. method to estimate the weight of military turbojet engines, whereas Chalmers University in collaboration with Stuttgart University developed WeiCo (Weight and Cost)[8] originating from the Onat and Klees variant of the method. WeiCo was used quite successfully in a series of EU projects within a TERA optimisation framework[10;11].

2.4 Other weight estimation methods

The latest version (12) of the gas turbine performance and design software GasTurb[44], provides also the capability to estimate turbofan engine weight. However, there is only a brief description of the parts that are included in each component and the detailed weight estimation method is not provided. This "component based" method is excluded from the present analysis, since GasTurb is a commercial software and the free demo version enables only the performance simulation of turbojet engines. Furthermore, even though it enables the design of GTF and intercool-recupated engines, it only allows a fixed number of engine configurations, restricting the study of any engine layout.

Several other methods are mentioned within the analysis of the methods that were presented. However, the author was unable to acquire the reports that describe them, since in most cases they are internal manufacturer documents. Sagerser[36] mentions the work of Merriman[45] as simplified scaling relations and Stevens method[46] as focused on specific designs and too detailed for parametric studies. Moreover, Gerend and Roundhill[33] refer to weight estimation techniques

by Parker and Love[47] and statistical studies on turbojet component weight by Holden[48]. These are only mentioned here for the sake of completeness.

2.5 Method comparison

2.5.1 Quantitative analysis

The above analysis has revealed that there are several methods available, which claim to perform preliminary gas turbine weight estimation with accuracy of $\pm 10\%$. However, most of these methods are more than 30 years old and derived from outdated engine databases. Therefore, they were unable to follow the technological advancements used in recent engines and most likely they are inaccurate or even unsuitable for estimating the weight of modern gas turbines. Furthermore, as presented in the previous section, several existing preliminary weight estimation methods use just a few variables to estimate engine weight and most likely don't capture all the parameters that affect it.

In order to obtain a better picture of the capabilities and limitations of each approach, all the existing preliminary weight estimation methods were used to estimate the weight of several actual engines, with special focus on the achieved accuracy and the required number of inputs. The method testing was performed on a wide spectrum of existing civil turbofan engines, of different sizes, characteristics, manufacturers and entry into service dates. This engine database was populated using public domain data, mainly sourced from the extensive Jane's aero engines encyclopaedia[30]. Notwithstanding the uncertainty of the supplied information, this source of data remains the best possible solution available in the public domain. Whenever the flight conditions of a thermodynamic parameter value are not given, the value was assumed to be the maximum in the flight envelope.

The results of this comparison are presented in figure 2.5 and table 2.4. Figure 2.5 shows a scatter plot of percentage error against the real engine weight for each method. Furthermore, table 2.4 not only presents the error margins illustrated

in figure 2.5, but also provides additional information regarding the method age, the number of engines that were calculated and the number of inputs that each method requires. The following paragraphs provide a more detailed analysis and discussion for each method.

Table 2.4: Comparison of preliminary weight estimation methods

Method	Year	No of Cases	No of Inputs	Error
Guha et al.	2012	64	1	$\sim \pm 30\%$
Svoboda	2000	64	1	$\sim \pm 30\%$
Raymer	1989	64	2	$\sim \pm 40\%$
Jenkinson et al.	1999	64	2	$\sim -60\%$
Clavier	2008	64	3	~ -40 - $+650\%$
Torenbeek	1975	56	4	$\sim \pm 25\%$
Gerend and Roundhill	1970	25	min 8	$\sim \pm 50\%$
Sagerser et al.	1971	7	min 45	$\sim \pm 25\%$
NASA WATE	1979	1	~ 80	(± 5 - 10%)

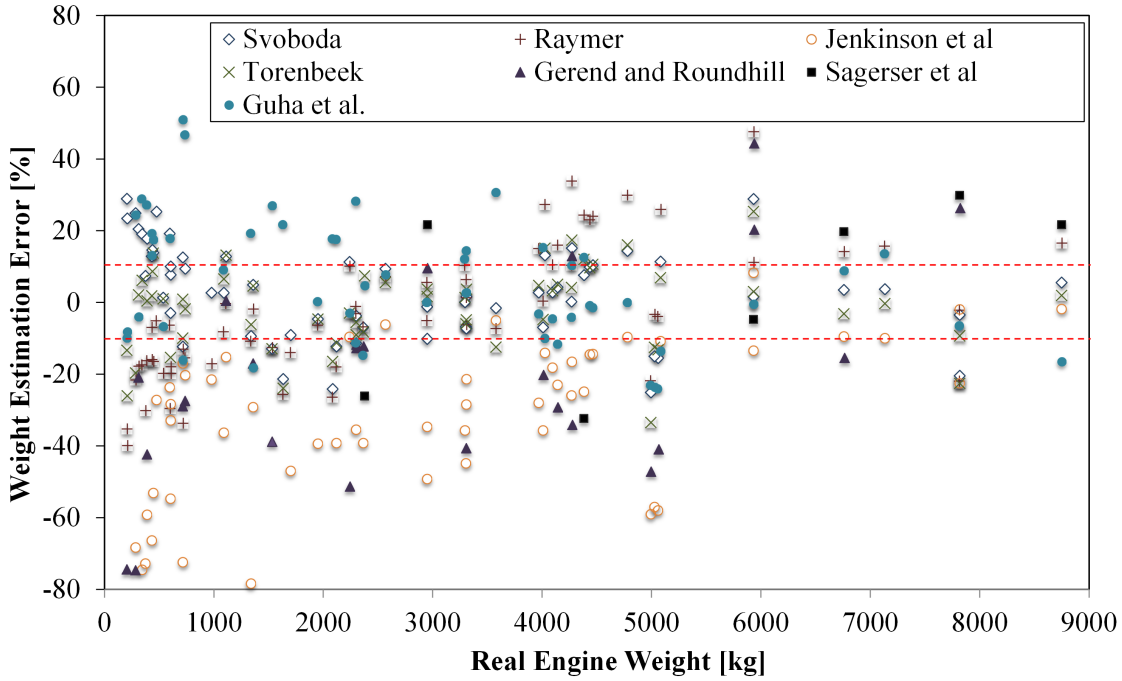

Figure 2.5: Percentage error of preliminary weight estimation methods

The method by Guha et al.[26] was first tested on all the engines of the database (64 civil turbofans), since fan diameter was available for all of them. As weight

does not only depend on fan diameter, the method error (±30%) was higher than the desired ±10% limit.

The methods by Raymer[28], Jenkinson et al.[29], and Svoboda[27] were consequently tested, since they are among the simplest to use methods, requiring up to two input variables, i.e. take-off thrust and BPR. Due to the availability of these parameters within the public domain, all the gas turbines in the database were used to estimate engine weight with these three methods. As shown by figure 2.5 and table 2.4 they all provide significantly lower accuracy than the target ±10%. Despite using only take-off thrust as input, Svoboda's method proved to be the most accurate, with its error lying within ±30%. On the other hand, the two-variable Raymer's equation is less accurate (±40% error) in general, but several distinct areas can be identified based on engine size. Dividing the engine into three categories, from figure 2.5 one can deduce that the method over-predicts the weight of gas turbines below 2200 kg, but is within the ±10% for engines that weigh between 2200 kg and 3700 kg. Regarding the large turbofans (above 3700 kg), no definite trends could be identified, even though the equation underestimates the weight of most engines. Finally, the method by Jenkinson et al. predicts lower weight for all engines, but this observation cannot be further exploited due to the big deviation from actual engine weight (60%).

Slightly increasing complexity, apart from take-off thrust and BPR, Torenbeek's equation (Eq. 2.9) includes also mass flow and OPR. However, these additional variables were not publicly available for all the database engines and restricted the studied cases to 56. The four-variable equation provided better accuracy (±25%), but still far from the acceptable limit.

The three variable weight estimation method by Clavier, despite being the most recent one, was the method that had the greatest error, especially for lightweight gas turbines. Up to 1500 kg engines, the error reduces, as the weight increases, but it starts from values as high as +650% reducing to a range of ±40% for larger engines. Due to the high error values, the points of the Clavier estimations were not included in figure 2.5, but only in table 2.4.

Finishing the study of the "whole engine based" preliminary weight estimation

methods, the method by Gerend and Roundhill[33] was used to estimate the weight of the gas turbines included in the database. As presented in the previous section, this method uses a lot of parameters to perform the calculations, which are not publicly available for most of the engines. Therefore, only 25 engines were tested, resulting in accuracy of around ±50%, significantly worse than the best achieved by "single equation" methods. This result can be attributed to the method's age and restrictions imposed by its authors, which combined with the significantly greater amount of input variables lead to the multiplication of the calculation error.

Similarly, the component based method by Sagerser et al.[36], due to the non-disclosure of engine data and the increased number of input variables, was used to calculate the weight of only 7 major engines. Once more, even though this method provided the best results among the examined methods, age and parameter limits led to an accuracy of around ±25%, instead of the expected ±10% that was quoted by the authors. Jackson[23] tested a variant of Sagerser's method for a short-range two-spool and a long-range three-spool engine and confirmed the error range of ±25%.

Finally, the NASA WATE method was tested on a single engine, due to the large number of input data required and their unavailability in the public domain. An engine performance model, built with Turbomatch[13;49], produced the thermodynamic cycle data needed to execute WATE.

Turbomatch is a FORTRAN-based gas turbine performance simulation software that has been validated over many years at Cranfield University. It is a 0-D aero-thermodynamic code that is based on component characteristic curves and solves the mass and energy balances between the engine components. Furthermore, it has been used in several studies in the past to predict the design and off-design performance of gas turbine engines[50;51], while it is also mentioned in the NATO report that sets out the principles of 0-D engine performance codes[52].

The engine model required for this study was based on publicly available data of the CFM56-7B engine, as shown in table 2.5[30]. The main design assumptions used in the WATE calculation are given in tables 2.6, 2.7 and 2.8. Figure 2.6

shows that the design calculated by WATE compares well with the real engine, while the engine dry weight estimate of 2289 kg is 4.8% lower than the value cited for the real engine. It is therefore concluded, that a correct use of the code can lead to a realistic engine design and thus a realistic weight prediction. This small case study also confirms the accuracy claimed by the authors of WATE ($\pm 5 - 10\%$).

Table 2.5: Baseline engine characteristics

Parameter	Value
Take-off Thrust (FN)	121.43 kN
Mass Flow ($\dot{m}$)	355 kg/s
Bypass Ratio (BPR)	5.1
Overall Pressure Ratio (OPR)	32.7
Cruise Specific Fuel Consumption $(\text{SFC})_{cr}$	17.06 $mg/N \cdot s$
Fan Diameter (D_{fan})	1.549 m

Table 2.6: WATE fan design parameters

Parameter	Fan
Inlet Mach Number (Ma_{in})	0.63
Outlet Mach Number (Ma_{out})	0.46
Configuration	Const. Tip
Inlet Hub to Tip Ratio $({}^{D_h}/_{D_t})_{in}$	0.323
Rotor Aspect Ratio (AR_R)	2.2
Stator Aspect Ratio (AR_S)	2.8

Table 2.7: WATE compressor design parameters

Parameter	IPC	HPC
Inlet Mach Number (Ma_{in})	0.42	0.46
Outlet Mach Number (Ma_{out})	0.41	0.27
Maximum Stage Presure Ratio (PR_{sg})	1.22	1.45
Configuration	-	Const. Tip
Inlet Hub to Tip Ratio $({}^{D_h}/_{D_t})_{in}$	0.8	0.725
Inlet Rotor Aspect Ratio ($AR_{R,in}$)	2.0	2.9
Outlet Rotor Aspect Ratio ($AR_{R,out}$)	1.5	1.34
Inlet Stator Aspect Ratio ($AR_{S,in}$)	2.2	2.9
Outlet Stator Aspect Ratio ($AR_{S,out}$)	2.8	1.34

Table 2.8: WATE turbine design parameters

Parameter	HPT	LPT
Inlet Mach Number (Ma_{in})	0.092	0.276
Outlet Mach Number (Ma_{out})	0.27	0.33
$MaximumStageLoading(\psi_{sg,max})$	1.51	6.41
Configuration	Const. Mean	Const. Hub
Inlet Rotor Aspect Ratio ($AR_{R,in}$)	1.3	1.85
Outlet Rotor Aspect Ratio ($AR_{R,out}$)	1.9	7.25
Inlet Stator Aspect Ratio ($AR_{S,in}$)	1.3	1.85
Outlet Stator Aspect Ratio ($AR_{S,out}$)	1.9	7.25

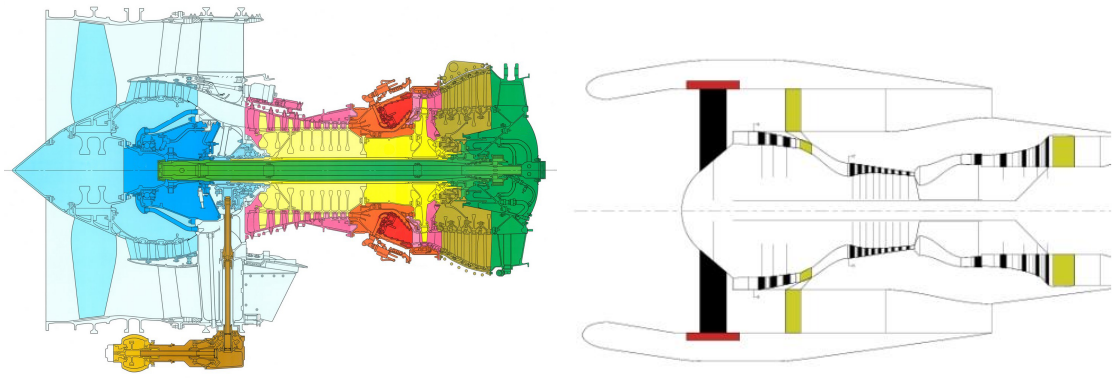

(a) CFM56-7B27 layout (b) Engine layout estimated by WATE

Figure 2.6: CFM56-7B27 NASA WATE design

2.5.2 Qualitative analysis

Having established the accuracy of each one of the reviewed methods in the previous section, it is now time to investigate how they capture the effect of the main preliminary design parameters on engine weight. For this purpose, a generic performance model is set up with Turbomatch in order to produce the thermodynamic data required by each method (mainly for the needs of the Gerend and Roundhill and WATE methods). The baseline performance values are given in table 2.9, for a typical two-spool turbofan with a booster architecture.

Table 2.9: Baseline engine performance values

Parameter	Value
Take-off Thrust (FN)	121 kN
Bypass Ratio (BPR)	5
Overall Pressure Ratio (OPR)	30
Take-off Specific Thrust (SFN_{to})	196 $mg/N \cdot s$
Turbine Entry Temperature (TET)	1400
Cruise Mach Number (Ma_{cr})	0.8
Entry Into Service (EIS)	1980
Engine Life	Long
By-Pass Duct Length	Short

The first parameter to be studied is the one included in all the available preliminary weight estimation methods, i.e. engine size. Each method captures the effect of size by correlating the weight either to the thrust, inlet mass flow or fan diameter. Figure 2.7 shows the trend predicted by the methods that use thrust as an input, along with real engine cases with the same characteristics as the baseline presented in table 2.9. All six methods link linearly or almost linearly take-off thrust with engine weight, starting from a common point at low thrust, and tending to diverge at higher values. Svoboda's method, having only the take-off thrust as variable, and being a relatively recent method derived by curve fitting techniques on existing data, appears to have the best fit on the real engine data.

At this point it is important to highlight a significant difference between thrust, mass flow and fan diameter as indicators of engine size. Fan diameter

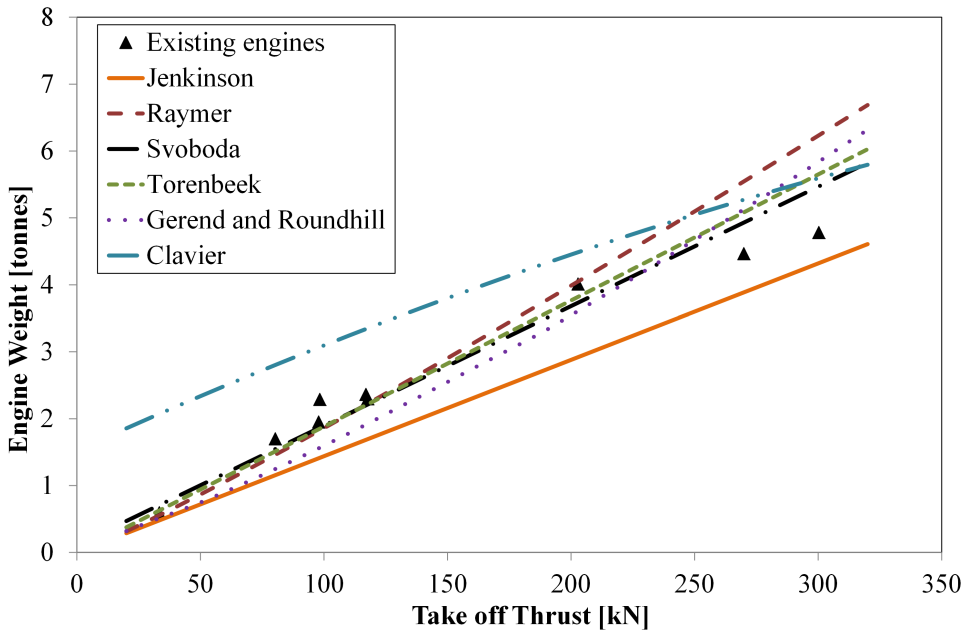

Figure 2.7: Take-off thrust effect on engine weight

has a direct impact on the volume and mass of the engine. Mass flow is a step further from weight, as it is proportional to the square of fan diameter for a given inlet hub to tip ratio and axial Mach number, determined by technological limits. If all the engines were at the same technology level, having the same inlet Mach number and hub to tip ratio, then the mass flow would have the same direct impact on weight as happens with fan diameter. On the other hand, the relation between thrust and weight is not as direct. Higher thrust can be produced either by a higher jet velocity or by a higher mass flow and diameter. In the first case the size of the engine remains unaffected by thrust variations resulting in small weight changes, while in the second there is a direct impact, corresponding to significant weight increase.

The above means that a method using thrust as input, cannot distinguish between engines that have the same thrust but different diameters. This is a common scenario at the preliminary engine design stage, where the diameter is selected for a specified thrust. Therefore, a method that only uses thrust as input could not be used in an engine optimisation analysis, and that is the rationale behind the use of diameter by Guha in his design studies[26].

Taking the analysis of existing preliminary weight estimation methods a step further, the effect of BPR was estimated for engines of the same thrust. Since Svoboda's method is only dependent on the take-off thrust, it was excluded from the analysis. Therefore, the methods by Raymer, Jenkinson et al., Torenbeek and Gerend and Roundhill were studied regarding the influence of BPR on engine weight, with the results presented in figure 2.8. Unfortunately, in this study there was not enough real engine data available with similar characteristics in order to compare with the equation predictions. As shown by equation 2.6 and figure 2.8, Raymer assumes that while the BPR increases, the decrease in core weight is higher than the increase in fan weight. Although not mentioned by Raymer, his method probably considers that the diameter of the engine is fixed by the thrust, and that is why the weight of the engine decreases with increasing BPR. Torenbeek's method also follows the same principle, since its behaviour is similar to Raymer's. Nonetheless, at low BPR the decrease of BPR results in a higher increase of weight, probably due to the "stricter" definition of engine diameter, by having a fixed thrust and specific thrust in equation 2.9. Raymer on the other hand might possibly imply that very low BPRs also lead to lower diameters. The Gerend and Roundhill method produces a curve similar to Torenbeek's, indicating thereby that it is based on the same fundamental principles.

On the other hand, Jenkinson et al. and Clavier follow the exact opposite approach. They consider that the fan size, and thus its weight, increases more than the reduction of engine core weight, and hence the total weight increases with increasing BPR. Both trends relative to BPR are valid, but based on different assumptions. Care should be taken that these "hidden" assumptions are respected when one of the methods is used, in order to ensure the validity of the results. Ideally, the effect of diameter and BPR should be taken into account separately, as done in the methods of Torenbeek, and Gerend and Roundhill.

The two major effects of diameter and BPR (core size) will be further studied for the methods of Gerend and Roundhill, and Torenbeek. These two, are the only whole engine based approaches that capture these effects independently and separate them from the definition of engine thrust. The comparison will also

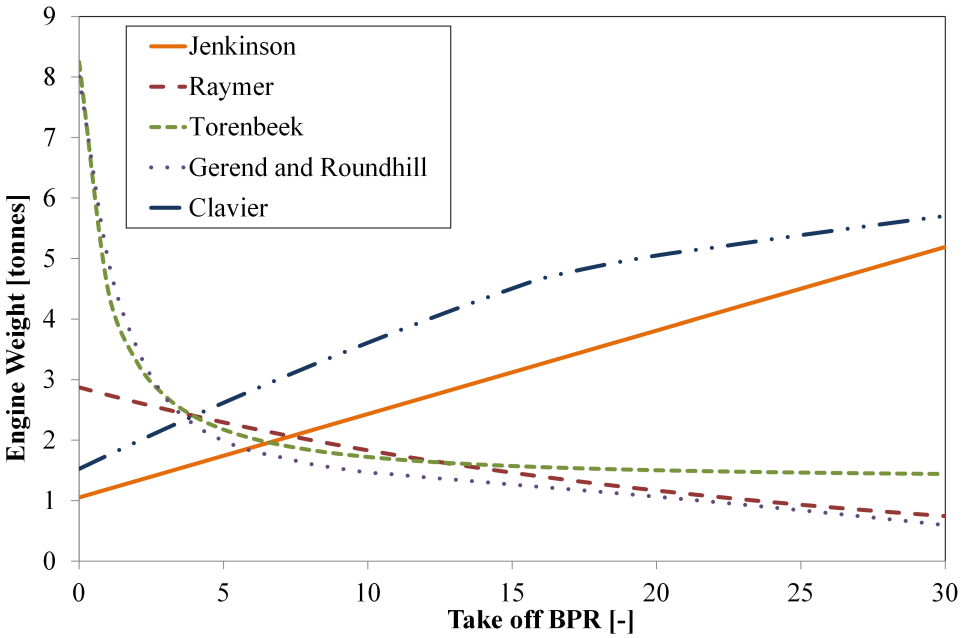

Figure 2.8: Bypass Ratio (BPR) effect on engine weight

include the WATE code as a baseline, which is expected to give the most realistic results, due to its analytical component based approach and its higher accuracy (as confirmed in the previous section). Due to confidentiality reasons, the latest version of WATE is not publicly available and an older version will be used in the present project.

The effects of diameter and core size will be studied concurrently in a design space where the TET and BPR are varied, while all the other variables are fixed to the baseline values given in table 2.9. These two variables have been chosen in order to facilitate the computation process (they are inputs to the performance code), while they also capture the desired effects; i.e. for a fixed BPR, the diameter varies for different TETs. Their design point values are given for a mid-cruise point of 20 kN, while the take-off values are calculated at off-design. A more detailed presentation of the calculation process can be sought in the work of Giannakakis[51;53].

The results produced by WATE are presented first in order to set the baseline for the comparison. Figure 2.9 shows that weight follows the variations of fan diameter, with BPR (or TET) having only a secondary effect.

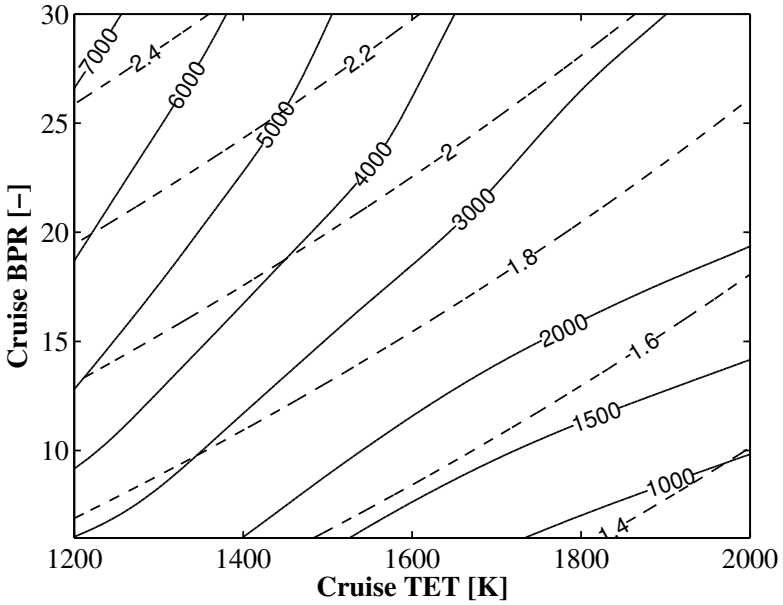

Figure 2.9: WATE engine weight prediction $[kg]$.
Dashed lines: engine diameter $[m]$

The weight predictions of the Torenbeek equation are shown in Figs 2.10 to 2.12. Figure 2.10 shows the variation of the first term of the equation, which represents the core weight. For a constant BPR the core size increases when the total fan diameter increases, and thus the core weight goes up. If now the fan diameter is kept constant while the BPR increases, the core diameter falls with a consequent reduction in core weight. At the same time the fan size gets bigger and its weight increases as shown by figure 2.11. On the other hand, at constant BPR the fan weight variation is rather unexpected. As shown by figure 2.11, increasing the diameter at a fixed BPR causes a decrease in the fan weight. This behaviour results probably from the fact that the fan weight term of Torenbeek's equation is only related to BPR and total thrust. This means that under constant thrust conditions, like the ones used in this study, the effect of diameter is not captured appropriately. Finally, figure 2.12 shows the variation of total weight, where it readily becomes apparent that the core weight variation dominates the total weight evolutions.

The analysis continues with the results of the approach by Gerend and Roundhill, shown in figure 2.13. Two distinct regions appear in the graph: a region with

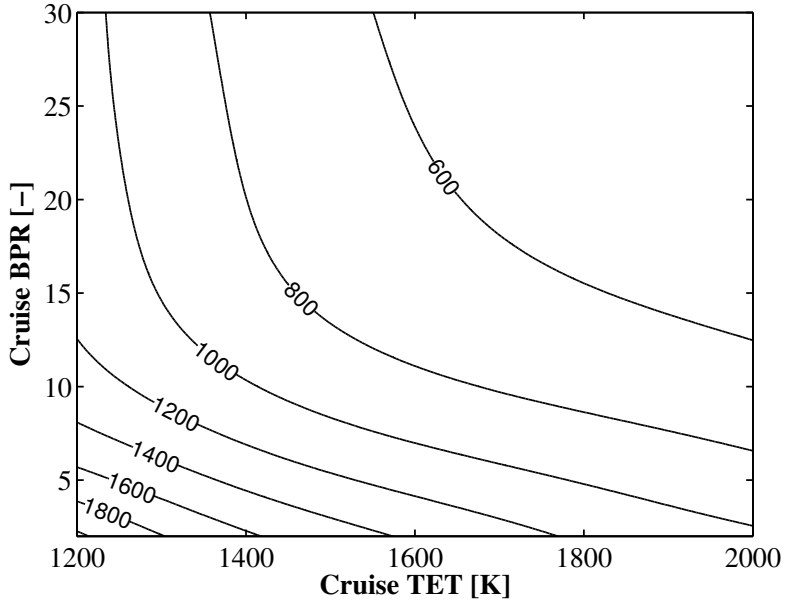

Figure 2.10: Torenbeek gas generator weight $[kg]$

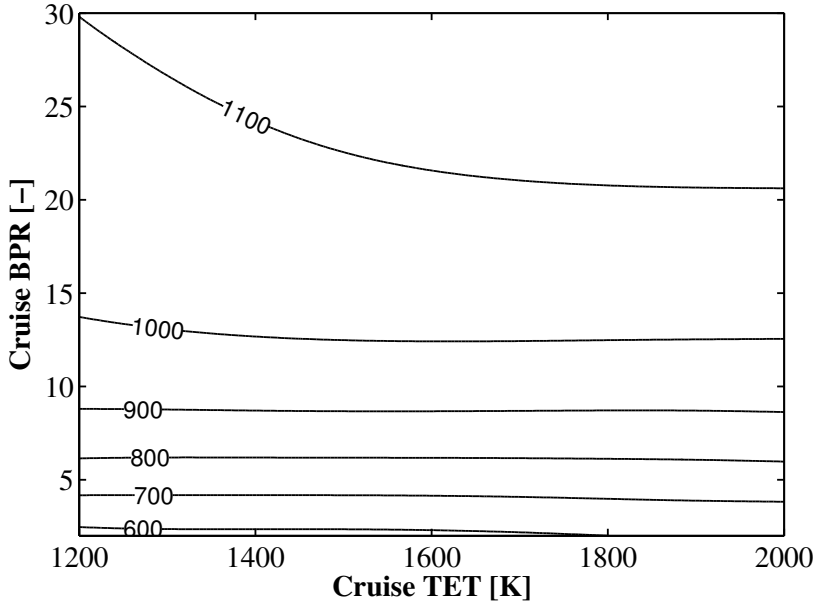

Figure 2.11: Torenbeek propulsive device weight $[kg]$

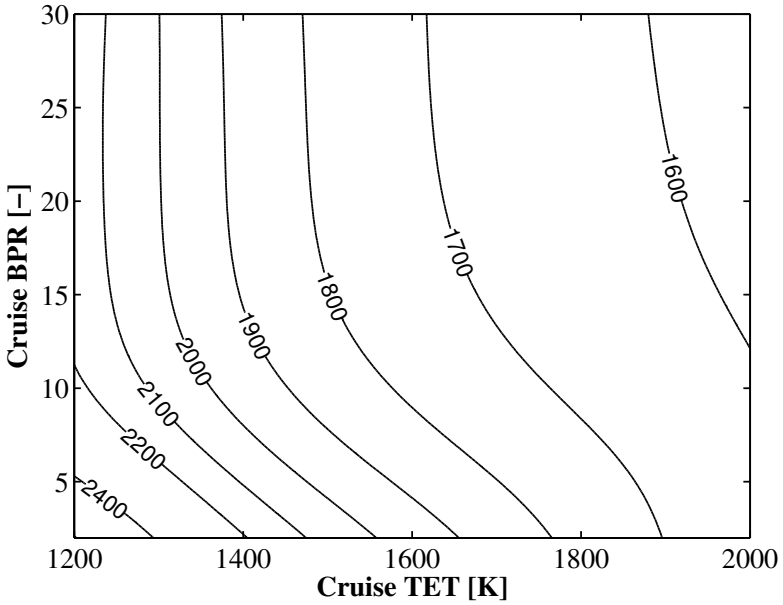

Figure 2.12: Torenbeek whole engine weight $[kg]$

BPR less than five, where the trends are similar to Torenbeek's, and a region of BPR higher than five where the results resemble the ones by WATE. In the first region, under constant BPR, increasing the diameter has little effect on weight, while in the high BPR area there is a more pronounced weight increase. In both graph regions, the increase of BPR under constant diameter clearly raises the engine weight. It is also interesting to add the constant TET point of view: following a vertical constant TET line, the weight initially decreases until a BPR of five, reaches a minimum and then starts rising. This happens due to the opposing effects of reducing the core size (dominating the first part) and increasing diameter (dominating the second part). This trend is not in agreement with the WATE results of figure 2.9, which shows that at constant TET, the increase of diameter always dominates over the increase of BPR and the weight finally increases.

A reason for the above effect can be sought in the reference engine used by Gerend and Roundhill, which corresponds to a 1962 turbojet engine, with BPR of one and a weight to mass flow ratio of 14. As shown by Doulgeris[54], modern turbofan engines have a weight to mass flow ratio closer to 16. This low and outdated value used by Gerend and Roundhill leads to an underestimation of the

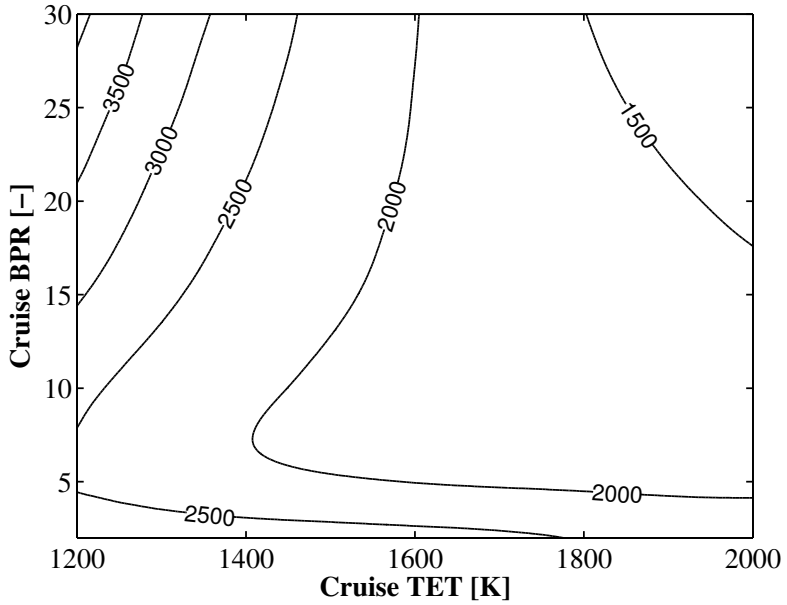

Figure 2.13: Gerend and Roundhill weight estimation $[kg]$

diameter effect and to the initial decrease of weight as the BPR increases in figure 2.13.

It is concluded that neither Torenbeek nor Gerend and Roundhill predict the same trends as the ones estimated by the higher fidelity WATE method, and hence they are not recommended for use at an engine preliminary design study.

2.6 Discussion and Conclusions

This short discussion section aims to explain the choices made in the past by other researchers and to present some recommendations for future implementations of weight estimation methods.

First of all, single equation models like the ones by Raymer, Jenkinson et al., Torenbeek and Svoboda, are usually proposed in aircraft design textbooks in order to provide a crude estimation of engine weight, in studies where the aircraft design varies while the engine remains constant. As these methods do not capture the effects of the basic engine design parameters, their use is not recommended for engine optimisation studies. For this kind of study, the weight calculation should

at least capture separately the effect of diameter and BPR, which correspond to the fan and core weight respectively.

Following the aforementioned principle, Guha et al. used equation 2.4 in order to select the optimum diameter for their turbofan design studies. In similar conventional turbofan optimisation studies, the method of Gerend and Roundhill was used, either in its original version[34], or extrapolated at higher BPRs[35], or recalibrated around a more modern turbofan[54;55]. The main disadvantage of even the most complete whole engine based analysis, such as the one of Gerend and Roundhill, is their dependency on engine data, which many times are not coherent and involve numerous uncertainties. The most common uncertainty encountered is the flight conditions associated with the value of an engine parameter; for example if the OPR is given at take-off for one engine and at top-of-climb for another, a false image will be given regarding its effect on weight. Furthermore, even if there is an adequate amount of coherent data, these will only apply to the conventional turbofan architecture and thus novel engine components or configurations cannot be captured.

In that case, researchers normally turn to component based methods, which can model the design and weight of each component separately, even if it is a novel one[10;11]. This involves a serious design effort, where a lot of knowledge is required to make the right design decisions and assumptions. Furthermore, this task can become more difficult, when a larger design space needs to be covered. Although this approach is the best for higher accuracy second level studies, it might be too time and resource consuming for a top-level thermodynamic design exercise. In such a case, it might be better to build a faster architecture specific whole engine based weight model that correctly captures the trends, within the limits and assumptions defined for the design study. For example, regarding a conventional turbofan study, WATE can be used to generate data, which are based on the same assumptions, and which can then be used in order to create a fast regression model that captures the effect of diameter and BPR. This model can subsequently be used for an extended turbofan design study, where for instance, the optimum diameter is sought, as done by Guha[26].

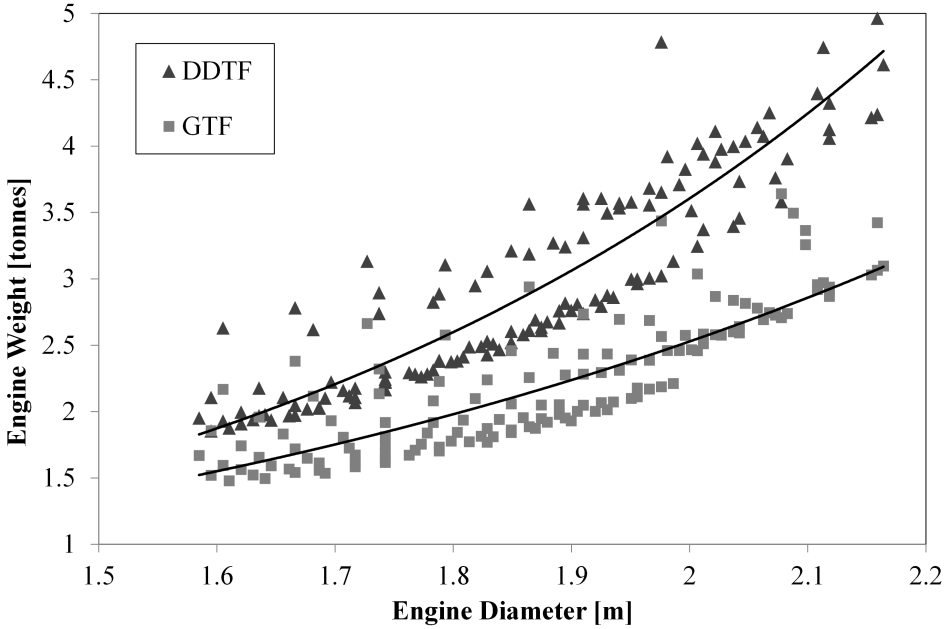

Figure 2.14: The effect of diameter on engine weight for a direct drive and geared configuration. Results produced with WATE. Gear ratio = 3

To better illustrate this approach, figure 2.14 regroups the results of figure 2.9 in order to generate a simple correlation between diameter and weight. In case a comparison with a GTF configuration is required, a different set of data has to be build, using the component based weight code, simply by adding a gearbox between the fan and the low-pressure turbine. Figure 2.14 shows these results for a gear ratio of 3, while all the other assumptions are kept fixed to the baseline values of table 2.9. Figure 2.14 reveals the importance of rebuilding the regression model when the engine configuration is modified, as the effect of diameter on weight also changes.

The proposed hybrid approach creates synergies and offers the following advantages compared to the two isolated approaches:

- It is faster and requires less effort than the component based methods. It is thus more suitable to extensive top-level thermodynamic design studies. The regression model needs only to be built once for each engine architecture.

- There is no need for real engine data. If a reliable component based method

is available, this can be used to generate the data needed for the regression model.

- Compared to real engine data, the data generated by the component based method, are coherent as they are based on the same assumptions and they concern the same engine architecture. There is no uncertainty relative to the flight condition associated with the values of the thermodynamic parameters, and no incoherencies due to different manufacturer practices or technology levels.

The aforementioned hybrid approach although seemingly obvious, has never been used in the past and promises a simple novel solution to the demand for a fast and reliable weight estimation method, independent of the availability of real weight data.

Chapter 3

New "component based" approach methodology

3.1 Introduction

In the previous chapter a variety of preliminary weight estimation methods was presented. However, the "whole engine based" methods lack accuracy, don't offer flexibility and don't fully capture the influence of parameters that are linked to engine weight. Furthermore, since most of them are based on existing engine data, they are unsuitable for studying novel engine configurations. On the other hand, the only detailed and robust "component based" method is the NASA WATE software, but the latest version is not available due to confidentiality restrictions. Furthermore, the method core is more than 30 years old and since then there have been no accompanying publications or documents to highlight any potential changes or improvements.

For the above reasons, following the WATE principles, a component based method including recent design methods was developed focusing on its robustness, accuracy, flexibility and expandability, that will enable the study of novel engine designs. Care was also taken to reduce the required inputs and minimise the necessary assumptions, in order to generalise the method for a wider group of engines.

The present chapter contains a presentation of the fundamental parameters and equations that are used in the "component based" method, followed by the component preliminary design and weight estimation models.

3.2 Fundamentals

In the present section several basic equations and calculation procedures applicable to multiple component design procedures are analysed. Furthermore, the flowpath designation used in the compressor and turbine components is presented.

3.2.1 Compressor and turbine flowpath designation

Prior to the analysis of the component design and weight estimation, the engine flowpath designation has to be defined. The main focus will be on compressors and turbines, which are described in a similar way according to Figures 3.1 and 3.2, but the analysis can be easily adapted to any component within the flowpath.

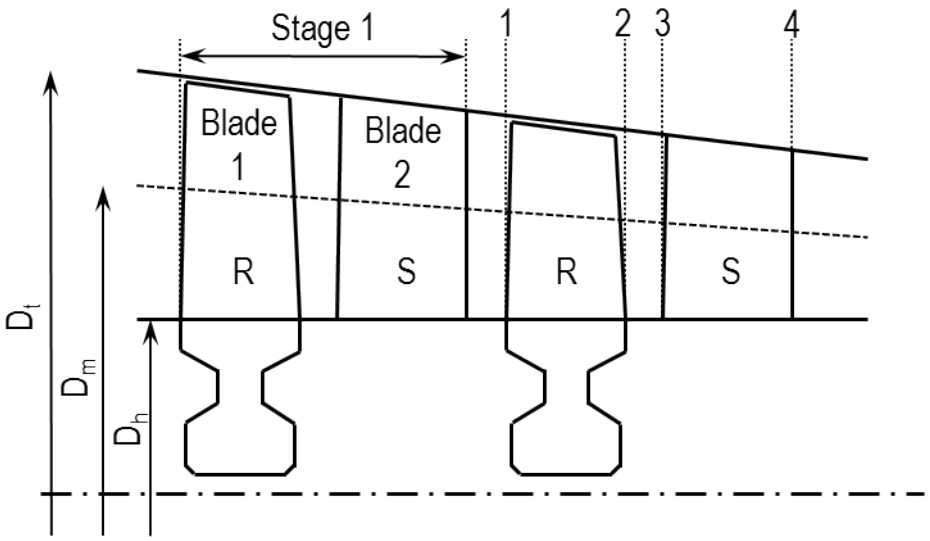

Figure 3.1: Compressor flowpath designation

Each of these components consists of several stages, with each one consisting, in turn, of a stator (S) and a rotor (R). In a compressor, blade 1 within a stage refers to the rotor blade (R), while blade 2 to the stator blade (S) (Fig. 3.1),

following the common design practice dictating that each rotor is followed by a stator. On the other hand, in a turbine the numbers are reversed with blade 1 assigned to the stator or Nozzle Guide Vane (NGV) and blade 2 to the rotor, according to the classical definition of a turbine stage (Fig. 3.2).

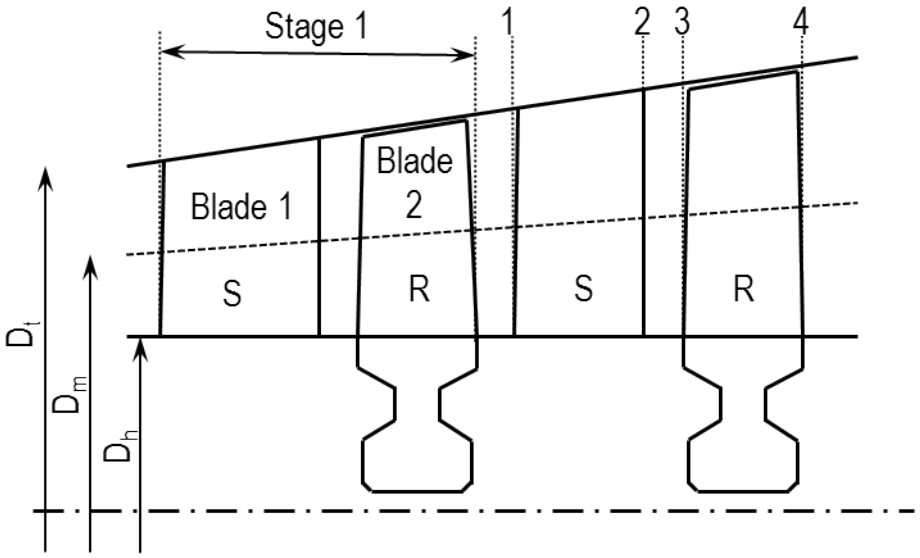

Figure 3.2: Turbine flowpath designation

In a similar manner, this time common for both components, each blade is assigned two stations, one at the blade inlet and one at the outlet, where all the flow parameters are calculated. For simplicity reasons, however, station numbering refers to the whole stage with the stage inlet and outlet being number 1 and 4 respectively, while the first blade outlet and the second blade inlet are assigned station numbers 2 and 3.

3.2.2 Velocity triangles

The velocity triangles of a compressor/fan (Fig. 3.3) or a turbine (Fig. 3.4) stage are a commonly used representation of the velocity vectors and their connection at each station. In the present analysis all the angles will be expressed relative to the axial direction and will be considered positive.

For both compressors and turbines, the fluid enters the stage at station 1 having an absolute velocity vector $\mathbf{C_{abs,1}}$ and it accelerates at station 2 to an

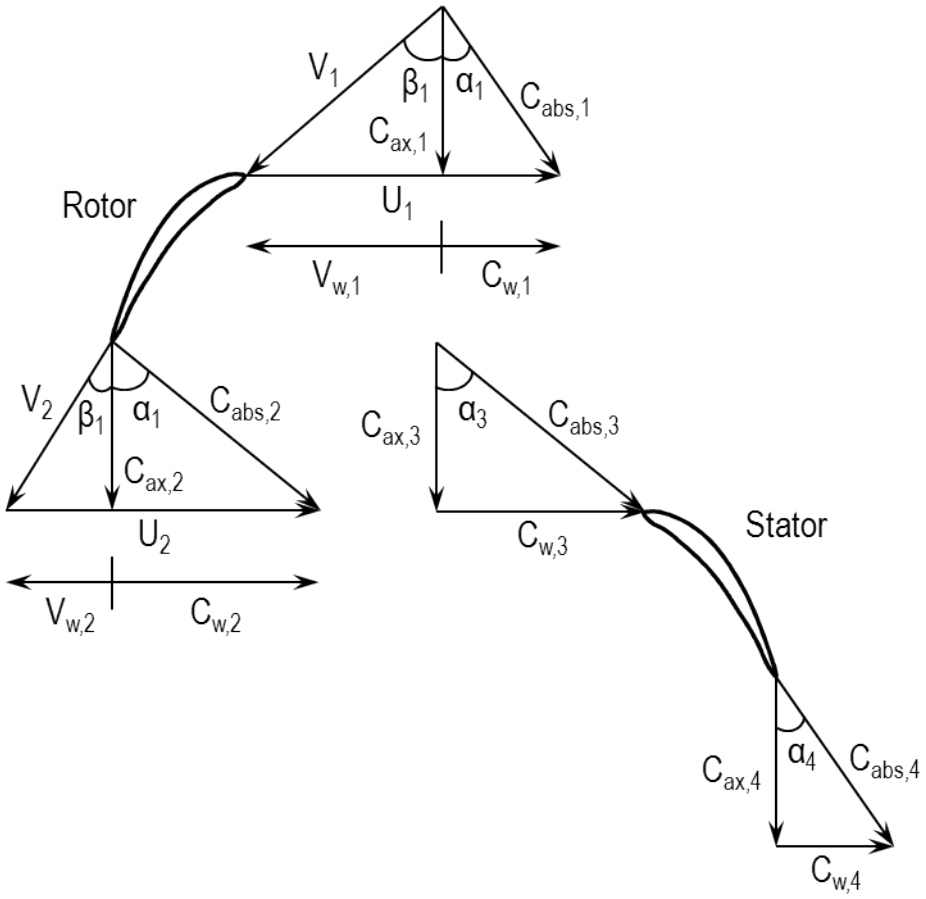

Figure 3.3: Compressor velocity triangles

absolute velocity vector $\mathbf{C_{abs,2}}$. For simplicity reasons, it is a common practice to assume that the velocity vector remains constant between stations 2 and 3[56], even though the change in annulus area (Fig. 3.1, 3.2) suggests that it should be different. Finally, the fluid is decelerated at station 4 ($\mathbf{C_{abs,4}}$), ideally to an absolute velocity vector with equal magnitude and direction to the ones at the inlet, achieving thus repeating stages.

The above velocities can be expressed in a scalar form if the axial direction is used as reference and an angle α is assumed. This way, the axial velocity (C_{ax}) and its connection to the absolute are also defined (Eq. 3.1).

$$\cos\alpha = \frac{C_{ax}}{C_{abs}} \tag{3.1}$$

The axial velocity vector ($\mathbf{C_{ax}}$) can also be linked to the absolute velocity

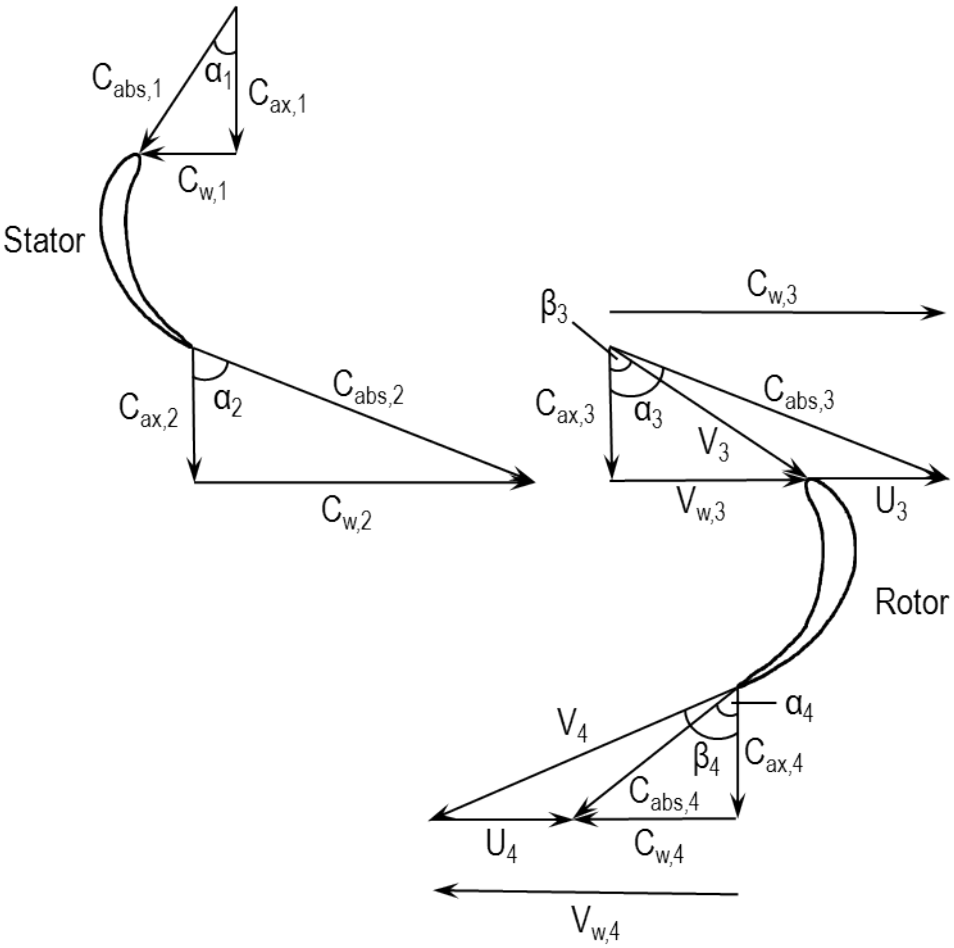

Figure 3.4: Turbine velocity triangles

vector ($\mathbf{C_{abs}}$) through the absolute swirl velocity vector ($\mathbf{C_w}$) as described by equation 3.2.

$$\mathbf{C_{abs}} = \mathbf{C_{ax}} + \mathbf{C_w} \tag{3.2}$$

In velocity triangles, the difference between compressors and turbines lies in the position of rotating blades, which are located between stations 1 and 2 for compressors and 3 and 4 for turbines. At the inlet and outlet of the rotating blades, apart from the absolute velocity vectors ($\mathbf{C_{abs}}$), relative to the blade motion velocity vectors ($\mathbf{V}$) are also defined, by subtracting the rotational velocity vector ($\mathbf{U}$) from the absolute one.

Similar to the absolute parameters, the relative velocity angle (β) and the relative swirl velocity vector (V_w) are described by equations 3.5 and 3.4 respectively.

$$\mathbf{C_{abs}} = \mathbf{V} + \mathbf{U} \tag{3.3}$$

$$\mathbf{V_{abs}} = \mathbf{C_{ax}} + \mathbf{V_w} \tag{3.4}$$

$$\cos\beta = \frac{C_{ax}}{V} \tag{3.5}$$

Further details on velocity triangles theory can be obtained from several turbomachinery handbooks[57].

3.2.3 Gas properties

Since the present work refers to aero engines, the working fluid is assumed to be dry air, while kerosene is selected as the engine fuel.

These two assumptions are essential to define the gas constant value (R_{air}), which is a sole function of Fuel to Air Ratio (FAR)[58] for a given fuel and working fluid. Moreover, the specific heat under constant pressure (c_p) and specific heat ratio (γ) can be calculated for kerosene combustion products in dry air as functions of the static temperature (t_{st}) and FAR[58]. For simplicity reasons, instead of static temperature, total temperature (T_{tot}) values are used within these estimations without significant error.

3.2.4 Component station calculation

In order to fully determine the annulus area, dimensions and velocities at a flowpath station different procedures are applicable, depending on the available inputs. In the following analysis it is assumed that the absolute Mach number

(Ma_{abs}) is an input, along with the total temperature (T_{tot}) and pressure (P_{tot}), mass flow ($\dot{m}$), FAR and absolute velocity angle (α). However, instead of absolute Mach number, either axial Mach number (Ma_{ax}), absolute velocity (C_{abs}) or axial velocity (C_{ax}) can be used as inputs.

If the absolute velocity is supplied, it can be converted to absolute Mach number by using equation 3.6. The static temperature that is required, can be calculated through equation 3.7 as a function of absolute velocity and total temperature. These are rudimentary equations in the gas turbine analysis and their origin can be found in many engineering handbooks[59].

$$Ma_{abs} = \frac{C_{abs}}{\sqrt{\gamma \cdot R_{air} \cdot t_{st}}} \tag{3.6}$$

$$\frac{T_{tot}}{t_{st}} = 1 + \frac{C_{abs}^2}{2 \cdot c_p \cdot t_{st}} \tag{3.7}$$

On the other hand, if the axial properties are known, they can be converted to absolute parameters by using the absolute velocity angle that is in any case a required input (Eq. 3.1 and 3.8).

$$\cos\alpha = \frac{Ma_{ax}}{Ma_{abs}} \tag{3.8}$$

The annulus axial flow area (A) at the station can be calculated by using the equation of continuity[57] (Eq. 3.9). The required density (ρ) is provided by means of the gas law equation (Eq. 3.10), which in turn requires the static temperature and pressure values, calculated with the help of equations 3.11 and 3.12.

$$\dot{m} = \rho \cdot C_{ax} \cdot A \tag{3.9}$$

$$\rho = \frac{p_{st}}{R_{air} \cdot t_{st}} \tag{3.10}$$

$$\frac{T_{tot}}{t_{st}} = 1 + \frac{\gamma - 1}{2} \cdot Ma_{abs}^2 \tag{3.11}$$

$$\frac{P_{tot}}{p_{st}} = \left(1 + \frac{\gamma - 1}{2} \cdot Ma_{abs}^2\right)^{\frac{\gamma}{\gamma - 1}} \tag{3.12}$$

When compressor stations are estimated, an empirical blockage factor (K_B) is introduced in equation 3.9, forming equation 3.13 to simulate the boundary layer effects at the walls, that effectively reduce the annulus flow area[56]. This factor is a function of the stage number and its values are given in table 3.1.

$$\dot{m} = \rho \cdot C_{ax} \cdot A \cdot K_B \tag{3.13}$$

Table 3.1: Compressor Blockage Factor

Stage	1	2	3	4	5 and above
Blockage Factor	0.99	0.95	0.92	0.90	0.88

The estimated annulus flow area is in turn used to calculate the dimensions of the examined station. However, in this case an extra input is required. Any one of the hub diameter (D_h), tip diameter (D_t), mean diameter (D_m) or hub to tip diameter ratio ($^{D_h}/_{D_t}$) has to be known so that the others can be determined through equation 3.14.

$$A = \frac{\pi}{4} \cdot (D_t^2 - D_h^2) \tag{3.14}$$

In the present analysis, the hub to tip diameter ratio ($^{D_h}/_{D_t}$) is selected as input, resulting, after manipulating 3.14, to the calculation of the tip diameter (D_t) by using equation 3.15.

$$D_t = \sqrt{\frac{\frac{4 \cdot A}{\pi}}{1 - \left(\frac{Dh}{Dt}\right)^2}} \tag{3.15}$$

The remaining dimensions can be easily produced by using the already known hub to tip diameter ratio ($^{D_h}/_{D_t}$). The process is identical if another input dimension is selected.

The calculation of the station parameters can be performed if different inputs are supplied. For instance the velocities can be determined if the annulus area is known by using the same set of equations.

3.2.5 Stage reaction

Stage reaction (R) is a parameter that describes the work load split in a compressor and a turbine stage. In a compressor it is defined as the static pressure rise in the rotor blade divided by the static pressure rise in the whole stage[57] (Eq. 3.16). Accordingly, in a turbine, stage reaction is the fraction of the static pressure drop at the rotor divided by the stage static pressure drop (Eq. 3.17).

$$R = \frac{p_{st,2} - p_{st,1}}{p_{st,4} - p_{st,1}} \tag{3.16}$$

$$R = \frac{p_{st,3} - p_{st,4}}{p_{st,1} - p_{st,4}} \tag{3.17}$$

Stage reaction is usually selected at 0.5 for optimal efficiency, but design and material limits can impose values up to 0.3[58].

3.2.6 Continuity equation

One of fundamental turbomachinery equations applicable to compressors and turbines is the continuity equation, which ensures the mass preservation in each stage and therefore in each component. For a stage without cooling or bleed flows the continuity equation states that the fluid mass flow is constant (Eq. 3.18).

$$\dot{m}_1 = \dot{m}_2 = \dot{m}_3 = \dot{m}_4 \tag{3.18}$$

Making use of equation 3.9 the continuity equation is expressed in the following form (Eq. 3.19).

$$\rho_1 \cdot C_{ax,1} \cdot A_1 = \rho_2 \cdot C_{ax,2} \cdot A_2 = \rho_3 \cdot C_{ax,3} \cdot A_3 = \rho_4 \cdot C_{ax,4} \cdot A_4 \tag{3.19}$$

3.2.7 Momentum equation

Newton's second law states that the rate of change in momentum of a system equals the sum of external forces that act on this system[60]. Considering also that momentum is mass multiplied by velocity, the momentum equation at the axial direction for steady flow is given by 3.20[57].

$$\sum F_x = \dot{m} \cdot \frac{d}{dt} C_{ax} \tag{3.20}$$

However, this equation is more useful for turbomachinery applications when moments instead of forces are considered, resulting in the momentum of momentum equation. For the axial direction, this states that the sum of the external moments [the torque (To) at the axis] is equal to the rate of change of angular momentum[57] (Eq. 3.21).

$$\sum To_x = \dot{m} \cdot \frac{d}{dt} (r \cdot C_w) \tag{3.21}$$

Respecting the velocity directions set in section 3.2.2 and considering the blade speed (Eq. 3.22) and work (Eq. 3.23) equations, the momentum of momentum equation can be used to produce the Euler compressor (Eq. 3.24) and turbine (Eq. 3.25) equations[57].

$$U = \omega \cdot r \tag{3.22}$$

$$\dot{W} = To \cdot \omega \tag{3.23}$$

$$\dot{W} = \dot{m} \cdot (U_2 \cdot C_{w,2} - U_1 \cdot C_{w,1}) \tag{3.24}$$

$$\dot{W} = \dot{m} \cdot (U_3 \cdot C_{w,3} + U_4 \cdot C_{w,4}) \tag{3.25}$$

A more detailed analysis on momentum and Euler turbomachinery equations can be found in several books[60;57].

3.2.8 Stage loading and flow coefficients

The stage loading coefficient (ψ) is defined as enthalpy change per unit of mass flow divided by the square of blade speed and is given by equation 3.26, considering also that enthalpy change can be expressed as a function of temperature difference. Stage loading is a measure of the work that a stage is able to deliver, but is also an indirect indicator of the component technology level[58].

Higher values are linked usually with more losses and decreased stage efficiency, but at the same time lower values increase the number of stages for the requested work, resulting in a trade-off to determine the optimal value.

$$\psi = \frac{c_p \cdot \Delta T}{U^2} \tag{3.26}$$

The flow coefficient (ϕ) is defined as the ratio of axial velocity divided by the blade speed (Eq. 3.27) and is linked to the stage mass flow. It is also related to the component size, since it affects its frontal area. As with the stage loading, it is also connected with stage efficiency, but further details will be provided at a following section (3.2.9).

$$\phi = \frac{C_{ax}}{U} \tag{3.27}$$

The combination of the momentum equation for turbines (Eq. 3.25) and the

stage reaction definition equation (Eq. 3.17) yields an equation that connects the stage loading coefficient with the flow coefficient (Eq. 3.28). To reach that correlation it is assumed that axial velocity is constant at all turbine stage stations, absolute velocity is constant at the inlet and outlet of the stage and blade speed has small variation between the inlet and outlet of the rotating blade.

$$\psi = 2 \cdot (1 - R + \phi \cdot \tan \alpha_4) \tag{3.28}$$

More details about the stage loading and flow coefficients can be found in several gas turbine books[58].

3.2.9 Stage efficiency

The isentropic efficiency (η_{ise}) in a compressor or turbine is defined as the ratio of the actual and isentropic work involved in the process[57]. However, isentropic efficiency can be misleading when components of different pressure ratios are compared.

To overcome this obstacle a common pressure ratio (PR) basis is established by assuming that the component consists of several equal efficiency small stages with the component isentropic efficiency being a function of the total pressure ratio, or in other words of the amount of small stages required. The small stage efficiency is called polytropic efficiency (η_{poly}) (Eq. 3.29) and is a measure of the technology level, considering that advanced technologies reduce losses and therefore fewer stages are required to achieve a given pressure ratio. Polytropic efficiency is linked to isentropic efficiency through equation 3.30 for compressors and equation 3.31 for turbines.

$$PR = (TR)^{\frac{\eta_{poly}}{\eta_{poly}-1}} \tag{3.29}$$

$$\eta_{ise} = \frac{PR^{\frac{\gamma-1}{\gamma}} - 1}{PR^{\frac{\gamma-1}{\gamma \cdot \eta_{poly}}} - 1}, \text{ for compressors} \tag{3.30}$$

$$\eta_{ise} = \frac{1 - PR^{\frac{\eta_{poly} \cdot (1-\gamma)}{\gamma}}}{1 - PR^{\frac{1-\gamma}{\gamma}}}, \text{ for turbines} \tag{3.31}$$

Further details on efficiencies can be acquired from the work of Dixon[57].

3.2.9.1 Smith chart

In order to define turbine stage isentropic efficiency, a plot of efficiency contours with the stage loading and flow coefficients as parameters, was developed by Smith in 1965[61], based on existing turbine designs (Fig. 3.5). Care should be taken that this tool, even though is widely used, is only valid if certain restrictions are respected. More specifically, it refers to the highest technology blading with 50% reaction, without taking into account any cooling related isentropic efficiency losses.

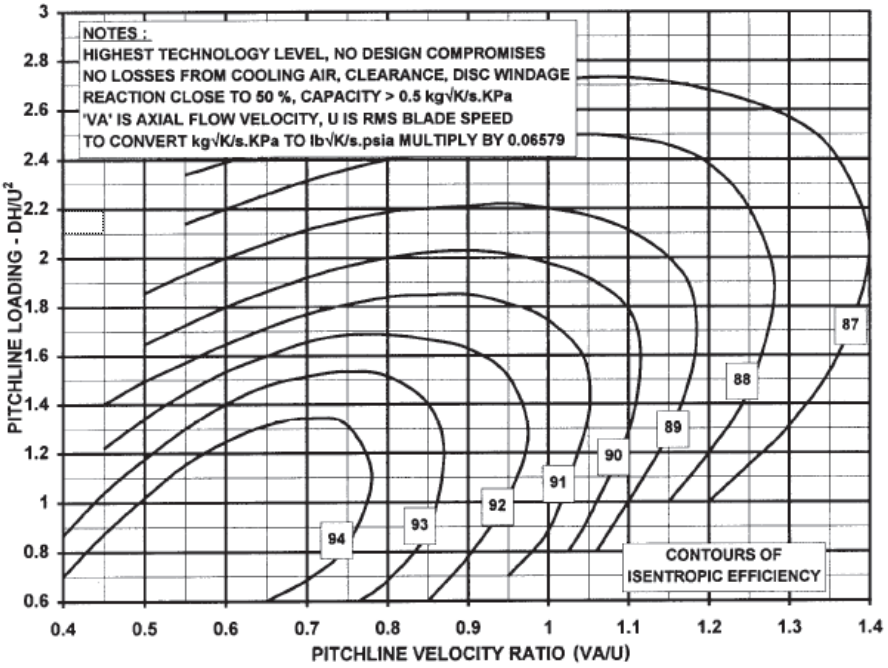

Figure 3.5: Smith chart[58]

In practice, for use in the preliminary design, all the major OEMs have developed their own Smith charts based on in-house data. Since they are not publicly available due to confidentiality restrictions, a Smith chart from a recent publication will be used[58].

3.2.10 Three dimensional flow

In the previous sections, the estimation of velocities is done at the mean line, assuming that the blade is relatively short and that the flow is two dimensional. However, this is just a simplification, since the compressor front and turbine rear stages can have long blades and the flow is affected by three dimensional effects.

A common practice that is adopted by most mean line design methods is to estimate the velocities and all the dependent parameters at the two blade span extremes, the hub and tip. Two of the assumptions used to estimate the three dimensional flow are the free vortex flow (Eq. 3.32) and the constant angle design (Eq. 3.33).

$$C_{ax} \cdot D = const \tag{3.32}$$

$$C_{ax} \cdot D^{sin^2\alpha_2} = const \tag{3.33}$$

In the following component design method the free vortex method is used to estimate the parameters at the hub and tip of blades. However, due to increased complexity, these results don't influence the design outcome, but are provided only for verification purposes.

3.2.11 Materials

Defining the materials of all the engine components is a necessary step to acquire the component density and therefore calculate the component mass. Furthermore, physical properties and stress limits are used, mainly in stress and strength related calculations.

The materials are selected primarily having in mind weight and temperature restrictions, but also by considering manufacturing, cost, life and stress restrictions. The most commonly used materials in aero engines are nickel and ceramic alloys in the "hot" section of the engine, because they can withstand the high temperatures[56] developed. On the other hand titanium that has low density is

used in the "cold" sections of the engine aiming for weight reduction. In some cases, further weight reduction is achieved through composite and titanium aluminide materials, where temperature and stress restrictions allow their use. Steel alloys are often used in shafts, casings and support structures in aero engines, due to their cost and machinability. The above are mere suggestions, because OEMs constantly develop and introduce new and improved materials.

In the present method, the materials can be manually selected for each part in each component. However, there is an option to automatically select the material based on temperature from a user supplied list with corresponding temperature ranges. This is sufficient for this project, but it is recommended that primarily stress and cost parameters are included in the material selection process.

3.2.12 Blade weight

The estimation of blade weight is performed by using the fundamental physics equation stating that blade mass is the product of its volume and density (Eq. 3.34).

$$m = Vol \cdot \rho \tag{3.34}$$

3.2.12.1 Blade density

The blade density (ρ) is readily available as soon as the blade material (3.2.11) is selected, a process that for aero engines is influenced more by temperature and weight and less by stress requirements. Furthermore, in the present method, blade density is adjusted to account for hollow blades or cooling passages, by introducing a blade solidity factor (sol). In the present weight estimation process, this is only an option for fan moving and stationary blades, that have a greater effect on engine weight, due to their big size.

3.2.12.2 Blade volume

On the other hand, blade volume is calculated as a product of blade profile area (A_{bl}) and height (h_{bl}), with the latter being a function of the blade station dimensions (Eq. 3.35).

$$h_{bl} = \frac{D_{t,in} - D_{h,in} + D_{t,out} - D_{h,out}}{4} \tag{3.35}$$

In order to estimate the blade profile area, a profile type is selected and the profile geometry is generated as function of the blade chord (c_{bl}), known during the blade weight estimation. It should be noted that the chord used is the axial chord of the blade, with camber and twist not applied, since their calculation introduces complexity without significant benefits in blade weight accuracy.

Another shape parameter that is not taken into account during blade weight estimation is the taper ratio of the blade (TRa). That refers to the fraction of the profile axial chord at the blade tip divided by the one at the blade hub (Eq. 3.36). In most blade designs the meanline chord is equal to the mean value of the tip and hub chords and therefore the omission of taper ratio doesn't influence blade weight. However, taper ratio should be taken into account when the engine layout is considered, since it mainly influences the axial clearance between the blades. Moreover, blade stress calculations are also affected, but are not a part of the present process.

$$TRa = \frac{c_{ax,t}}{c_{ax,h}} \tag{3.36}$$

3.2.12.3 Blade count

The procedure described so far provides only the weight of only a single blade, but each component blade row, as known, consists of multiple blades. Therefore the total weight in a single row ($m_{bl,row}$) is estimated through equation 3.37, that multiplies the single blade mass (m_{bl}) with the total number of blades (Nr_{bl}).

$$m_{bl,row} = m_{bl} \cdot Nr_{bl} \tag{3.37}$$

The number of blades is not readily available for each blade row, but can be estimated if the non-dimensional parameter space to chord ratio (s/c) is available (Fig. 3.6), as stated in equation 3.38.

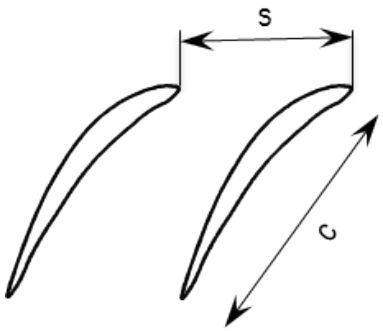

Figure 3.6: Space to chord ratio

$$Nr_{bl} = \frac{\pi \cdot D_m}{{}^{s}/_{c} \cdot c} \tag{3.38}$$

Realistic values for space to chord ratio can be selected for moving and stationary blades by following recommendations in the literature[58]. Nevertheless, there are also available methodologies and correlations for compressors and turbines that estimate space to chord ratio.

Regarding compressors, in the present analysis, the diffusion factor[56] (Eq. 3.39) criterion is used, describing the relation between the blade velocities and space to chord ratio. The former are calculated during the design process, enabling the estimation of the latter by setting limiting diffusion factor values that are available in the literature[58]. These are 0.6 for the hub of the blade and 0.4 for the tip.

$$DF = 1 - \frac{V_1}{V_2} + \frac{\Delta C_w}{V_1} \cdot \frac{s}{c} \tag{3.39}$$

Similarly, correlations that link space to chord with the fluid angle at the stations of a turbine have been developed. The most commonly used are the Zweifel[63] and the Ainley-Mathieson[62] methods. In the following method the optimum space to chord ratio values for a turbine are estimated by using a graphical

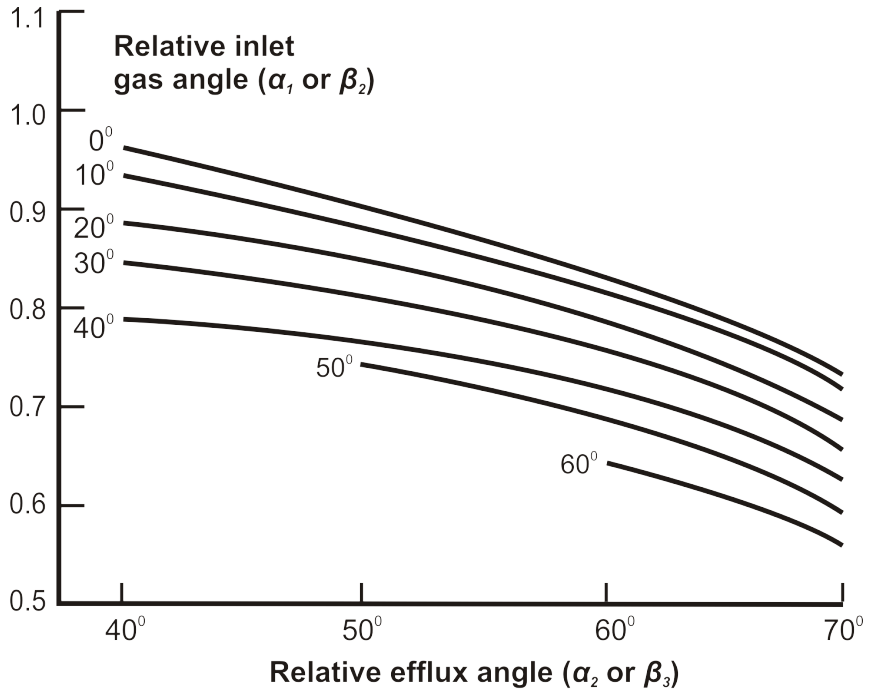

Figure 3.7: Turbine optimum space to chord ratio by Ainley and Mathieson[62]

representation of the Ainley-Mathieson method[56].

3.2.12.4 Inlet Guide Vanes (IGVs) and Outlet Guide Vanes (OGVs)

The flow at a compressor inlet, as expected, is heavily influenced by the upstream components. Therefore, in order to achieve the desirable velocity profile at the first rotating blade inlet, almost all of the modern compressor designs make use of an IGVs blade row upstream of the first rotor row. Furthermore, since the aero engines have to cover a wide variety of operating conditions, avoiding stall and surge phenomena in the compressors, IGVs are usually designed with the ability to change their angle and are then named Variable Inlet Guide Vanes (VIGVs). However, in most cases VIGVs are not sufficient, resulting in variable geometry vanes (Variable Guide Vanes (VGVs)) at several of the following stages. For simplicity reasons, in the following methodology the weight increase associated with variable geometry vanes is not estimated.

Similarly, in a turbine, the flow characteristics at the component exit are not ideal for the downstream component inlet or the engine outlet, resolved with the

introduction of a blade row that "corrects" the flow at the turbine outlet. This row is similar to an IGV, but due to its function and position, it is named Outlet Guide Vane (OGV) and downstream of an LPT, it is usually integrated into the rear frame providing also structural support.

Finally, in the fan, a vane row in the bypass duct, downstream of the fan stator with similar function to OGVs, is used, widely known as struts[58]. The struts provide flow correction to minimise losses in the bypass duct and structural support for the whole engine, as well as passage for service ducts.

For simplicity reasons, if an IGV, OGV or strut row is selected in one of the components, the outlet and inlet parameters at this blade row are assumed to be equal to the neighbouring blade station parameters. This interpretation doesn't impose a significant error on the final weight estimation, but if a more realistic approach is required, a different assumption can be used. The blade weight and the number of blades per row are calculated in a similar fashion as in the regular blade rows.

3.3 Design philosophy

As was mentioned above, the preliminary weight estimation of turbofan engines method, presented in the present chapter, uses design methods to estimate the size and shape of the various components.

In the following sections, the methodology that was used in order to determine the design of each component is analysed. Furthermore, the weight estimation process of each component based on the resulting design is presented.

3.3.1 Compressor

The philosophy followed in the present method assumes that compressor weight consists of several parts, as shown in figure 3.8. Only the annulus design and blade weight are analysed in detail in this section, with the remaining parts presented in following sections, since the process for estimating their weight is common for several components.

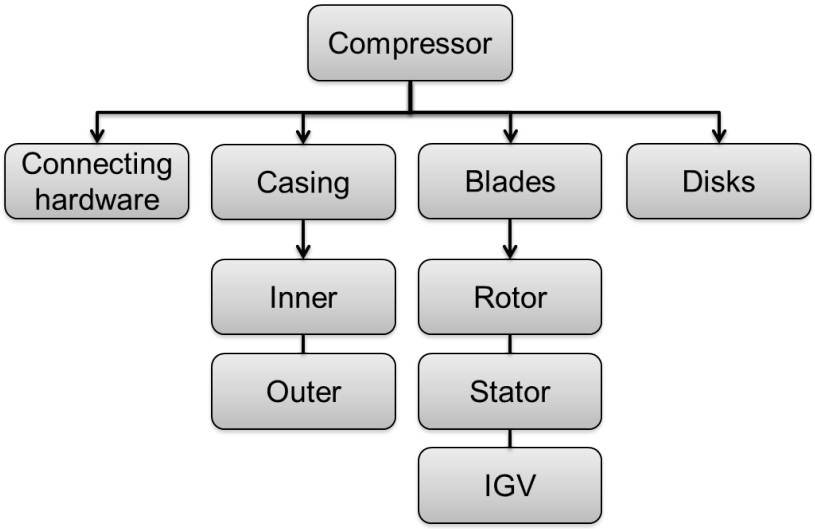

Figure 3.8: Compressor weight parts

3.3.1.1 Annulus design

In order to estimate the weight of the compressor blades, it is necessary to determine first their shape and dimensions, along with the shape and dimensions of the compressor annulus. The general principles behind the design method that was used to determine them can be found in several gas turbine handbooks[56;57;64;65]. However, several modifications and improvements have been implemented in the initial methodologies and will be analysed in detail in the following paragraphs.

Several input parameters are required to uniquely define the annulus shape of a compressor, with several of them deriving from the component characteristics and requirements, but also with others chosen based on experience or engineering judgement. In the present analysis, typical values are given for most of the parameters, but it should be noted that they are mere suggestions valid only for common engine cases. The input parameters can be categorised in four major groups and are analysed in the next points.

Input parameters

I **Cycle parameters**

Several parameters that are estimated during the engine cycle simulation are used as inputs to the compressor preliminary design methodology. These

include mass flow ($\dot{m}$) at the component inlet, and total pressure (P_{tot}) and total temperature (T_{tot}) at the inlet and outlet of the component. These essentially describe the component work requirement and are crucial when defining the component design. Furthermore, FAR at the component inlet and the non dimensional rotational speed (PCN) are also values that are provided from the cycle simulation analysis, with the latter reflecting the design point of the component, through the change in rotational speed compared to the nominal shaft speed.

Taking into account that almost in all aero gas turbine engines the compressors are located before the combustion chamber, the FAR can be assumed to be zero. On the other hand, regarding the non dimensional rotational speed, even though there are no typical values, the Top of Climb (TOC) is usually selected as the design point. Nowadays, a common practice for the acquisition of the cycle parameters is the use of a performance simulation code.

II **Velocities**

A velocity vector at the compressor inlet is also required as input, contributing mainly towards the calculation of the necessary annulus area of the component at different stations. More specifically, one out of absolute Mach number (Ma_{abs}), axial Mach number (Ma_{ax}), absolute velocity (C_{abs}) or axial velocity (C_{ax}) at the component inlet is required. To fully define the velocity vector, the absolute velocity angle (α) at the component inlet is also necessary.

These parameters are usually selected based on previous experience from similar cases. Based on suggestions from the literature[58], typical values for the absolute Mach number at the component inlet (Ma_{abs}) lie between 0.4 and 0.6. However, when the component is integrated into the whole engine design, care should be taken that there is continuity between the upstream exit velocity vector and the compressor inlet velocity vector, in order to avoid the use of extra parts that introduce additional losses. Furthermore, in most

cases the compressor shaft rotational speed is fixed by imposing aerodynamic and stress limits on the compressor itself or on another component connected to the same shaft. Therefore, the inlet velocity has to be carefully selected to provide reasonable flow coefficient (ϕ) and acceptable component dimensions.

III **Annulus Dimensions**

To fully define the dimensions of the compressor annulus, as mentioned in Section 3.2.4, a dimension input is also required at each station. Therefore, one out of hub diameter (D_h), tip diameter (D_t), mean diameter (D_m) or hub to tip ratio ($^{D_h}/_{Dt}$) at the inlet of the component has to be provided. Similarly, at the outlet of the component one of these dimensions is also required, but alternatively, they can be also expressed as a ratio of any of the inlet dimensions. Furthermore, through the given outlet dimension any rising or falling line configuration can be achieved.

To avoid having a dimension input at each station, the necessary dimensions within the components are defined by use of a cubic spline interpolation[66], selected also in order to provide a smooth annulus curve. However, apart from inlet and outlet dimensions, the spline estimation, requires two further inputs. The annulus slope angles (a_{sl}) at the inlet and outlet of the component have to be provided, but if the component is not connected to others, these can be set equal to zero.

The annulus dimension inputs are defined usually having in mind the whole engine layout, but there are some typical values available in the literature that can be used in all cases. Regarding hub to tip diameter ratio ($^{D_h}/_{Dt}$), a value greater than 0.65 is proposed[58].

IV **Blade Dimensions**

The last input category includes variables that refer to blade dimensions. The aspect ratio (AR) of the first rotor blade is required to determine the blade chords (c), which in turn shape the component through the spline interpolation. The aspect ratios of the first stator and/or the aspect ratios of the last rotor and stator are not necessary inputs, but contribute towards

the increase of the calculation accuracy. Common design aspect ratio values for compressors range between 1.5 to 3.5[58].

The axial distance between the blades, even though it is not a blade dimension, is included in this group because it is defined as a percentage of the upstream blade axial chord. The size of the gap is selected having in mind the axial movement of the blades and their possible vibrational interaction. Usually it is selected as 20% of the upstream blade chord[58].

Apart from the required inputs, several design limits can also be set for the calculation of the compressor annulus. However, values are available for all of them based on suggestions from the literature[58]. The most important ones are mentioned in the following list.

Design limits

i **Rotational speed limits**

The rotational speed (N) in a compressor is limited based on two mechanisms. The first one suggests that the relative Mach number at the tip of the first rotor blade ($Ma_{rel,t}$) has to be limited to restrain the aerodynamic losses. On the contrary, the second one refers to the blade speed limits that are applied for mechanical integrity purposes. For the latter, one out of hub (U_h), mean (U_m) or tip (U_t) blade speed has to be provided. The proposed rotational speed limiting values for compressors specify that, when titanium is used, the hub blade speed (U_h) is limited to 350 m/s, whereas the tip blade speed (U_t) to 500 m/s. However, when nickel disks are used at the back stages of the compressor the hub blade speed is constrained to 400 m/s. Regarding the relative tip Mach number ($Ma_{rel,t}$), a value of 1.3 is suggested as the uppermost limit[58].

ii **De Haller number (DH) limit**

This is a common design limit that is applied at rotor and stator blades alike. It is defined as the ratio of the relative velocity at the blade outlet, divided by the relative velocity at the blade inlet (Eq. 3.40). However, in the stator case

the absolute velocity values are used. The purpose behind DeHaller number is to restrain the diffusion that is performed at each blade row, avoiding thus high losses. It is evident that this is an indicator of the technology level and therefore the exact values are not disclosed by the OEMs. However, during the design phase the DeHaller number limit can be set to 0.72, which is an acceptable value for current engines[56].

$$DH = \frac{V_2}{V_1} \tag{3.40}$$

The design of a compressor is a complex procedure if all the parameters are considered. However, at the preliminary design stage, only a limited amount of variables is available making this task very difficult. Moreover, the accuracy that is required during this procedure is not very high, since the general component layout is examined with great margin for amendments. Therefore, to simplify this procedure or even enable the calculation of several parameters, several assumptions, that are listed below, are adopted.

Design assumptions

a **Constant polytropic efficiency (η_{poly}) at all stages**

The compressor polytropic efficiency (η_{poly}) was assumed to be equal for all the component stages. According to literature[56;64] this is a common design assumption, representing the technology level of the component, which has to be constant. However, due to secondary effects that influence the polytropic efficiency (η_{poly}), it differs between the stages.

b **Constant absolute velocity (C_{abs}) at the inlet of the component and outlet of each stage**

This assumption is a common design practice and suggested by several authors[56;64]. It greatly simplifies the calculation process, even though in real engine designs none of the velocities is held constant, but are readjusted in the

detailed design process. Alternatively, either the axial velocity (C_{ax}) or the absolute Mach number (Ma_{abs}) could be held constant, assumptions that lead to a different design outcome.

c **Constant absolute velocity angle (α) at the inlet and outlet of each stage**

This assumption is also a common design practice[56;64] but as with assumption b, the final absolute velocity angle (α) values are redefined in the detailed design process.

d **The component annulus shape is simulated by a cubic spline**

Taking into consideration current component designs, it is evident that the annulus shape is a smooth line. Therefore, a cubic spline was selected as the most appropriate curve to simulate the annulus boundaries.

e **Constant absolute velocity angle (α) between two adjacent stages**

Even though the shape of the annulus is fixed by the spline interpolation, an extra assumption is required to achieve velocity continuity between stages. For this purpose constant absolute velocity angle (α) was assumed between the stages as the most realistic solution.

By combining these assumptions and the inputs that are provided, the method calculates the minimum number of stages (Nr_{sg}) that corresponds to a feasible design, matches the given output pressure ($P_{tot,out}$) for the compressor, and provides DeHaller number (DH) values for the stators and rotors that are higher than the defined limit. This is achieved by finding feasible values for the stage temperature rise (ΔT_{sg}) and the component polytropic efficiency (η_{poly}), as well as for the other design parameters. This process leads to the determination of the compressor annulus and blade geometries, that are used to estimate the component weight.

If the compressor rotational speed (N) is not provided, based on the limits (Compressor design limit i), the maximum allowable number of rpm is estimated prior to the component calculation.

More specifically the steps that are followed for the determination of the compressor annulus shape and dimensions are:

Design process

1. **Assume polytropic efficiency (η_{poly})**

   Assume a value for the polytropic efficiency (η_{poly}) constant for all stages according to assumption a. An iterative process is then utilised aiming to match the desired outlet pressure. A numerical solver is used in this process to achieve numerical stability, starting with low efficiency values.

2. **Assume number of stages**

   In order to reduce the engine weight and the number of parts, it is desirable to have as few stages as possible. However, if a low number of stages is assumed, the blades will be highly loaded resulting in incorrect results and numerical instabilities. Therefore, the starting value for the number of stages is defined by respecting a maximum temperature rise per stage (ΔT_{sg}) limit. The final number of stages is defined when all blade DeHaller number (DH) values are within limits.

3. **Assume temperature distribution to the stages**

   Initially the temperature rise at the compressor is equally distributed to the stages. In a later stage it will be adjusted to achieve DeHaller number (DH) within limits for rotors and stators.

4. **Component inlet and outlet calculations**

   By using the available inputs and assumptions, the velocities, annulus area and dimensions are calculated for the inlet of the component. The same process is followed for the component outlet as well, since the necessary values are either known or a function of the inlet values.

5. **Component spline interpolation**

Based on the configuration that was chosen, interpolate a cubic spline between the inlet and outlet of the component. This provides one annular dimension (D_h, D_m or D_t, according to the configuration that is chosen) at each station within every stage.

6. **Calculate the velocities, areas and dimensions for all the stage outlets**

   Applying the assumptions, the stage exit parameters are calculated for all stages. The stage outlet temperature is provided, since the temperature distribution is assumed.

7. **Spline interpolation**

   A cubic spline is again used to define all the annulus dimensions based on the component inlet and stage outlet dimensions.

8. **Stage calculation**

   All the remaining velocities, areas and dimensions are calculated for all stages and all stations. This is performed based on the assumptions that were made and some basic equations. Euler's momentum equation (Eq. 3.24) is used to define the rotor outlet (station 2) velocities and angles, while care is taken so that the continuity equation is not violated (Eq. 3.19).

9. **Stage parameters calculation**

   At this stage, there are enough data available to calculate the remaining stage parameters. These include the rotor and stator DeHaller number (DH) (Eq. 3.40), the loading (ψ) (Eq. 3.26), the flow coefficient (ϕ) (Eq. 3.27), the reaction (R) (Eq. 3.16) and the blade height (h_{bl}).

10. **Check the DeHaller numbers (DH)**

    A check is performed to verify that the calculated DeHaller numbers for the rotors and stators are above the defined limit. If most of these are far from the limit, the number of stages is increased and the calculation is repeated

from step 2 until all of them are above the limit. On the other hand, if the calculated DeHaller numbers are close to the limit, the temperature is redistributed to the stages and the calculation is resumed from step 3. This is performed by increasing the temperature rise at the stage with the highest DeHaller number, while the temperature is equally decreased at the stage with the lowest one.

11. **Check the outlet pressure**

    The outlet pressure has to be equal with the pressure that is assigned at the inputs. Since the temperature rise is fixed, this can only be achieved by modifying the compressor polytropic efficiency (n_{poly}). Therefore, the calculation is repeated by changing the assumption at step 1, until the desired outlet pressure is achieved.

12. **Blade hub and tip calculations**

    Through the analysed process, all velocity values are estimated at the mean line and therefore a calculation follows to estimate their values at the hub and tip of the blades. This is achieved by assuming a free vortex condition (Eq. 3.32), where the absolute swirl velocity varies inversely with the radius[56].

3.3.1.2 Blade weight

As was described in a previous section (3.2.12), compressor blade weight is calculated based on equation 3.34. The two parameters of the equation are already known from previous calculation procedures and assumptions.

The total blade weight per row is then calculated by using equation 3.37 and the number of blades is estimated through equation 3.38. Typical values for compressor diffusion factor are used to estimate space to chord ratio (Eq. 3.39)

3.3.2 Fan

The fan of a gas turbine is its biggest and easiest recognisable component, located, in turbofan engines, at their front end. It can be considered similar to a compressor, since in principle they perform the same function. However, by looking at a typical fan layout, as presented in figure 3.9, it is evident that the fan is significantly different from a compressor and therefore its design process is notably modified.

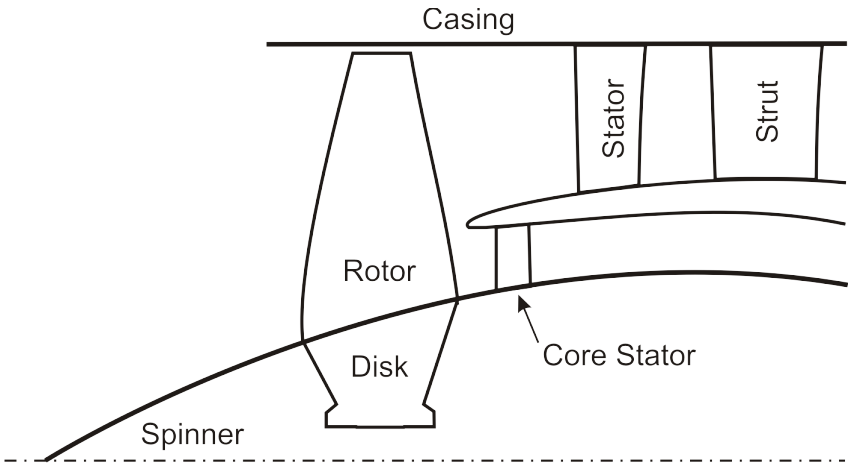

Figure 3.9: Fan layout

Unlike a typical compressor, the flow is divided into two parts downstream of the fan rotor blade, according to the BPR (Eq. 3.41), with one part diverted to the fan nozzle and the other guided into the engine core[58]. Therefore, the fan consists of one rotor and two stator blades, one for the bypass and one for the core stream. In the current study only single stage fans are considered, even though multi stage fans have been used in low BPR existing engines[30]. Furthermore, the fan outlet refers to the area downstream of the bypass duct stator and should not be confused with the area downstream of the core stator, even though they share several parameters.

$$BPR = \frac{\dot{m}_{bp}}{\dot{m}_{co}} \tag{3.41}$$

In order to simplify the weight estimation process, the fan weight is broken

down in several parts, as presented in figure 3.10. The weight estimation processes for the connecting hardware, disks and casing will be analysed in following sections, common for all components.

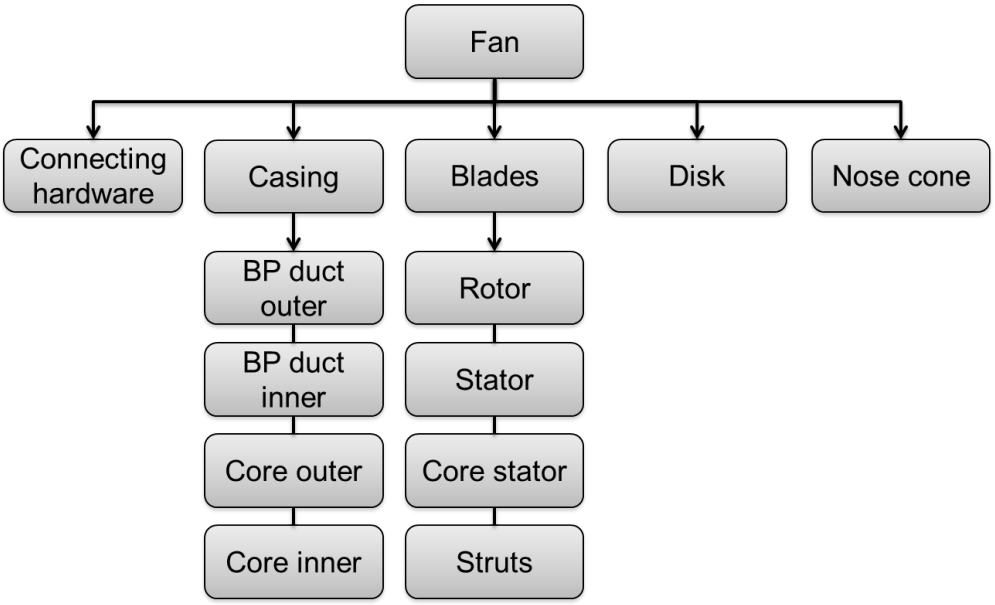

Figure 3.10: Fan weight parts

3.3.2.1 Annulus design

Despite the differences, the fan requires similar input parameters to the compressor for the annulus design, which will enable the weight estimation. These are divided into four categories and are described in the following points.

Input parameters

I **Cycle parameters**

Similar to the compressor, the total pressure (P_{tot}) and total temperature (T_{tot}) at the inlet and outlet of the fan have to be provided, along with the mass flow ($\dot{m}$) at the inlet. Furthermore, the non dimensional rotational speed (PCN) is also a necessary input for the annulus geometry estimation. However, the flow division dictates the use of an extra input variable that indicates the mass flow split between the bypass and the core, which is commonly known as BPR.

All the above cycle input parameters, as their name implies, are provided from the cycle simulation analysis. Regarding the non dimensional rotational speed (PCN), the value at the TOC is used, since this is the most common design point of a fan[67].

II **Velocities**

Identical to the compressor process, a velocity vector at the inlet of the fan and one at the outlet are required. Furthermore, one downstream of the core stator is also a necessary input. As was mentioned above, a velocity vector consists of a magnitude, given by one of the absolute Mach number (Ma_{abs}), axial Mach number (Ma_{ax}), absolute velocity (C_{abs}) or axial velocity (C_{ax}), and a direction specified by the absolute velocity angle (α).

At the inlet of the fan, the flow is usually considered axial ($\alpha = 0$), with the absolute Mach number ranging between 0.55 and 0.65. Similarly, at the outlet, the flow is ideally axial to minimise the downstream duct losses and for the same reason the absolute Mach number should be between 0.3 and 0.35[58]. In the present methodology, there is an option to estimate the outlet absolute Mach number, if it is not given, or correct it, if it is not conforming with the other inputs, but this will be further analysed in the design process. Finally, the velocity vector downstream of the core stator, if it is not supplied, is taken equal to the one at the fan outlet. Alternatively, if another component is connected downstream of the core stator, which usually is a compressor, its inlet velocity vector is used.

III **Annulus Dimensions**

In accordance to the compressor, the annulus dimension required at the fan inlet is one out of hub diameter (D_h), tip diameter (D_t), mean diameter (D_m) or hub to tip ratio ($^{D_h}/_{Dt}$). In a similar manner, one of these parameters is also a requirement at the fan outlet, which in this case can also be given as a ratio of one of the inlet dimensions. The supplied outlet dimension defines also whether the fan will have a falling or a rising line layout.

The hub to tip ratio at the fan inlet is a typical input, aiming for low values

that reduce the fan frontal area, blade size and centrifugal stresses. However, at the same time, it has to be sufficiently big to ensure enough space for the disk and restrain secondary losses. The compromise between the above requirements, results in inlet hub to tip ratio values between 0.3 and 0.4[58].

In order to simulate more accurately the existing fan designs, a parameter that defines a fan rotor outlet dimension is introduced. This is selected based on the given outlet dimension and is defined as a ratio of the rotor outlet divided by rotor inlet diameter. For simplicity reasons, it can be selected equal to 1, but slightly lower values (0.97) for the tip diameter, yield more accurate results.

IV **Blade Dimensions**

The aspect ratios (AR) of the fan rotor, the bypass stator and the core stator are necessary inputs for the determination of the annulus shape. Along with the blade axial distance, these aspect ratios contribute towards the estimation of the fan and blade axial length and position.

Typical values for the fan rotor aspect ratio range between 2 and 2.5, but they are usually a bit higher for the stators (up to 3.5). The blade axial distance is again given as a percentage of the upstream blade chord and it can be different between the rotor and the core or the bypass stator[58].

Design limits

i **Rotational speed limits**

Similarly to the compressor, two limits are also used to estimate the fan rotational speed (N), one related to aerodynamic performance and the other to mechanical integrity. The former one limits the relative Mach number at the fan rotor tip ($Ma_{rel,t}$), with typical values ranging between 1.4 and 1.6. On the other hand, the latter limit requires either the hub (U_h), tip (U_t) or mean (U_m) blade speed. Bibliography guidelines suggest that the the hub blade speed should be lower than 180 m/s, while the tip blade speed should remain below 500 m/s[58].

ii **De Haller number (DH) limit**

The De Haller number (Eq. 3.40) is a common design limit of the fan design, following the compressor practice and should be restricted to values higher than 0.72[58].

Design assumptions

a **The axial velocity (C_{ax}) remains constant at the rotor outlet and at the stator inlet and outlet**

For simplification purposes the axial velocity (C_{ax}) is assumed constant at the rotor outlet and stator inlet and outlet. This selection of this assumption was based on the fact that provides consistently results that resemble the existing engine design.

b **The absolute velocity angle (α) at the rotor outlet equals the one at the stator inlet**

To achieve continuity between the rotor outlet and stator inlet, the absolute velocity angle is kept constant between the rotor outlet and the stator inlet.

Design process

1. **Assume absolute Mach number (Ma_{abs}) at the fan stator outlet**

   The absolute Mach number (Ma_{abs}) at the fan stator outlet can be provided as input in the design calculation procedure. If it is not, or the value that is supplied doesn't produce a feasible design, it is adjusted iteratively by means of a Newton-Raphson method, until the default, or provided DeHaller number (DH) target is matched.

2. **Calculate the fan inlet parameters**

   By following the method analysed in section 3.2.4, calculate all the station parameters at the fan inlet using the inputs provided.

3. **Calculate the fan rotational speed**

   If the fan rotational speed is not already known, it is estimated by using the above mentioned limits (Limit i).

4. **Assume the hub or tip diameter at the fan rotor outlet**

   According to the fan design configuration that is selected, the hub or the tip diameter is assumed. This step is the beginning of an iteration process, that is ended when the fan rotor outlet mass flow is matched as will be shown in a later step.

5. **Calculate the rotor outlet velocities**

   Making use of the above assumption, the rotor outlet mean diameter is calculated and is used along with the fan rotational speed to estimate the blade velocity as per equation 3.22. This, along with the rotor inlet parameters, enables the calculation of the rotor outlet absolute swirl velocity by using Euler's pump equation (Eq. 3.24). Finally, through equations 3.2 and 3.1 the absolute velocity at the rotor outlet is defined.

6. **Check the mass flow at the fan rotor outlet**

   The calculated mass flow is checked against the fan mass flow at the rotor outlet. If they don't match, a new hub or tip diameter is assumed at step 4, by using a bisection method, and the calculation resumes from that point.

7. **Calculate all the station parameters at the outlet of the rotor**

   Since all the required inputs are known, the station parameters at the rotor outlet can be calculated by following the process described in section 3.2.4.

8. **Estimate the station parameters at the inlet and outlet of the core and fan duct stators**

   The process followed for the determination of the velocities and dimensions at the inlet and outlet of both the core and fan duct stators, depends on the design configuration that has been selected. If the fan hub diameter is known at each station, the fan core stator values are calculated initially and the core stator tip diameter is used to produce the fan duct stator hub diameter, allowing the estimation of the remaining parameters. The reverse process is followed if the fan tip diameter is known, with the fan duct stator calculated first, followed by the core stator.

9. **Check if the calculated DeHaller (DH) number matches the target value**

   If the calculated and target DeHaller (DH) numbers don't match, iterate by returning to step 1. This step is included in the process only if the Mach number at the stator outlet is not given.

10. **Perform the blade hub and tip calculations**

    Similarly to the compressor process, this step provides the velocity triangles at the hub and tip of all the fan blades based on the mean line velocity triangles. In order to achieve that, the free vortex theory is adopted (Eq. 3.32), assuming that the absolute swirl velocity is inversely proportional to the radial position.

3.3.2.2 Blade weight

The weight of rotating and stationary blades of the fan is estimated according to section 3.2.12. As the fan is similar to a compressor, the same approach is followed.

3.3.2.3 Nose cone

The nose cone covers the area between the fan blade hub and the centreline and its main task is to provide suitable flow conditions to the hub of the fan rotating blade. Furthermore, it should sustain bird impacts and prevent the accumulation of ice, with the former defining the thickness and the latter influencing the cone angle[68].

Due to limited data, the thickness of the nose cone is assumed to be equal to $5\,mm$, based on existing engine schematics. Following the same approach, the nose cone angle is assumed to follow the fan rotor hub angle, limited to twice the length of the fan rotor chord. The material selected is glass fibre, used in modern designs due to its low density[68].

The nose cone weight is calculated by multiplying its volume with the material density.

3.3.3 Turbine

Even though the turbine serves a different purpose in a gas turbine engine, the parts that form it are similar to the ones in a compressor. Therefore, as presented in figure 3.11, the part breakdown of the turbine weight is the same as in the compressor analysis.

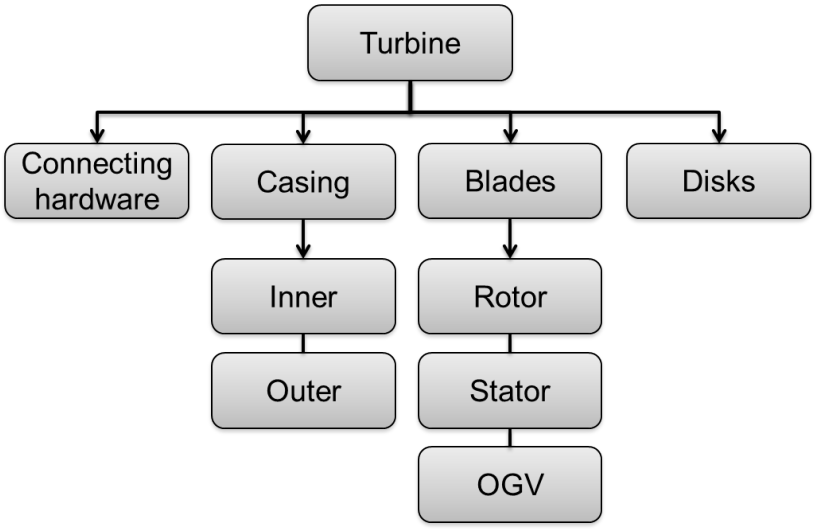

Figure 3.11: Turbine weight parts

The casing, disks and connecting hardware are presented in a later section, since their weight estimation method is adopted by several components.

3.3.3.1 Annulus design

The weight estimation of turbine blades fundamentally follows the same principles as the methodology that was presented for compressor blades. However, the turbine annulus design method is significantly different as will be presented in the following paragraphs.

The input parameters used in the turbine annulus design, categorised in four groups, are presented in the following section.

Input parameters

I **Cycle parameters**

Similar to compressors, the preliminary design of turbines also requires several parameters as inputs, which are the product of the cycle simulation analysis. More specifically, the mass flow ($\dot{m}$), total pressure (P_{tot}) and total temperature (T_{tot}) are required at the inlet of the turbine. The same parameters are also necessary at the component outlet, with the exception of mass flow, that is only required when it is added in the component due to cooling. Moreover, as in compressors, FAR and non dimensional rotational speed (PCN) are also cycle related inputs.

Unlike compressors, FAR has significant values and affects gas properties in turbines, since they are downstream of the combustion chamber. Furthermore, Take Off (TO) is selected as the design point for turbines, because they have to deliver their maximum power output at that phase.

II **Velocities**

In accordance with the compressor, a velocity vector at the turbine inlet is required. In order to fully define it, along with the absolute velocity angle (α), the axial (Ma_{ax}) or absolute (Ma_{abs}) Mach number, or the axial (C_{ax}) or absolute (C_{abs}) velocity are considered as inputs. At the outlet of the turbine, however, a different approach is followed, since there is an option to supply a similar velocity vector to define the desirable output conditions.

Empirical guidelines[58] dictate that the inlet absolute Mach number (Ma_{abs}) for HPTs should be below 0.2, but higher for LPTs. On the other hand, at the outlet of the LPT, the absolute Mach number should ideally have a value around 0.3 to avoid excessive losses at the outlet duct. Regarding the absolute velocity angle (α), it should be equal to 0 before the HPT, since it is located directly downstream of the combustor, but assumes higher values at the HPT outlet to achieve desirable reaction values. Furthermore, on grounds of minimising losses, the absolute velocity angle should be restricted below 20 deg at the LPT outlet.

III **Annulus Dimensions**

The dimension inputs that are required for the turbine preliminary design

are identical to the ones for the compressors. At the component inlet and outlet one of hub diameter (D_h), tip diameter (D_t), mean diameter (D_m) or hub to tip ratio ($^{D_h}/_{Dt}$) has to be given as an input. Alternatively, the outlet dimensions can be expressed as a ratio of the inlet dimensions, or by taking into account the whole engine perspective, the outlet tip diameter can be adjusted so that it doesn't interfere with the fan duct.

There are no indicated values for the inlet and outlet dimensions of a turbine, but they are usually defined within the whole engine arrangement context, trying to achieve the minimum component size and maximum efficiency. As a guideline, the hub to tip ratio ($^{D_h}/_{D_t}$) is advised to be between 0.5 and 0.85 to avoid undesirable losses[58].

To achieve a smooth annulus geometry and to define the dimensions of each stage, a cubic spline interpolation[66] is also used in this case. The inlet and outlet slope angles (a_{sl}) are again assumed to be zero, if there are no input values provided.

IV **Blade Dimensions**

The blade aspect ratios (AR) and axial distance are also inputs, as defined in the compressor section[58]. Typical aspect ratio values lie between 2.5 and 3.5, but for LPTs values up to 6 can be selected. Regarding the axial distance, it is chosen at 25% of the upstream blade chord.

Design limits

i **Rotational speed limits**

The rotational speed (N) of a turbine is restricted by imposing two limits that ensure that the stresses are acceptable[58]. The first criterion is a limit placed on either the hub (U_h), mean (U_m) or tip (U_t) blade speed, while the second one refers to the product of the annulus area at the middle of the rotor blade and the square of the rotational speed (AN^2). An aerodynamic limit is also used in practise, keeping the blade inlet hub relative Mach number ($Ma_{rel,1}$) below a certain value, but it is not followed in the present study. Furthermore,

the rotational speed is tweaked to achieve the maximum performance and efficiency, but these considerations are not taken into account in the initial design stages.

Based on publicly available guidelines[58], the blade hub speed should be limited to 400 m/s for HPT cases, while the corresponding value for LPTs is a bit lower (350 m/s). Furthermore, the AN^2 factor assumes values around $20E06\ rpm^2 \cdot m^2$ for low technology HPTs, ranging up to $50E06\ rpm^2 \cdot m^2$ for LPTs.

ii **Stage loading limit**

The stage loading (ψ), as mentioned in a previous section (3.2.8), is a depiction of the turbine technology level and is defined by a trade-off between the stage efficiency and the number of stages. In the present study, a limit is introduced in order to avoid low efficiency turbines, defining thus the number of required stages. This is selected based on the technology level of each design, but common values lie between 1.5 and 2.5[58].

Design assumptions

a **Constant stage loading (ψ) for all stages except the last**

During the preliminary design of a turbine, one of the initial design choices is the number of stages and the work split among them. Since the work split among the stages assumes its final values at the detailed design stages, this task can be quite challenging at the preliminary design stage and most of the existing preliminary design methodologies adopt assumptions to overcome that. One of the most common states that the number of stages is defined by an empirical temperature drop limit per stage, to restrict loading, which is also assumed to be equal for all stages[64]. On the other hand, a more realistic approach defines the number of stages in the same way, but assumes a constant stage loading[69]. In the present study, the number of stages is estimated iteratively based on a loading limit and similarly to the second assumption the stage loading is kept constant for all stages apart from the last. The last stage loading is lower,

accounting for the turbine outlet absolute velocity angle restriction.

b **Interpolate axial velocity (C_{ax}) at the outlet of each stage**

The axial velocity (C_{ax}) is linearly interpolated between the inlet and outlet of the component to produce the corresponding values at the exit of each stage, since this yields consistently realistic results. Any of the available Mach numbers (Ma_{ax} or Ma_{abs}) or the absolute velocity (C_{abs}) can be interpolated instead, without any change in the calculation process.

c **Constant absolute velocity (C_{abs}) between the rotor and stator of a stage**

The common design practice is to consider that between the rotor and the stator the velocity vector remains the same. However, this doesn't depict the reality, where the annulus area change implies a different velocity vector at the stator outlet and rotor inlet. To enable the estimation of these velocities, the constant absolute velocity (C_{abs}) is selected to be kept constant between these two stations, as the option that gives the more realistic results.

d **The component annulus shape is simulated by a cubic spline**

As in the compressor design, the existing turbine annuli are defined by curved surfaces that can be simulated by a cubic spline curve.

e **Constant absolute velocity angle (α) between two adjacent stages**

Similar to the compressor design and in order to achieve continuity, the absolute velocity angle is preserved between two adjacent stages.

f **Constant stage reaction (R) for all stages**

The stage reaction (R) is assumed to be constant for all stages to simplify the calculation procedure and is equal to 0.5 for most cases[56].

Design process

1. **Assume isentropic efficiency**

   A value for the component isentropic efficiency (η_{ise}) is assumed, even

though both the component inlet and outlet pressures and temperatures are supplied by the cycle simulation analysis, defining thus its value. The component efficiency value is selected during the cycle calculations without any insight to the number of stages and design parameters of the turbine, resulting in inconsistencies during the design process. In this study, the cycle-supplied outlet temperature value is preserved, in order to match the required work output, but the outlet pressure is recalculated based on the new value.

2. **Assume the component outlet absolute velocity angle (α) for HPT**
   If the designed turbine is a HPT, then there are no inputs or restrictions regarding the component outlet velocity angle (α). In order to progress with the calculation this is assumed at this point, with a starting value of 0.

3. **Assume number of stages**
   The number of stages is required so that the turbine design can be performed, but it is not known at this stage. Therefore, an assumption is made starting from low values that yield less component weight and they are iteratively increased until the stage loading (ψ) limitations are met.

4. **Component inlet and outlet calculations**
   By following the process that is described in section 3.2.4, the velocities, annulus area and dimensions are estimated for the inlet and outlet of the turbine.

5. **Component spline interpolation**
   Based on the selected component configuration, one of D_h, D_t or D_m is interpolated by using a cubic spline between the inlet and outlet for all the stations within the component.

6. **Stage outlet velocity distribution**
   The velocities between the inlet and outlet of the component are linearly interpolated as per assumption b.

7. **Assume stage loading (ψ)**

   A stage loading constant for all the stages, apart from the last, is assumed (a). The final value is defined by matching the component outlet temperature and should be below the given limit. A bisection numerical formulation is used to reduce calculation time, avoiding the faster converging gradient methods which cause numerical instabilities.

8. **Stage connection**

   Several parameter values are propagated from the upstream to the downstream stage to ensure continuity and to enable the calculation process. These include the fluid total pressure (P_{tot}), total temperature (T_{tot}) and mass flow ($\dot{m}$), as well as the absolute velocity angle according to assumption e.

9. **Calculate stage inlet parameters**

   The stage connection supplies all the necessary inputs for the stage inlet calculation parameters as presented in section 3.2.4.

10. **Assume stage outlet mean diameter (D_m)**

    At this stage of the calculation, one out of hub (D_h), tip (D_t) or mean (D_m) diameters is known at the stage outlet, due to the initial spline interpolation. If the mean diameter is not known, it has to be assumed, thus initialising an iterative process, which is accelerated by a bisection method, avoiding the faster gradient methods due to numerical instabilities.

11. **Calculate stage outlet absolute velocity angle (α) or stage loading (ψ)**

    For all the stages apart from the last stage, the outlet absolute velocity angle (α) is estimated by using equation 3.28. Since the absolute velocity angle is known at the turbine outlet, the same equation is used to define the stage loading for the last stage.

12. **Calculate stage temperature drop**

    Through the stage loading definition (Eq. 3.26), the stage temperature drop

and the stage outlet temperature are calculated.

13. **Estimate stage efficiency**

    Since the stage loading and flow coefficients are known the stage isentropic efficiency can be derived from the Smith chart (3.2.9.1).

14. **Calculate stage outlet parameters**

    The stage outlet density, area and dimensions are estimated to fully define this station.

15. **Check the stage outlet mass flow ($\dot{m}$)**

    Based on the calculated stage outlet parameters, a value for the mass flow at the same station is derived. This is checked against the actual mass flow value and if they differ more than the set accuracy, the calculation process returns to step 10 with a new mean diameter value, according to the bisection method.

16. **Cubic spline interpolation**

    A cubic spline is fitted to the annulus boundaries (hub or tip diameters) that are not yet defined. The points at stations one and four of the stages are used, while the points at stations two and three are defined.

17. **Stage parameter calculation**

    The remaining stage parameters are estimated based on the station estimation (3.2.4), having as an input the annulus dimensions and the assumed velocities.

18. **Check the component outlet temperature**

    The calculated outlet temperature, according to the assumed stage loading, is checked against the temperature that is supplied by the cycle calculations. If they don't match, then the calculation returns to step 7 with a new stage loading value given by the bisection method.

19. **Increase the number of stages**

    If there is no feasible solution for stage loading below the chosen limit,

increase the number of stages, return to step 3 and repeat the calculation process.

20. **Check the last stage reaction (R)**
    The calculated stage reaction is checked against the reaction target that was selected and if it doesn't fall within the limit, the outlet angle is increased and the process is resumed from step 2.

21. **Check the component isentropic efficiency**
    The component isentropic efficiency (η_{ise}) is calculated and checked against the assumption that was made in the beginning of the calculation process. If they don't match within the error limit, then a new assumption is made and the process is restarted from step 1. In order to reduce calculation time, a Newton-Raphson method is utilised for the iterative process.

    According to the authors view, this approach is simulating more accurately the engine design processes. However, the new efficiency, resulting from this iterative process, should be an input to the performance simulation that comes before the present engine design method, initialising a new iterative process. Due to time and tools restrictions, this is omitted in the present study resulting in a mismatch between the LPT estimated and the optimal rotational speed.

22. **Blade hub and tip calculations**
    As with the compressor design, the velocity triangles at the hub and tip of each blade are calculated for reference and checking purposes by assuming a free vortex design (Eq. 3.32).

3.3.3.2 Blade weight

The turbine blade weight estimation process is similar to the one used for compressors, following the method described in section 3.2.12.

3.3.4 Disk

3.3.4.1 Introduction

The majority of the modern aero engines use disks in fan, compressor and turbine components, that act mainly as blade carriers. Due to the high blade loads that the disk has to sustain, its size and in extend its weight is a significant part of the component total weight, rendering the disk weight estimation an important task[56].

In the present study, the disk weight estimation method by Tong et al.[41], implemented in NASA WATE, is used as a guideline, but significant improvements[70] and simplifications are also applied. The main idea behind this approach is to find the minimum volume, and subsequently the minimum weight, disk shape that satisfies the stress limitations imposed by its shape and its material. This is of course a realistic approach, as a minimum mass disk would be also the choice of an aero engine design engineer.

According to the NASA WATE method, most of the existing disk designs can be included in three major groups, the web (Fig. 3.12), hyberbolic (Fig. 3.13) and ring (Fig. 3.14) disks. There are also studies that consider disks with spline sections[71], but they are not included in this work.

For calculation purposes, as is presented in figures 3.12, 3.13 and 3.14, each of the three disk types is divided in five sections by selecting six radial positions, chosen based on thickness variation. Contrary to the sections presented in figures 3.12, 3.13 and 3.14, in this study, for simplification purposes, the blade root and platform are included in the disk, and more specifically in section six, introducing inaccuracy in case the weight of only the single disk or the blade is estimated.

3.3.4.2 Disk stress calculation

The stress analysis of the disk under centrifugal load is usually performed by considering an infinitesimal ring-shaped disk part of constant thickness[70;41;72] (Fig. 3.15).

The force equilibrium at the tangential and radial directions produces equa-

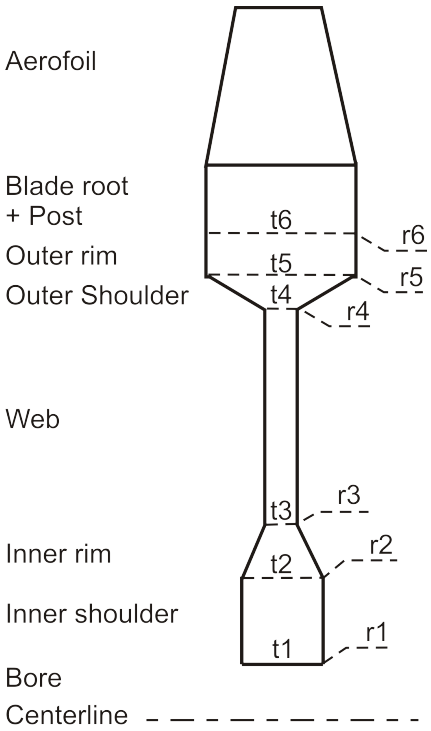

Figure 3.12: Web disk[41]

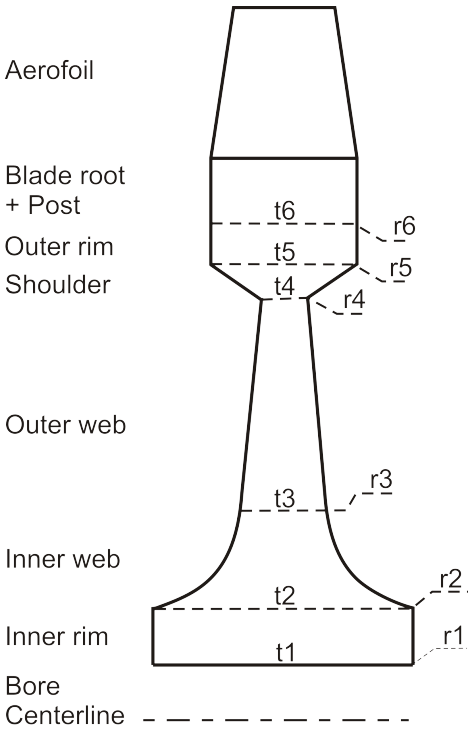

Figure 3.13: Hyperbolic disk[41]

tions 3.42 and 3.43, with F_θ and F_r being the forces in tangential and radial directions respectively, θ and r the tangential and radial distance to the centroid of the element, ρ the disk density and ω the rotational velocity. Furthermore, for the radial and hoop stresses, the symbols σ_r and σ_h are used.

$$\sum F_\theta = 0 \tag{3.42}$$

$$\sum F_r = 0 \Rightarrow \sigma_r \cdot r \cdot d\theta + \sigma_h \cdot dr \cdot d\theta - \left(\sigma_r + \frac{d\sigma_r}{dr} \cdot dr\right) \cdot (r + dr) \cdot d\theta - \rho \cdot \omega^2 \cdot r^2 \cdot dr \cdot d\theta = 0 \tag{3.43}$$

After some algebra, equation 3.43 can be written in a simpler form (Eq. 3.44) and by integrating the stress-radial displacement (u) equations (Eqs. 3.45, 3.46), it produces equation 3.47.

$$\sigma_h - \sigma_r - r \cdot \frac{d\sigma_r}{dr} - \rho \cdot \omega^2 \cdot r^2 = 0 \tag{3.44}$$

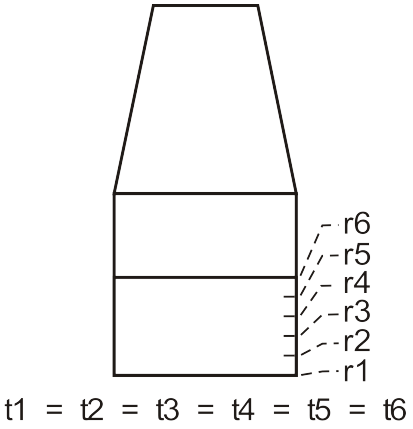

Figure 3.14: Ring disk[41]

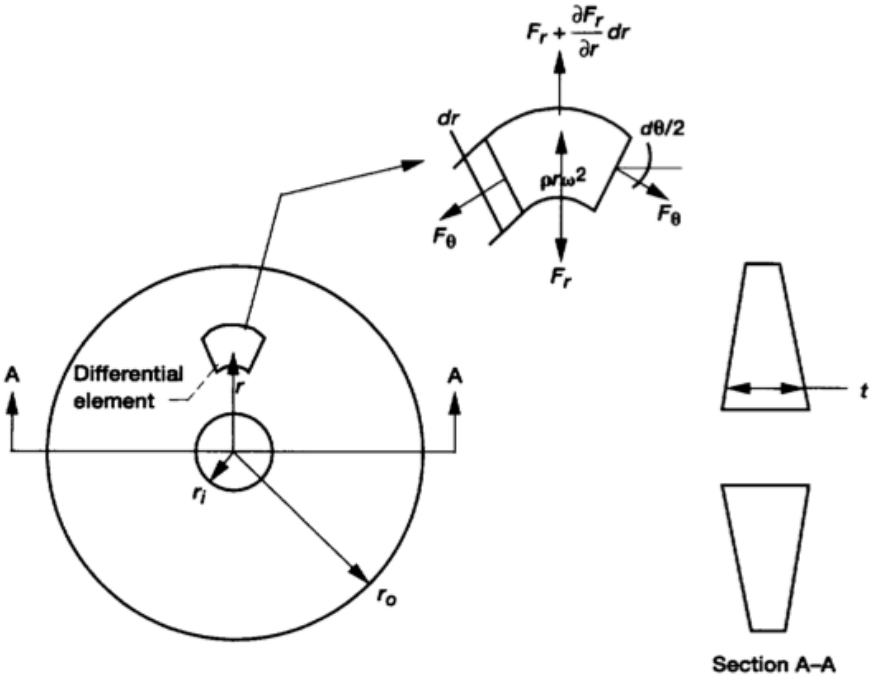

Figure 3.15: Rotating disk analysis[72]

$$\sigma_h = \frac{E}{1-\nu^2} \cdot \left(\frac{u}{r} + \nu \cdot \frac{du}{dr} \right) \tag{3.45}$$

$$\sigma_r = \frac{E}{1-\nu^2} \cdot \left(\frac{du}{dr} + \nu \cdot \frac{u}{r} \right) \tag{3.46}$$

$$\frac{d^2u}{dr^2} + \frac{1}{r} \cdot \frac{du}{dr} - \frac{u}{r^2} + \frac{1-\nu^2}{E} \cdot \rho \cdot \omega^2 \cdot r = 0 \tag{3.47}$$

Equation 3.47 is a second order linear inhomogeneous differential equation and therefore its solution consists of a homogeneous solution term and a particular solution term. The calculation process can be found in several textbooks[73] and will not be analysed here. Substituting this solution in equations 3.45 and 3.46, equations 3.48 and 3.49 are produced. The constants A and B are integration constants that can be selected according to the disk boundary conditions.

$$\sigma_h = \frac{E}{1-\nu^2} \cdot \left[A \cdot (1+\nu) + (1-\nu) \cdot \frac{B}{r^2} - \frac{(1+3\cdot\nu)\cdot(1-\nu^2)\cdot\rho\cdot\omega^2\cdot r^2}{8\cdot E} \right] \tag{3.48}$$

$$\sigma_r = \frac{E}{1-\nu^2} \cdot \left[A \cdot (1+\nu) - (1-\nu) \cdot \frac{B}{r^2} - \frac{(3+\nu)\cdot(1-\nu^2)\cdot\rho\cdot\omega^2\cdot r^2}{8\cdot E} \right] \tag{3.49}$$

The two equations (Eqs. 3.48 and 3.49), that were acquired from the small ring-shaped disk piece analysis, can also be applied on each of the ring sections that were assumed for each disk type at the beginning of this section. However, the connections between the sections have to be taken into account to ensure continuity and the elimination of constants A and B. Focusing on two adjacent sections (Fig. 3.16), the combination of the available equations and boundary conditions through a sum and difference method yields equations 3.50 to 3.55. These provide the radial and tangential stresses at the outer radius of each section due to centrifugal and thermal loads when the stresses at the inner radius are known.

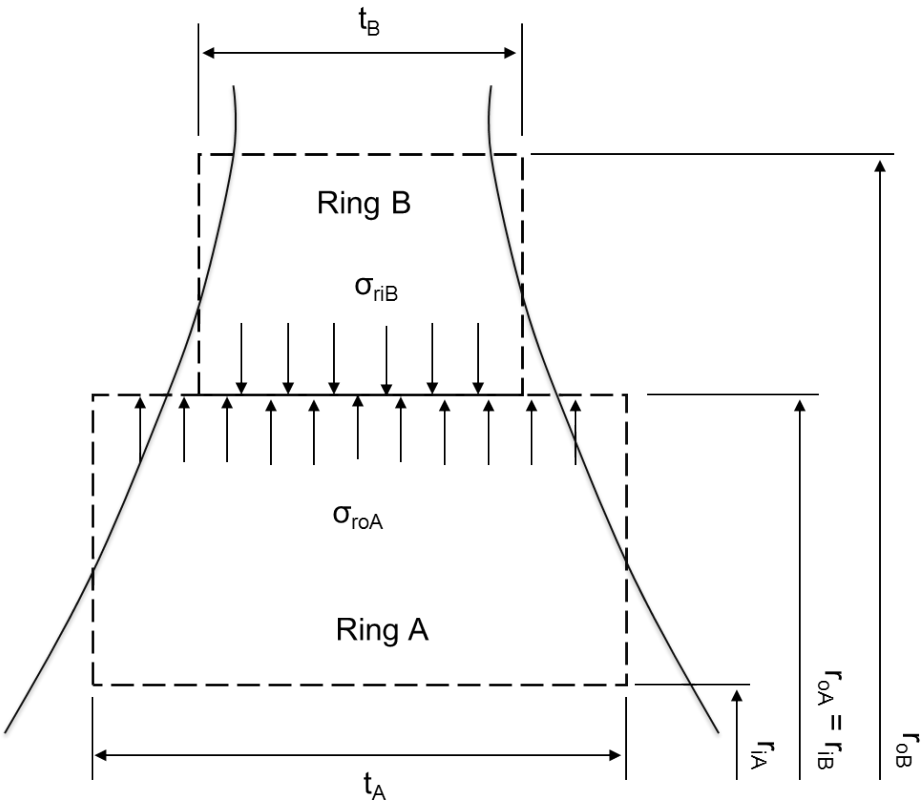

Figure 3.16: Disk ring elements[70]

$$\sigma_{hoA} = \frac{S_{oA} + D_{oA}}{2} \tag{3.50}$$

$$\sigma_{roA} = \frac{S_{oA} - D_{oA}}{2} \tag{3.51}$$

$$S_{oA} = S_{iA} - \frac{1+\nu}{2} \cdot \rho \cdot \omega^2 \cdot \left(r_{oA}^2 - r_{iA}^2\right) \tag{3.52}$$

$$D_{oA} = D_{iA} \cdot \left(\frac{r_{iA}^2}{r_{oA}^2}\right) - \frac{(1-\nu) \cdot \rho \cdot \omega^2}{4} \cdot \left(\frac{r_{iA}^4}{r_{oA}^2} - r_{oA}^2\right) \tag{3.53}$$

$$\delta\sigma_r = \sigma_{roA} \cdot \left(\frac{h_A}{h_B} - 1\right) \tag{3.54}$$

$$\delta\sigma_h = (\sigma_{hoA} - \nu \cdot \sigma_{roA}) \cdot \left(\frac{E_B}{E_A} - 1\right) + E_B \cdot (\alpha_A \cdot T_A - \alpha_B \cdot T_B) + \nu \cdot \delta\sigma_r \tag{3.55}$$

The connection between the outer radius stresses of a ring sections and the inner radius stresses of the next one is achieved through equations 3.56 and 3.57.

$$\sigma_{riB} = \sigma_{roA} + \delta\sigma_r \tag{3.56}$$

$$\sigma_{hiB} = \sigma_{hoA} + \delta\sigma_h \tag{3.57}$$

Zooming out from the sections to take a look at the whole disk, arises the question of the stress values at the inner radius of the innermost disk section that are required to commence the calculation process. Regarding the radial stress, it can assumed that it is equal to zero, since there are no centrifugal loads at the inner diameter of the disk. The tangential stress, however, is not known, but it can be selected through a trial and error method so that the calculated outer disk diameter radial stress matches the blade centrifugal stress that is received by the disk at that position (Eq. 3.58). Considering that this process requires the

calculation of the stresses for all the sections multiple times, a Newton-Raphson numerical method is utilised to improve computational speed.

$$\sigma_{rim} = \frac{Nr_{bl} \cdot m_{bl} \cdot r_{bl,cog} \cdot \omega^2}{\pi \cdot D_h \cdot c_{ax}} \tag{3.58}$$

The calculated tangential and radial stresses are then used in failure criteria to answer if the disk is within the acceptable stress limits. Two criteria, widely used in similar studies which are also adopted here, are the yield and burst criteria[41]. The former is a classic mechanical strength criterion that compares the von Mises stress (σ_e) against the material yield strength (σ_y), including also a safety factor (S_f) (Eq. 3.59). The latter, on the other hand, captures plastic material behaviour, appearing mostly at overspeed and compares the material ultimate tensile stress (σ_{UTS}) with the average tangential stress ($\sigma_{\theta,avg}$) (Eq. 3.60).

$$\frac{\sigma_y}{S_f \cdot \sigma_e} - 1 > 0 \tag{3.59}$$

$$\frac{0.47 \cdot \sigma_{UTS}}{\sigma_{\theta,avg}} - 1 > 0 \tag{3.60}$$

3.3.4.3 Disk temperature

The calculation process for the disk stresses, presented in the previous section, includes also temperature related terms (Eq. 3.55). Due to significant temperature gradients present in disks, combined with the fact that for every degree of temperature difference the permissible stress drops by approximately 3 MPa[74], the omission of these temperature terms can result in significant errors. However, the calculation of the temperature distribution is not a trivial task and involves the use of heat transfer principles. Since this will add complexity in the present analysis, without any significant accuracy improvement, a simple empirical curve 3.17 that describes the temperature drop as a function of the radial position is used.

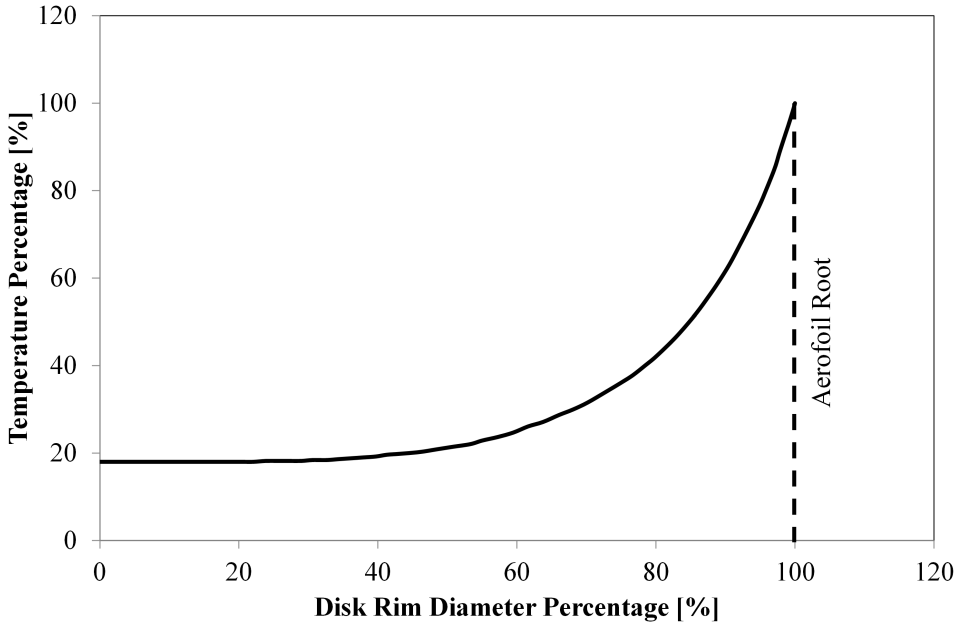

Figure 3.17: Disk temperature distribution[70]

3.3.4.4 Disk materials

The disk materials that are used in turbomachinery applications are similar to the materials used for blades, as a consequence of the stress and temperature levels being similar. Therefore, the use of nickel-based materials at the turbines is necessary to cope with the high temperatures, whereas titanium materials, that offer reduction in weight, are common for fans and compressors[56].

3.3.4.5 Minimum volume disk

The present method aims to select the minimum volume/weight disk that satisfies the stress criteria, where the volume of the disk is purely a function of its dimensions. Based on the discretisation assumptions introduced at the beginning of this section, the disk dimensions can be determined by defining only the radii and thicknesses of the six positions. However, the process requires the calculation of stresses as presented in section 3.3.4.2, which in turn needs the disk dimensions to produce results. Therefore, the problem needs to be solved iteratively, by using an optimisation process which minimises the disk volume by varying the twelve dimension inputs, respecting also the two stress constraints. Furthermore,

bounds to the variables should be introduced to have a disk that doesn't exceed the available space and assumes a reasonable shape.

The outlined problem, due to its complexity and number of independent variables, requires the use of a non-gradient based optimisation method[75] to avoid numerical instabilities and local optima. On the downside, these methods require increased calculation time and taking into account that a single engine includes several disks, a full engine preliminary weight estimation would require significant amount of time, jeopardising the efficiency of a TERA study.

To enable the use of a gradient method to solve this problem, the model has to assume a simpler form. Therefore, based on existing disk designs, correlations between the unknowns are devised pursuing reduction in variables, but also existing design rules are introduced to achieve numerical stability. In the present analysis these will be presented initially for a web disk type (Fig. 3.12) and will adjusted to the hyperbolic (Fig. 3.13) and ring (Fig. 3.14) disk types. In the end, when the minimum volume disk shape is defined for each type, the overall minimum weight disk is selected as the final design solution.

Web disk. The correlations between the thickness and radius variables for a web disk are presented in the following list.

1. The thickness at position six is equal to the blade chord and the thickness at position five (Eq. 3.61)

$$t_5 = t_6 = c_{bl,ax} \tag{3.61}$$

2. The thickness at position four is taken equal to the one at position three (Eq. 3.62)

$$t_3 = t_4 \tag{3.62}$$

3. The thickness at position two is equal to thickness at position one (Eq. 3.63)

$$t_1 = t_2 \tag{3.63}$$

4. The disk radius at position six is assumed to be equal to the radius at the hub of the blade (Eq. 3.64).

$$r_6 = r_{h,bl} \tag{3.64}$$

5. The disk radius at five is expressed as a function of blade height and, radius and thickness at position six (Eq. 3.65)

$$r_5 = \begin{cases} r_6 - \min(0.25 \cdot h_{bl}, 0.1 \cdot t_6) & \text{for fans} \\ r_6 - \min(0.75 \cdot h_{bl}, 0.75 \cdot t_6) & \text{for compressors/turbines} \end{cases} \tag{3.65}$$

6. By assuming a fixed angle between positions two and three, the radius at three is given by equation 3.66

$$r_3 = r_2 + 0.5 \cdot \frac{t_2 - t_3}{\tan(\pi/5)} \tag{3.66}$$

7. The fixed angle assumption between positions four and five provides a correlation for the radius at four (Eq. 3.67)

$$r_4 = r_5 + 0.5 \cdot \frac{t_5 - t_4}{\tan(\pi/5)} \tag{3.67}$$

For simplicity reasons, the angles used in the last two correlations are assumed to be equal and have a value of $\pi/5$, which provides realistic designs.

The first assumption, indicating that the disk rim thickness is equal to the blade chord, includes the blade fixation, as mentioned above, and is also used by NASA WATE[41]. However, the root of the blade should not designed based on chord, but on the blade centrifugal load, which is a function of mass, rotational speed and diameter. This was not possible in the present work, due to the absence of a publicly available correlation, but it will greatly improve the component weight and is suggested as future work.

Taking into account the above mentioned correlations the amount of unknown dimension variables is reduced from 12 to just four (r_1, r_2, t_2, t_4), greatly simplifying and accelerating the calculation process. Even so, some additional constraints

are necessary to ensure that the shapes of the estimated disks are reasonable and ensure the stability of the numerical process. They are presented in the following points.

1. The disk inner radius has to be greater than the maximum shaft radius ($r_{sh,max}$) multiplied by a spacing factor (Eq. 3.68).

$$r_1 \geq 1.1 \cdot r_{sh,max} \tag{3.68}$$

2. The radius at section two (r_2) is greater than the disk inner radius (r_1) multiplied by a spacing factor (Eq. 3.69).

$$r_2 \geq 1.1 \cdot r_1 \tag{3.69}$$

3. The radius at section four (r_4) has to be bigger than the radius at section three (r_3) multiplied by a spacing factor (Eq. 3.70).

$$r_4 \geq 1.1 \cdot r_3 \tag{3.70}$$

4. The thickness at two (t_2) is greater than 1.5 times the thickness at four (t_4), but at the same time less than 2 times the thickness at six (t_6) (Eq. 3.71)

$$1.5 \cdot t_6 \leq t_2 \leq 2 \cdot t_4 \tag{3.71}$$

5. The thickness at two (t_4) has to be between 0.3 and 0.8 times the thickness at six (t_6) (Eq. 3.72)

$$0.3 \cdot t_6 \leq t_4 \leq 0.8 \cdot t_6 \tag{3.72}$$

The above correlations enable the use of a gradient based optimisation method and specifically a non-linear sequential quadratic programming method[76] was chosen for the estimation of the minimum volume/weight web disk.

Hyperbolic disk. The hyperbolic disk type is similar to the web disk, apart from the inner web area that follows a hyperbolic curve and the outer web that has variable thickness (Fig. 3.13). Therefore most of the equations, assumptions and limits presented for the web disk are also valid at this case. More specifically, only equations 3.62 and 3.66 that describe correlations regarding the inner and outer web shape have to be replaced. For simplicity reasons, the hyperbolic part of the disk will be modelled by a straight line, simplifying thus the equations that describe it, without introducing significant inaccuracies in the estimation of the disk volume. The two new equations that describe this geometry are presented in the following list.

1. The radius at position three is bigger that the one at two by one third of the radius difference of four and two (Eq. 3.73).

$$r_3 = r_2 + \frac{r_4 - r_2}{3} \tag{3.73}$$

2. The angle between positions two and three is considered fixed and equal to $\pi/4$, defining thus the thickness at position three (Eq. 3.74).

$$t_3 = t_2 - \frac{2 \cdot (r_3 - r_2)}{tan\,(\pi/4)} \tag{3.74}$$

Ring disk. Due to its shape the ring disk can be considered as one section, with the outer and inner radii and the corresponding thicknesses being the only parameters. Regarding the thickness of the ring, it is evident from its shape that it remains constant and by adopting equation 3.61, it is assumed to be equal to the blade axial chord. Similarly, the outer radius of the disk is equal to the blade hub radius according to equation 3.64, while the inner disk radius has to be bigger than the maximum shaft radius with an added necessary clearance (Eq. 3.68). Since the final problem has only one variable with one limit, after the application of the correlations, there is no need for a sophisticated optimisation method, but it can be solved by means of a Newton-Raphson method.

3.3.5 Combustor

3.3.5.1 Introduction

Combustor is the gas turbine component that performs the fuel burn, raising by heat addition the energy of the working fluid. In aero gas turbines, it is usually situated after the high pressure compressor and before the high pressure turbine, a configuration that is also followed in the present study.

In aero applications, combustors follow in most cases three characteristic designs, as presented in figure 3.18[68]. One of the first designs for aero engines was the tubular combustor (Fig. 3.18a), which consists of several chambers. Each chamber includes a flame tube enclosed in a cooling duct and handles a portion of the air flow.

An evolution of the tubular combustor, aiming for reduced size and weight, is the tubo-annular design (Fig. 3.18b). In this case, a single cooling duct includes all the flame tubes that are arranged in a circular pattern.

Finally, the most common design for modern aero gas turbine engines is the annular combustor that is formed by two concentric rings, design that reduces even more its weight and size for a given power output (Fig. 3.18c). In the present study, only the annular combustor will be examined, since the other two types are considered obsolete for modern applications. However, the flexibility of the method allows for the preliminary weight prediction of any combustor type, if the appropriate component design process is implemented.

Taking a more detailed look into the annular combustor layout, its main parts are presented in figure 3.19[77] . Downstream of the high pressure compressor, the air enters the pre-diffuser, where as its name implies, a diffusion process takes place. This is followed by a second diffusion, performed by the dump diffuser before the working medium is split into two streams, one led to the dome and the other driven into the passage. There also available configurations that include a faired diffuser instead of a dump diffuser, but the latter is preferred for aero applications due to better performance and reduced dimensions[78]. At the dome the fuel is introduced in the flow by the fuel injectors and the combustion pro-

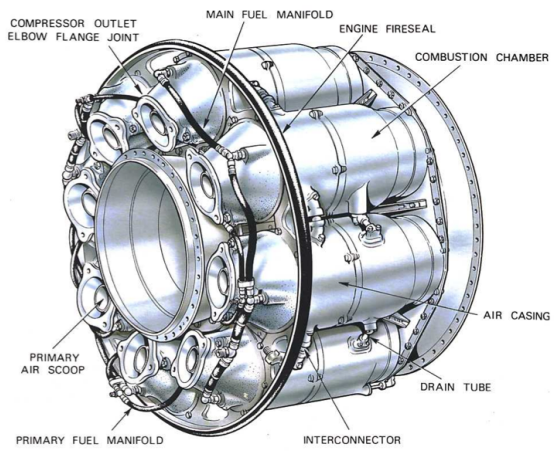

(a) Tubular

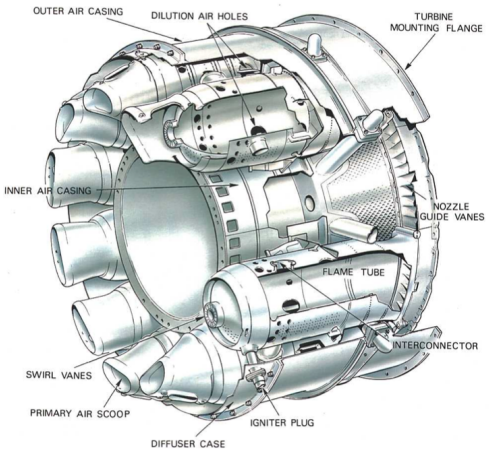

(b) Tubo-Annular

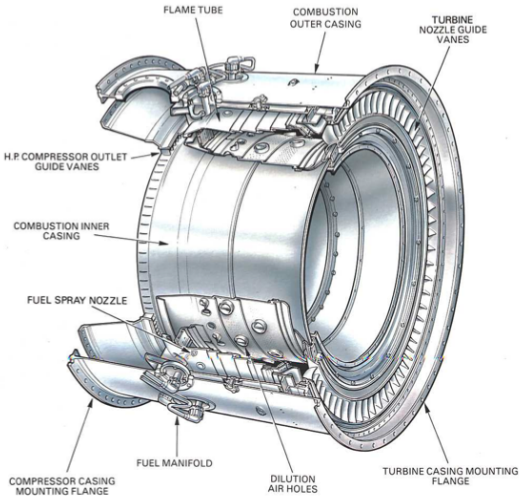

(c) Annular

Figure 3.18: Aero combustion chamber types[68]

cess takes place, pushing the local temperature environment above the material melting point. For this reason, the passage stream is of critical importance, since it acts as coolant that helps to avoid the combustor melting, but also lowers the dome flow temperature at acceptable levels for the downstream component.

Each one of the these combustor parts is formed by an outer and inner ring, being very similar to ducts. Therefore the duct preliminary weight estimation process will be used to define the weight of the combustor. However, this approach requires the annulus dimensions and length of each part, which are defined by applying a combustor preliminary design process.

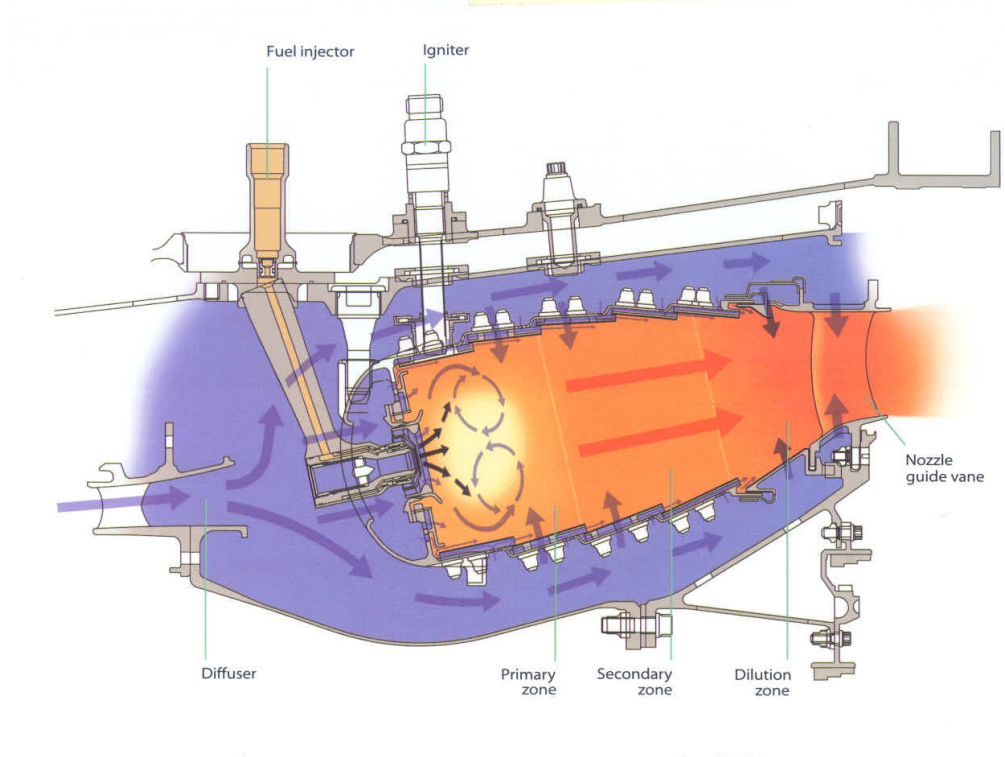

Figure 3.19: Combustor chamber layout[68]

Figure 3.20 summarises the parts that form the combustor weight.

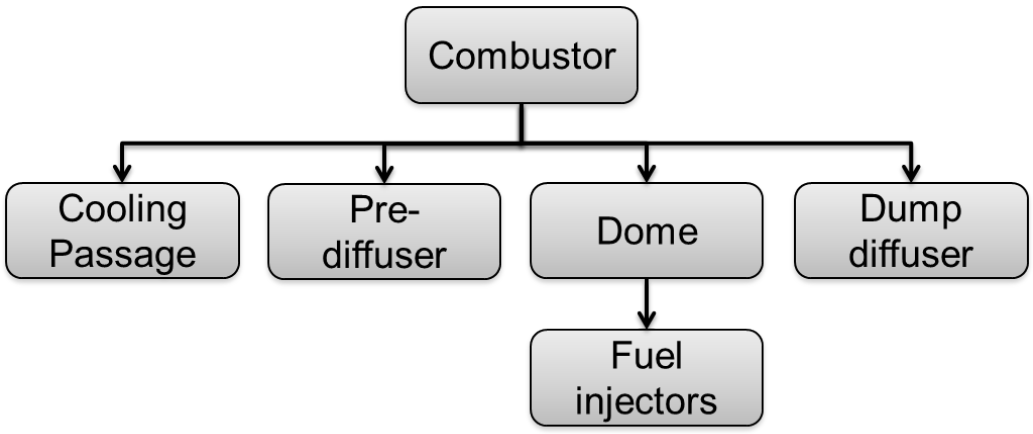

Figure 3.20: Combustor weight parts

3.3.5.2 Design process

The combustor design process in the present study uses the method developed by Mohammad and Jeng[79] as a basis, but includes significant modifications, addi-

tions and improvements. The choice was made taking into account this is a recent and straightforward method that requires few inputs and covers the design of the whole combustor geometry.

Input parameters

I **Cycle parameters**

Similar to the components that were analysed in the previous sections, the combustor preliminary design uses parameters that derive from the cycle simulation analysis. These inputs include the mass flow ($\dot{m}$), total pressure (P_{tot}), total temperature (T_{tot}) and FAR for the inlet and outlet of the combustor. As these are usually required or estimated for the upstream and downstream components, they can be extracted from the outlet of the upstream component for the combustor inlet and from the inlet of the downstream component for the outlet if known.

II **Velocities**

As with the cycle parameters, the required input velocity vectors are similar to the ones for the other examined components and can be retrieved from the upstream and downstream parts. Therefore, one of axial Mach number (Ma_{ax}), absolute Mach number (Ma_{abs}), axial velocity (C_{ax}) and absolute velocity (C_{abs}) has to be supplied as input at both the inlet and outlet of the combustor. Furthermore, the absolute velocity angle (α) at both stations is also required to complete the velocity vector definitions.

Following the recommendations for the HPT, the combustor outlet Mach number should be ideally less than 0.2. Regarding the absolute velocity angle at the same station, it can be safely assumed that the flow exits axially from the combustor.

In order to estimate the parameters at the dome inlet station, the axial velocity (C_{ax}) has to be provided. According to literature[79], values between 35 and 60 m/s can be used. In a similar manner, the axial velocity at the passage inlet is also required and can be selected between 7 and 12 m/s.

III **Annulus dimensions**

The annulus dimensions required at the inlet and outlet of the combustor in order to perform the preliminary design and weight estimation can be either supplied or taken from the upstream and downstream components. They are also similar to the ones required for the components that have been analysed above and include one of hub diameter (D_h), tip diameter (D_t), mean diameter (D_m) or hub to tip ratio ($^{D_h}/_{Dt}$) for the inlet and outlet stations. The required outlet dimension can be also supplied as a function of either the hub, tip, or mean diameter at the inlet. Furthermore, the outlet dimension input is not required if the combustor angle (a_{cob}) relative to the engine axis is given.

IV **Combustor dimension parameters**

The dimension parameter input group includes parameters that are essential to dimensionalise a combustor.

The atomising flow ratio (AFR) is the parameter that defines the ratio between the mass of fuel ($\dot{m}_f$) and the mass of air ($\dot{m}_a$) in the atomiser in order to achieve sufficient fuel atomisation. Characteristic values assume that the atomiser air flow is two to three times the required fuel flow[77].

The dome cooling flow rate ($DCFR$) should also be supplied as an input. It is defined as the ratio of the dome cooling flow ($\dot{m}_c$) and the total combustor airflow ($\dot{m}$) and lies between 0.1 and 0.15 for typical applications. The dome cooling flow is required for the dome to withstand the extremely high combustion temperatures.

The stoichoimetric FAR is also a required input, indicating the amount of air required to fully burn a unit of fuel and for kerosine it is equal to 0.0641026[58].

The primary zone equivalence ratio (ϕ), defined as the fuel to air ratio (FAR) divided by the stoichiometric fuel to air ratio (FAR_{stoi}) is also among the inputs and is associated with flame temperature and emissions[78]. Studies showed that the equivalence ratio has to be lower that 1.5[77], with suggested values at 1.02 for maximum rating at sea level static conditions[58].

The length to height ratio (l/h) of the combustor dome is a non-dimensional parameter that defines its length and volume. Its value is dependent on requirements for flame stabilisation, mixing and residence time with characteristic values ranging between 2 and 3[77].

Finally, the dome gap ratio (DGR), which influences pressure recovery and losses at the dump diffuser has to be also supplied as input[80]. It is defined as the ratio of the distance between the dump diffuser axial length divided by the dump diffuser inlet area.

Design assumptions

a **Assume prediffuser angle**

In order to simplify the design process, the prediffuser angle is assumed equal to 8 degrees. That value is in agreement with the limits given by Reneau et al.[81] and designs used in recent aero gas turbines.

b **Straight walls for each combustor part**

The walls of each combustor part are assumed to be straight lines. This is not an unrealistic approach, but lacks the detail and complexity of several existing combustor designs.

c **Assume axial flow at all combustor stations**

The velocity vector at each combustor station is assumed to be axial. This is realistic throughout the combustor, apart from inside the dome, where sufficient swirl is required to perform the combustion process.

d **The combustor annulus is symmetric around the mean diameter line**

Several modern combustor designs use an asymmetric shape[30]. However, for simplicity reasons, the combustor shape is assumed to be symmetric around the mean diameter line without significant difference in the estimated weight.

e **The passage mass flow is fully introduced in the dome flow**

In the present method, the amount of air that enters into the combustor is maintained at its outlet. This also includes the assumption that the passage

mass flow is introduced fully to the dome airflow before or at the combustor outlet.

f **The distance between the dome and passage annuli is kept constant**
Unlike existing combustor designs, the present method, without any significant influence on the weight estimation, considers that the distance between the dome and the passage remains constant.

Design process

1. **Estimation of combustor mass flows**

   The combustor flow downstream of the dump diffuser is split into two separate streams, one driven into the dome, while the other goes to the passage area (Fig. 3.19). The dome mass flow ($\dot{m}_d$) performs three different functions. One part is used to atomise the fuel ($\dot{m}_a$), one to cool the dome ($\dot{m}_c$) and the last to create a stabilising swirl flow ($\dot{m}_w$)[77]. According to equation 3.75, the fuel atomising mass flow is estimated as a product of the atomising flow rate (AFR) and the fuel mass flow ($\dot{m}_f$), which can be calculated with equation 3.76 at the combustor outlet, since the FAR and combustor mass flow ($\dot{m}$) are known.

$$\dot{m}_a = AFR \cdot \dot{m}_f \tag{3.75}$$

$$\dot{m}_f = \frac{FAR \cdot \dot{m}}{FAR} \tag{3.76}$$

   The dome cooling mass flow ($\dot{m}_c$) is calculated by multiplying the dome cooling flow rate ($DCFR$) with the combustor mass flow ($\dot{m}$).

$$\dot{m}_c = DCFR \cdot \dot{m} \tag{3.77}$$

   The dome swirl mass flow is estimated as a function of the fuel flow ($\dot{m}_f$), the atomising mass flow ($\dot{m}_a$) the stoichiometric FAR and the primary zone

equivalence ratio (*phi*) (Eq. 3.78).

$$\dot{m}_w = \frac{\dot{m}_f}{FAR_{stoi} \cdot \phi} - \dot{m}_a \tag{3.78}$$

Finally, these three components are added to produce the dome mass flow ($\dot{m}_d$) (Eq. 3.79), which in turn substracted from the total combustor mass flow produces the passage mass flow ($\dot{m}_p$) (Eq. 3.80).

$$\dot{m}_d = \dot{m}_a + \dot{m}_c + \dot{m}_w \tag{3.79}$$

$$\dot{m}_p = \dot{m} - \dot{m}_d \tag{3.80}$$

Taking into account assumption e, the dome outlet mass flow equals the combustor outlet mass flow, while the passage mass flow at the same station is zero.

2. **Calculate station parameters at the combustor inlet**

   The station parameters at the combustor inlet station are calculated following the procedure described at section 3.2.4. The prediffuser inlet station parameters are also known, since it is located at the combustor inlet.

3. **Estimate prediffuser parameters**

   Having assumed the prediffusser angle equal to 8 degrees, the prediffuser axial length to inlet height ratio (l_{ax}/h_{in}) and the outlet to inlet area ratio (A_{out}/A_{in}) are estimated according to Renau et al.[81] Both the values derive by assuming no appreciable stall. The axial length to inlet height ratio is used to estimate the prediffuser axial length, since its height is known at this step.

4. **Assume the combustor axial length**

   The combustor axial length is assumed at this point of the calculation. It

is used within the following steps to determine the mean diameter at all stations, by interpolation between the inlet and outlet mean diameter.

5. **Calculate combustor outlet station parameters**

   The velocity vectors, area and dimensions of the combustor outlet are calculated, by using the parameters that were taken from the downstream component inlet. These parameters are also common to the dome outlet, since the passage mass flow is reduced to zero at this station.

6. **Estimate prediffuser outlet station parameters**

   Initially, the area at the prediffuser outlet, estimated by using the inlet to outlet area ratio, is used to calculate the prediffuser outlet Mach number. The station parameter estimation procedure is then used to acquire the rest of the unknown values, which are also common to the dump diffuser inlet station. During this step, the dump diffuser axial length is also estimated as the product of dome gap ratio (DGR) and the dump diffuser inlet height.

7. **Calculate passage inlet station parameters**

   The passage inlet station parameters can be estimated, since all the required inputs are known at this stage.

8. **Estimate dome inlet station parameters**

   Following the station calculation procedure, the velocity vectors, area and dimensions are estimated at the dome inlet. This step also includes the determination of the dome axial length. It is defined as a product of the dome length to height ratio and the dome inlet height.

9. **Calculate dump diffuser outlet station parameters**

   The outlet of the dump diffuser is attached to the inlet of the dome and the inlet of the passage. Therefore, the dump diffuser outlet area is the sum of the dome inlet and the passage inlet flow areas and can be used to estimate the dump diffuser outlet Mach number by using equation 3.6.

10. **Check the combustor axial length**

The axial lengths of prediffuser, dump diffuser and dome are summed to produce the final combustor axial length, which is checked against the assumed value. If they don't match, a new value is assumed and the calculation resumes from step 4.

11. **Estimate the passage outlet station parameters**
    To complete the dimensioning of the combustor, the passage outlet station parameters are calculated by following the guidelines in section 3.2.4.

12. **Calculate the number of fuel nozzles**
    The number of fuel nozzles is estimated as a function of the mean diameter ($D_{m,d,in}$) and the height ($h_{d,in}$) of the dome inlet according to equation 3.81.

$$Nr_{fnz} = round\left(\frac{\pi \cdot D_{m,d,in}}{h_{d,in}}\right) \tag{3.81}$$

As was mentioned above, the combustor wall thickness and the final weight are acquired by following the duct preliminary weight estimation, presented in a later section.

3.3.5.3 Materials

The combustor material is selected by considering the high temperatures that develop during the combustion process, but also the requirement for reduced weight. Therefore, it should exhibit adequate resistance to high temperatures, along with good thermal conductivity to assist cooling and low thermal expansion to avoid excessive deformations[78]. Furthermore, increased resistance to oxidation and corrosion is required, since they are promoted at high temperatures. However, the development and application of Thermal Barrier Coatings (TBCs) has enabled higher combustor temperatures, while providing good corrosion and oxidation resistance, reducing thus the material requirements.

According to the literature, the materials that satisfy the above requirements and are used in aero gas turbine applications are nickel-based alloys, with Nimonic 263 being the most common. However, ceramic materials are also considered for

future applications, since they exhibit good properties that satisfy all the selection criteria.

In the present study, the Nimonic 263 alloy will be used for the combustor, but any other nickel-based alloy will yield similar results, since only the density of the material is used to estimate combustor weight.

3.3.6 Duct

3.3.6.1 Introduction

Ducts in a gas turbine engine are considered the flowpath sections that link two components, as well as the parts that guide the flow before the first, or after the last component. They should occupy minimum space, otherwise they have a negative impact on engine size and weight, but due to engine layout and flow losses restrictions this isn't always feasible. For the same reasons, the desire for flow characteristics that suit the downstream component at the duct exit is not always met. It is therefore evident that the design of a duct is no trivial task and involves some difficult decisions and compromises.

3.3.6.2 Sizing

In order to estimate the weight of a duct, an approach similar to the ones for the components that have been analysed, will be followed, with the weight of a duct being equal to the product of the duct volume and material density, according to equation 3.34. Therefore, to define the duct volume, its dimensions have to be estimated through a design process. For simplicity reasons, the duct will be considered as two concentric conical parts, with the inner subject to outer pressure and the outer to inner pressure.

The geometry of the duct is fully defined if the dimensions and flow characteristics of the components that is connecting are known. These information are usually provided by the component design teams, missing though the exact axial positions. It is not uncommon, however, for a duct to be part of an iterative design that introduces compromises in the component positions to minimise weight,

dimensions and losses of the duct.

In the present study, the introduction of a duct in the flowpath requires that not only the dimensions and flow characteristics of the upstream component are known, but also of the downstream, otherwise constant values are assumed throughout the duct. Regarding the length of the duct, no data is provided and therefore one of the two design assumptions presented in the following list is introduced.

1. **The duct angle is known.** The duct angle has to be limited to avoid excessive losses that are associated with the turning of the fluid. In practice, this limit isn't always respected, due to arrangement and weight restrictions and swan neck ducts with high turning angles are used[58].

2. **The duct length to inlet height ratio is known.** A common non-dimensional parameter that is used to define the length of a duct, so that reasonable shapes are produced, is the length to inlet height ratio[58]. There are no guideline values for this parameter, but is selected for each engine configuration.

The thickness of the duct is also not known, but it can be estimated based on the assumption that the duct is a cylinder under pressure. Following the pressure vessel theory, it can be estimated by using equation 3.82[82].

$$t_{pr} = \frac{p_{st} \cdot D}{2 \cdot \sigma_y} \tag{3.82}$$

The final duct volume can be estimated by using the formula for the volume of a cylinder.

3.3.6.3 Material

Since ducts are not usually subject to high stresses, the material selection is mainly driven nowadays by weight reduction and less by cost and manufacturability, that were also issues in the past. Therefore, steel, titanium and aluminium ducts are replaced by composite ones, where possible[68].

3.3.6.4 Component Casing

Although there are several component casing designs available[83], for simplicity reasons and due to similarities in shape and function, the weight estimation methodology that was used for ducts is adopted. However, casings, apart from containing the high pressure fluid, have to contain also fragments in the event of a blade release, adding an extra factor when their thickness is estimated. Furthermore, the casing is usually the carrier of mechanisms such as variable vane actuators[58] and active clearance control systems[84], but the detailed design of these cases introduces complexity, without significant improvement in weight estimation accuracy.

According to Bretschneider et al.[83], the required thickness for containment of blade fragments surpasses by far the one for pressure containment and is estimated by using equation 3.83.

$$t_{con} = \frac{0.4 \cdot E_{kin,bl} \cdot E}{\sigma_y^2 \cdot h_{bl} \cdot c_{bl}} \tag{3.83}$$

The thickness estimation is performed for each stage, since the blade kinetic energy varies, allowing for a variable thickness casing.

In order to contain large fan rotor blades in the event of a blade release, due to their mass, a very thick casing is required with adverse effects on the total engine weight. Therefore, materials that can withstand high energy impact, such as kevlar, are installed on the inner surface of fan casings[68]. To include this in the current weight estimation process, the thickness of the steel casing is estimated for pressure containment, while the lining thickness for blade containment. Finally, as mentioned above, the duct weight estimation methodology is then applied on each stage to get the casing weight.

3.3.7 Shaft

The shaft is the part of the gas turbine engine that transmits power between the rotating components, but also provides support for them. Apart from the requirement for power transmission, the shaft design is dictated by bending and

vibrations requirements, due to its size and limited supports[85].

In the present study, the preliminary design of the shaft is performed based only on the transmitted torque, omitting bending and vibrations, as they introduce complexity and many additional required inputs. Furthermore, this approach is also followed by other preliminary weight estimation methodologies[86].

Therefore, shafts are considered concentric, with reducing length from the inner to the outer one, as is the practice in aero gas turbine engines. Each one is assumed to have constant thickness and the innermost is solid, having an inner diameter of 0, while its outer diameter is selected in order to satisfy the torque criterion (Eq. 3.84). Due to the higher order of the equation, an outer diameter (D_{out}) is assumed and the maximum allowable stress (σ_{max}) is checked against the material yield stress. If it is not within the limits, then a new outer diameter is assumed and the calculation that involves also the transmitted power ($\dot{W}$), the angular velocity (ω) and the inner diameter (D_{in}) is repeated. A Newton numerical method is used to determine the final answer, reducing thus the calculation time. The procedure is repeated for the next shaft, after its inner diameter is defined by assuming a gap proportional to the inner shaft outer diameter.

$$\sigma_{max} = \frac{16 \cdot \dot{W} \cdot D_{out}}{\omega \cdot \pi \cdot (D_{out}^4 - D_{in}^4)} \tag{3.84}$$

The estimated shaft inner and outer diameters, along with its length, which is taken equal to the length of all the components that it connects, are used to estimate its volume. Multiplied with the material density provides the final shaft weight.

3.3.8 Frames

The term frame, also known as support structure, refers to the aero engine part that provides structural support and carries the loads to the engine fixings. In general, frames have a cylindical/conical shape and intersect the flowpath usually at the bearing position. Apart from the bearing housing, they may include

support struts and mounting lugs.

Typical frames of a three shaft engine are presented in figure 3.21[68]. The forward bearing housing frame, which is also a part of almost all turbofan engines, includes apart from the fore bearing housing support, struts in the bypass duct or reinforced stators, that provide support for the fan casing. Also common to most aero engines is the rear frame that includes the aft bearing housing, the rear engine mount and the LPT OGVs, that act as support elements for the rear engine part. Moreover, most engines include up to two more frames between the previous two, but their design and position is dependent upon the engine layout.

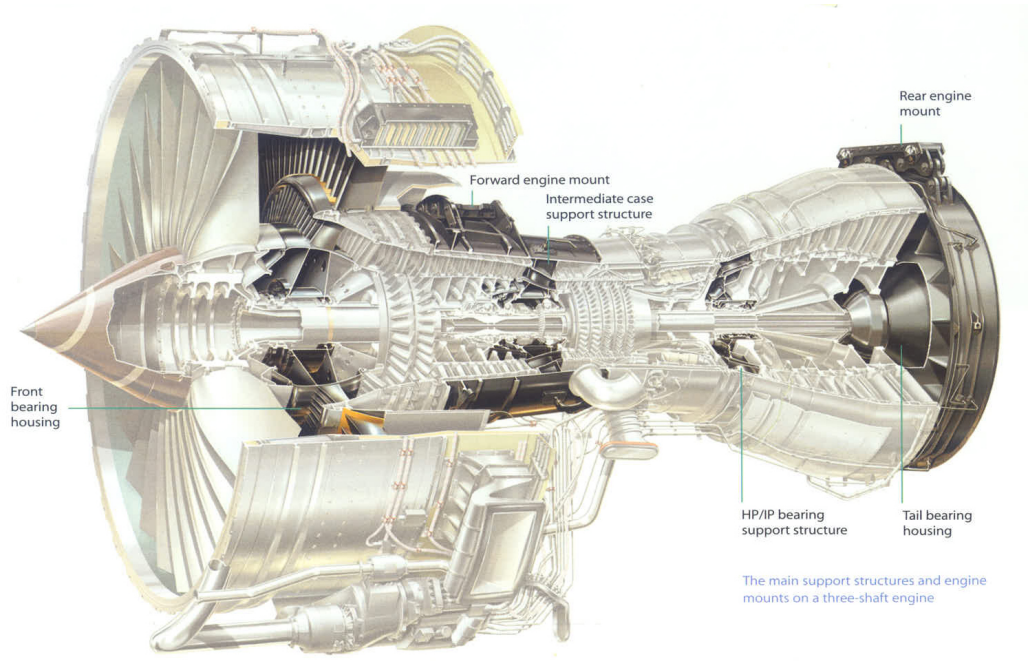

Figure 3.21: Three shaft engine frames[68]

The frame design is restricted by the available space and load requirements, aiming also for minimum weight. Even though they are a significant part of an aero gas turbine, there are limited bibliographic references on their preliminary design and/or weight prediction. This can be attributed to their sizing complexity and customised design for one engine or engine family. For this reason, the frame weight estimation is usually based on empirical correlations that derive from existing frame data.

The approach that is adopted in the present method is the one proposed by Onat and Klees[86] and is part of the NASA WATE method. It considers four frame types, which are the one bearing type, with or without power off-take (PTO), the turbine exit and the intermediate or two bearing type. The weight is estimated by using curves for each type (3.22), derived from engine data, that connect the frame diameter, defined by the adjacent components, with its weight.

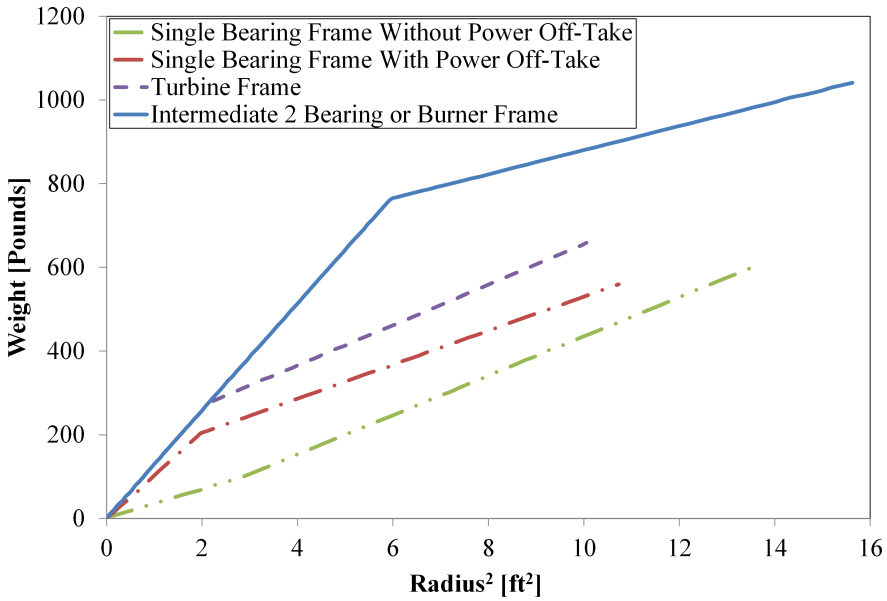

Figure 3.22: Frame weight estimation[39]

3.3.9 Connecting hardware

The rotating parts of the flowpath (i.e. fan, compressor and turbine) use in most cases spacers and bolts to connect the moving parts, with a charecteristic case being the CFM56-7 LPT (Fig. 3.23). The weight of these parts is not negligible and therefore has to be included in the final engine weight.

Due to lack of available methods, the approach suggested by Onat and Klees[86] for the NASA WATE method is followed. The connecting hardware centre of gravity is assumed to be at 75% of the blade hub diameter, as is the practice in existing gas turbine engines. Furthermore, it is assumed to have thickness of 2 mm and length equal to the one of the stage. Therefore, the weight of

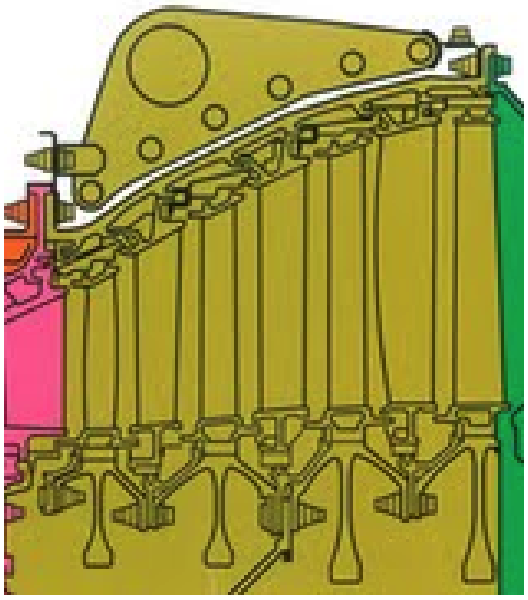

Figure 3.23: CFM56-7 LPT

connecting hardware per stage is given by equation 3.85 and is a function of stage length (l_{sg}), thickness (t), blade hub diameter ($D_{h,bl}$) and material density (ρ).

$$WT_{CHW,sg} = 0.75 \cdot D_{h,bl} \cdot \pi \cdot l_{sg} \cdot t \cdot \rho \tag{3.85}$$

3.3.10 Gearbox

A gearbox is only included in the total engine weight, when a GTF configuration is examined. Since the GTF concept was utilised recently, with only one engine of this type with high BPR currently in production (PW1000G)[87], the available gearbox preliminary weight estimation methods are limited.

In order to avoid complex gearbox weight estimation methods, an empirical method that requires only three readily available inputs (shaft power ($\dot{W}$) in $\frac{lbf \cdot in}{s}$, angular velocity (ω) and gear ratio (z)) was selected[88]. According to it, based on existing gearbox designs[87], the weight of an epicyclic gearbox is estimated by using equation 3.86. Care should be taken to convert all the inputs to imperial units for use with this equation.

$$WT_{gear} = 0.5 \cdot \frac{\dot{W}}{K \cdot \omega} \cdot \left(\frac{1}{Nr_{pl}} + \frac{1}{Nr_{pl} \cdot z_s} + z_s + z_s^2 + \frac{0.4 \cdot z^2}{Nr_{pl} \cdot z_s} + \frac{0.4 \cdot z^2}{Nr_{pl}} \right) \quad (3.86)$$

The gear ratio between the sun and the planet gear (z_s) can be estimated by equation 3.87, while the optimum number of planets (Nr_{pl}) is calculated by equation 3.88.

$$2 \cdot z_s^3 + z_s^2 = \frac{0.4 \cdot z^2 + 1}{Nr_{pl}} \quad (3.87)$$

$$Nr_{pl} = \frac{16.3677}{3 \cdot sin^{-1}\left(\frac{z-1}{z+1}\right) \cdot 1.1736} \quad (3.88)$$

The method provides also suggested correction factors (K) for several applications, but since it is more than 50 years old, there is no reference to a gearbox for a GTF. Therefore, the correction factor (K) was recalibrated with publicly available data of Pratt and Whitney's PW1000G. The gearbox of this engine, being the only one of its type in production, reduces the approximately $10000\,rpm$[89] of the LP shaft with a gear ratio of 3.1[90], delivering $22370\,kW$[91] to the fan. In order to match its approximately $115\,kg$[91] of weight, the correction factor (K) is set to $1200\,{}^{lb}/_{in^2}$.

The above calculated weight refers only to the gearbox itself, without including its accessories that impose a significant weight increase. These include the oil cooling, circulation, control and valve systems, which depend primarily on the heat dissipation requirement. This can be calculated based on the mechanical losses, and the starting oil temperature.

Even though the gearbox accessories have significant weight, they are not calculated in the present work, because there is no publicly available data or a calculation method.

3.3.11 Controls and accessories

The control and accessories component includes the weight of the fuel, oil, control and starting systems and the accessory gearbox. Since the weight of these components cannot be easily calculated analytically, it is assumed to be 10% of the total engine weight[39], following the suggestions of existing studies[36].

$$WT_{C\&A} = 0.1 \cdot WT_{eng,tot} \tag{3.89}$$

The weight of the controls and accessories as a percentage of the total engine weight is considered sufficient for the present study, but it could be unrealistic for some engine types and if a different technology is used. The most characteristic example is the replacement of mechanical systems by electrical in recent engines, with the latter being usually lighter. Furthermore, it has to be considered that there is a minimum size for the control and accessories and that they may not scale as expected for small engines, if the fixed percentage weight estimation method is used.

In order to improve the weight estimation accuracy, a more detailed calculation process that addresses each of the components included in controls and accessories should be introduced in future updates of the method.

3.3.12 Nacelle

The nacelle weight is not included in the total engine weight in the present "component based" weight estimation method, since the whole engine weight quoted by the OEMs refers to the "bare" engine weight. However, when the installed performance of an engine is calculated, the nacelle weight is a big part of the total installed engine weight.

Due to the variety of nacelle designs, there are only empirical correlations that estimate its weight. The correlation that is used in the present study was developed by Jackson[23] and is described by equation 3.90.

$$WT_{Nac} = k\pi \cdot (2 \cdot l_{ca} \cdot D_{ca} + l_{bo} \cdot D_{af} + 2 \cdot l_{af} \cdot D_{af}) \tag{3.90}$$

The coefficient $k\pi$, representing the nacelle material density, was estimated by Jackson at $24.88\,kg/m^2$, while the geometrical parameters of the equation are presented in figure 3.24.

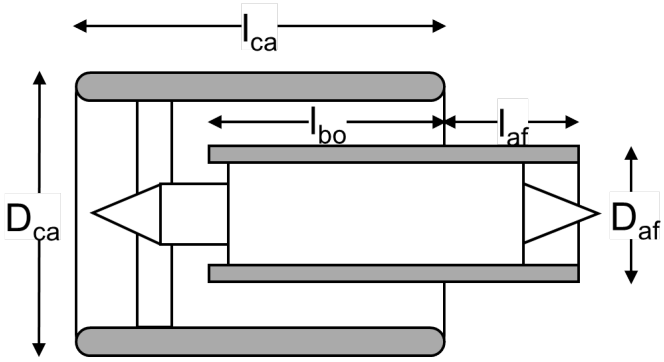

Figure 3.24: Nacelle dimensions[53]

A simplified version of this method was also used by Giannakakis[53] by taking into account the weight of the afterbody only once. This approach was also followed in the present study.

3.4 Summary and discussion

The "component based" preliminary weight estimation method, that was presented in this chapter performs a complete engine design and sizing, used to calculate the whole engine weight. As its name implies, this is achieved by performing the sizing and weight estimation at each individual component by using or adapting proven existing design methods. Furthermore, the components interact, exchanging data, such as basic dimensions and inlet and outlet flow conditions, in order to achieve a realistic whole engine integration.

Even though this method is identical to the NASA WATE preliminary weight estimation method, its development is justified by the differences in the component design practices used in each one. For instance, WATE calculates the component diameter by setting a loading limit, a method applicable to cases when the optimum diameter is sought. Moreover, it reaches the solution by assuming constant temperature rise or drop per stage, which is a common design

practice, but not realistic for existing engines. On the other hand, the new "component based" preliminary weight estimation method is able to simulate variable temperature rise or drop per stage and can be used when diameter restrictions are applicable, since it uses dimension inputs.

Furthermore, there is an inconsistency between the WATE version available to the author and the publications that describe its component design and weight prediction methodology. Clearly, the improvements that have been introduced over the years were not fully documented and therefore there are uncertainties about the weight estimation process.

In addition, the development of the new preliminary weight estimation method simplifies the integration in the TERA framework and allows for the introduction of new components for novel engine arrangements. In order to enable the former, the "component based" preliminary weight estimation method was built in a computer software, named ATLAS, in order to integrate in the TERA optimisation process. ATLAS, created by using the FORTRAN programming language, is built by using modules, strengthening its flexibility and expandability, allowing for easy integration of new components and design methods.

Based on the above characteristics, ATLAS, despite its complexity, aims to achieve higher accuracy and flexibility, enabling the weight estimation of complex and novel engine configurations. Furthermore, the use of simple methods allows for reduced calculation time, an advantage for engine optimisation studies.

However, several of the component design methods in ATLAS can be further improved, increasing thus the accuracy of the results. The main tasks are listed below:

- Improve the fidelity of efficiency estimation in compressor and fan design. The currently estimated efficiency value by the performance calculation should be recalculated in ATLAS, respecting turbomachinery restrictions. This is also an essential step towards the coupling of ATLAS with a performance code in a feedback loop, that will redefine the cycle parameters, raising the accuracy of both.

- New components, including a propeller, an intercooler, a recuperator and a contra-rotating turbine, could be included in ATLAS to enable the weight estimation of novel configurations.

- The weight of the gearbox accessories should be estimated in ATLAS, since it is a critical component for the weight estimation of a GTF engine.

- The optimisation process to define the volume of the disks is currently the slowest process in ATLAS. This could be improved by implementing faster optimisation methods or redefining the problem to reduce the unknown variables, but without compromising the weight estimation accuracy.

- The empirical weight estimation method of the frames was based on old data and should be updated. Ideally, it could be substituted by a detailed frame design method that will also yield weight. This should also include the bearings and their housings.

- The estimation of shaft thickness is done considering only the transmitted power and torque. Ideally, shaft bending and rotor dynamics should also be part of the calculation process. Furthermore, the assumption of a solid inner shaft is not realistic and a methodology to estimate the minimum weight shaft, by modifying the inner diameter, can be developed. However, this approach may increase the weight of other engine components that are affected by the outer diameter of the shafts, such as the disks.

- A more accurate modelling of the turbine cooling is required in order to estimate the passages that reduce the blade volume. Alternatively, an empirical correlation that uses blade solidity can be used.

- The hub and tip calculations at the fans, compressors and turbines are currently informative only. These should be integrated into the design process and new limits should be set for critical hub and tip parameters.

- Apart from temperature, other criteria, such as stress, cost and life, have to be included in the material selection process for all parts.

- Introduce the blade taper ratio at all blades for more accurate preliminary weight estimations. Even though the taper ratio is not expected to have a big effect on individual blade weight accuracy, this will affect the spacing of the components at the hub area and thus their total length.

- Since the adopted nacelle weight estimation method is empirical, an analytic design method should be developed. This should also include thrust reversers, since they also contribute to nacelle weight.

- Only single stage fans are currently supported by ATLAS, but that needs to be modified to cover multi-stage fans for low BPR values.

- The estimation of the space to chord ratio used in ATLAS was developed considering primarily compressor blades. It is currently used for fans as well in ATLAS, but it has to be verified against existing fan designs.

- The turbine rotational speed limits should be expanded to include not only mechanical integrity restrictions, but also aerodynamic as well.

Many of the above improvements though could result in reduced calculation speed, but this could be mitigated with the hybrid method concept, as described in the previous chapter. Despite the increase in calculation speed, the hybrid method has to be retrained for engines with different characteristics.

Chapter 4

Method validation

4.1 Introduction

Due to disclosure policies followed by the OEMs, there are limited component weight data available in the public domain for turbofan engines. This poses a serious obstacle in verifying any "component based" preliminary weight estimation method and allows only for comparisons against the whole engine weight that is quoted in most cases.

However, if the weight of the engine is estimated by performing the preliminary design of the engine components, as is the case with ATLAS, the validation of the flowpath dimensions provides a solid base for verifying the engine's volume, the first of the two terms in the engine weight equation (3.34). The engine dimensions can be retrieved from the literature[30] or from 2D cutaways, which are available in the public domain for the majority of engines. Furthermore, several information about the engine components, including materials, blade numbers per row or design choices, that can be used either as input or as validation values, are publicly available.

Moreover, existing "component based" preliminary weight estimation methods can be used to verify the accuracy of the new "component based" method, provided that their accuracy is proven and their limitations are respected. From the examined existing methods, only NASA WATE could be used for verification

purposes, since it is similar to ATLAS and has been validated against existing turbofan engines.

4.2 Verification of component based method

In the present study, two different engine designs were compared against the ATLAS output in order to verify its accuracy. Care was taken to include engines with different number of spools and to cover a wide spectrum of design philosophies if possible.

The two shaft engine is the popular CFM56 and more specifically the variant CFM56-7B27[92], which is the result of the joint venture by the American General Electric and the French Snecma. On the other hand, the three shaft engine is manufactured in the UK by Rolls Royce plc and is designated as Trent 892[30].

Apart from the different performance characteristics, these two engines have also striking differences in their architecture, primarily due to the number of shafts each one uses. The 2-spool CFM56 has a small three stage booster compressor connected to the LPT and a big HPC, which provides most of the pressure ratio and is driven by the HPT. On the other hand, the 3-spool Trent 892 gets the majority of its pressure ratio from the eight stage Intermediate Pressure Compressor (IPC) that is driven by the Intermediate Pressure Turbine (IPT). Furthermore, the arrangement restrictions and the philosophy of each company are primarily visible at the engine frames, with the most characteristic case being the fan duct support frame that is positioned downstream of the booster compressor in CFM56-7B27, but upstream of the IPC in Trent 892.

4.2.1 Two shaft engine verification

Initially, the cycle related inputs required by ATLAS were retrieved from the results of the CFM56-7B27 performance simulation analysis. The engine model used was built in TURBOMATCH[13] and matched the publicly available key engine characteristics, summarised in table 4.1.

Table 4.1: CFM56-7B27 performance parameters

Take-off thrust	121.43 kN
Take-off mass flow	355 kg/s
BPR	5.1
OPR	32.7
Cruise SFC	16.06 mg/Ns

The majority of input dimensions required by the method were extracted by proportion from the engine 2D cutaway (Fig. 4.1), using the known fan diameter ($D_f = 1.549\,m$) as reference. Furthermore, several other geometry related inputs were acquired from public domain databases[92] and books[30;93]. These included among others, published number of blades, materials, number of stages and design choices. The remaining required inputs were assumed by following general suggestions available in literature[58].

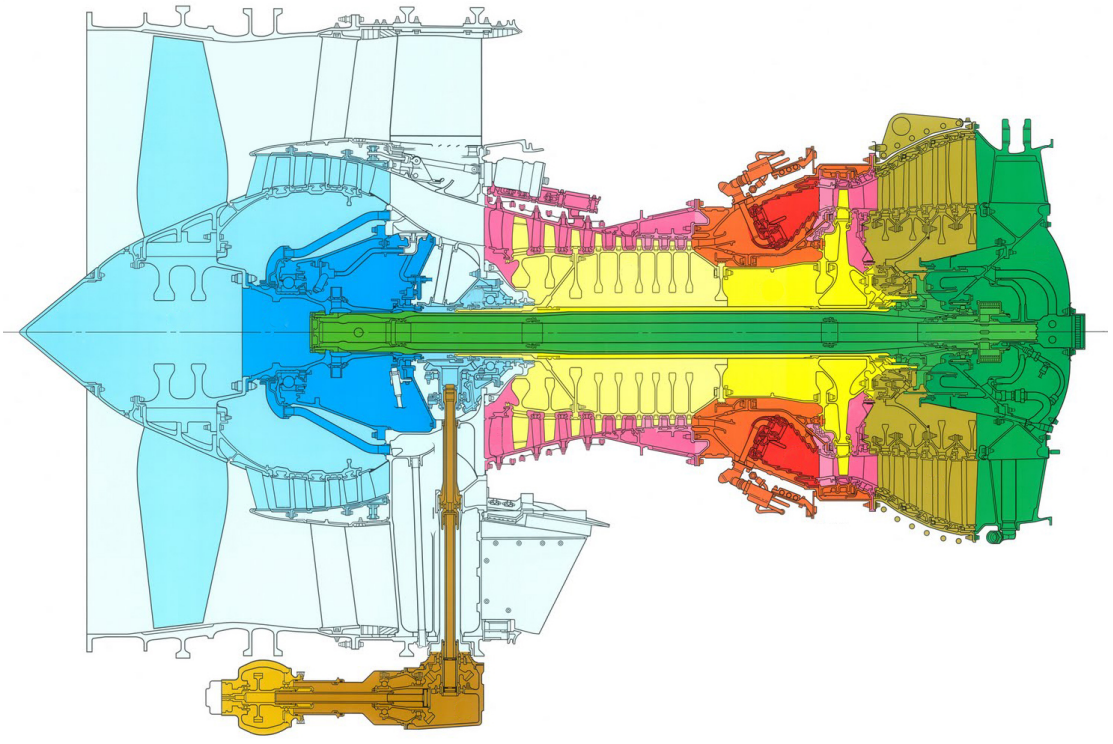

Figure 4.1: CFM56-7 2D cutaway

The performance and design input parameters were then used by ATLAS to perform the preliminary design, sizing and weight estimation of the engine

components. The estimated 2D engine layout plot was produced (Fig. 4.2) and can be directly compared with the available CFM56-7B27 2D cutaway (Fig. 4.3).

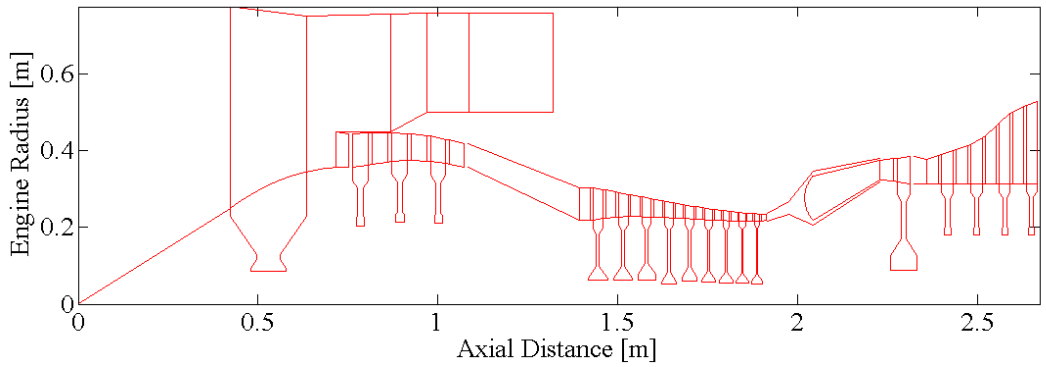

Figure 4.2: Estimated CFM56-7 2D annulus

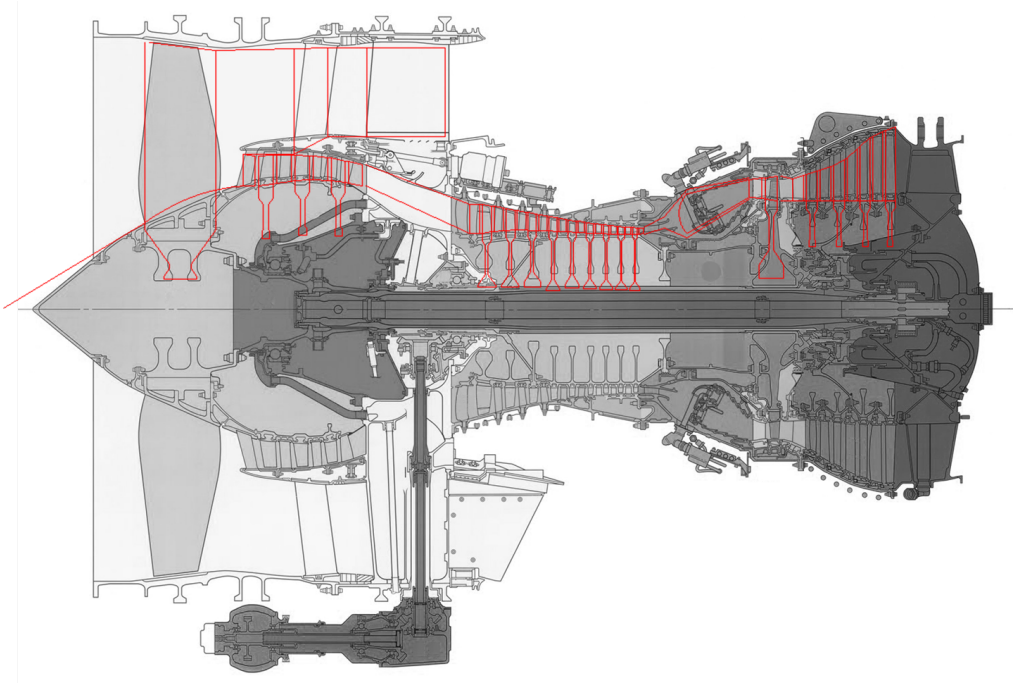

Figure 4.3: Estimated-real CFM56-7 overlay

The ATLAS estimated layout of the CFM56-7B27 engine is similar to the real engine with only minimal differences, confirming that the preliminary weight estimation method is able to simulate existing engine layouts. In order to reach an accurate representation of the components, the shafts' rotational speeds are estimated with minimal error. Consequently, the number of stages for all the com-

ponents are also estimated accurately, avoiding inaccuracies at the engine weight estimation, since the component weight is considered to be primarily dependent on the number of stages.

Small differences are observed at the geometry of the disks and more specifically in the fan, booster and HPC, where due to the design assumptions and the use of the web disk only in ATLAS, the optimised shape of the CFM56-7B27 disks is only partially matched. For example, the booster compressor disks are larger than expected, contrary to the HPT which has one smaller than anticipated. This results in wrong component weights, but the whole engine weight could be still correct when these errors are added.

The reason for this discrepancy can be found in the definition of the disk rim thickness that is a function of the blade chord, following the suggestion of NASA WATE[41]. As a result, unrealistic disk rim stresses are estimated, since they are also a function of diameter and rotational speed, giving wrong disk shapes. Therefore, this correlation has to be improved and the disk rim thickness should be calculated based on the blade centrifugal load.

Apart from the engine design that is produced by ATLAS, the estimated weight is also compared against the quoted real engine weight. As presented in table 4.2, the estimated weight is only 4.97% less than the actual engine weight, falling within the desired maximum error limit of ±10%.

Table 4.2: CFM56-7 weight estimation

	Real	**Estimated**	**Difference**
Weight	2405 kg	2285.5 kg	-4.97%

The component weights are also estimated by ATLAS, but there are no published data to perform the comparison. However, the weight breakdown that is estimated (Table 4.3) seems to be be reasonable, if the component sizes and number of parts are considered.

Table 4.3: CFM56-7B27 estimated weight breakdown

Fan	30.8%
IPC	7.5%
HPC	9.8%
Combustor	2.4%
HPT	4.6%
LPT	11.3%
Ducts	0.9%
Shafts	2.4%
Frames	20.2%
Controls and Accessories	10.0%

4.2.2 Three shaft engine verification

The engine design validation process that was used for the 2-spool engine was also applied on the selected Rolls Royce Trent 892 3-spool engine.

Similarly to the 2-spool, the required cycle inputs for ATLAS were extracted by using TURBOMATCH. The required parameters(Table 4.4) were acquired from Jane's encyclopaedia[30] and the work of Jackson[23], where the performance simulation analysis was performed for the examined engine by using the GasTurb software[44]. Furthermore, Jackson's work was also the source of several geometric parameters, which were supplemented by data found in the public domain[94] or extracted from the 2D annulus plot[30] (Fig. 4.4). The remaining required ATLAS inputs were assumed based on engineering judgement and guidelines found in the literature[58].

Table 4.4: Trent 892 performance parameters

Take-off thrust	407.5 kN
Take-off mass flow	1200 kg/s
BPR	5.8
OPR	40.8
Cruise SFC	15.86 mg/Ns

The inputs are then introduced in ATLAS and an estimation of the 2D engine layout(Fig. 4.5) is generated and overlaid on the Trent 892 2D representation (Fig. 4.6).

Similar to the two shaft configuration, the generated flow path, along with the

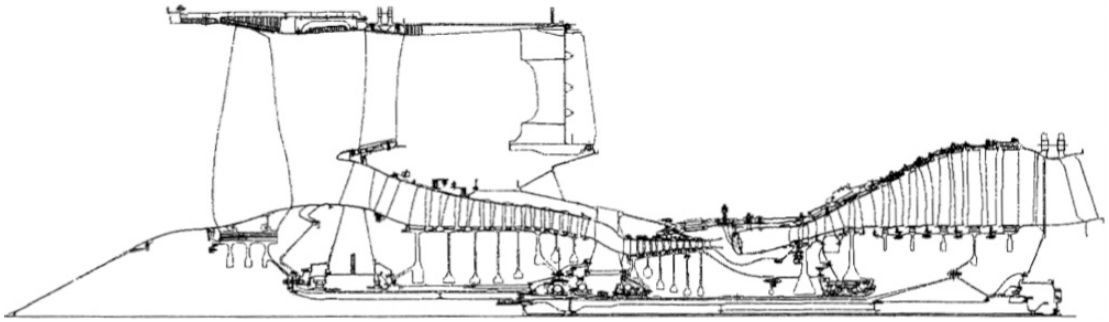

Figure 4.4: Trent 800 2D cutaway

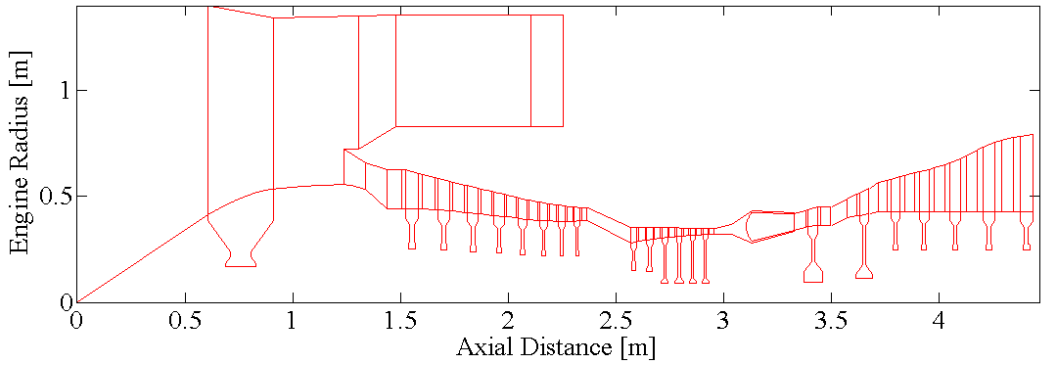

Figure 4.5: Estimated Trent 892 2D annulus

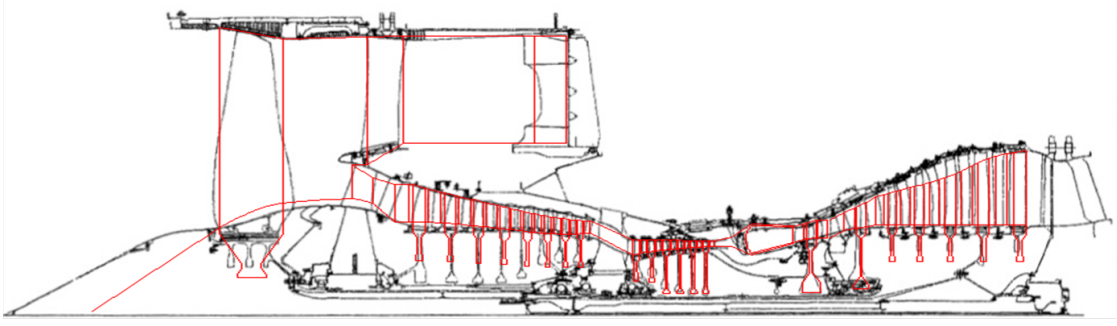

Figure 4.6: Estimated-real Trent 800 overlay

axial positions of the blades and disks is identical to Trent 892, with only small differences. The disk shape problem is again repeated in this case. Furthermore, the accurate estimation of the rotational speed contributes to the calculation of the actual stage number for all the components.

However, a small difference is observed at the tip diameter of the LPT, attributed to the design assumptions in the ATLAS engine model. Even though ATLAS is estimating the correct inlet and outlet dimensions at the LPT, the tip diameters don't match. Trent 892 does not follow a simple spline contour, but there is an asymptote towards the component outlet, possibly due to restrictions imposed by the fan duct.

The same also applies to the nose cone geometry, since in the estimated geometry it follows the slope of the annulus, but in Trent 892 there is a surface parallel to the engine axis at the leading edge of the fan blade. This is clearly an engine specific design and cannot be easily predicted by a simplified design method.

The verified 3-spool engine design is used by ATLAS to perform the preliminary weight estimation of the engine components. The total Trent 892 weight is calculated 5.6% lower than the actual weight (Table 4.5), but is still within the target accuracy of $\pm 10\%$.

Table 4.5: Trent 892 weight estimation

	Real	**Estimated**	**Difference**
Weight	5942 kg	5609 kg	-5.6%

As with the two shaft engine, the component weights are not available for the three shaft engine either, and no direct comparison can be made against the estimated values. However, the calculated weight breakdown is similar to the 2-spool case, considering also the differences in component sizes.

The estimated whole engine weight for both verification engines is lower than the real engine weight, but still within the target accuracy limit. This indicates that ATLAS may underestimate weight and apart from improving the weight estimation of components, the whole engine weight can be also adjusted with a

Table 4.6: Trent 892 estimated weight breakdown

Fan	33.7%
IPC	10.0%
HPC	3.8%
Combustor	1.3%
HPT	3.2%
IPT	2.9%
LPT	17.8%
Ducts	0.6%
Shafts	3.0%
Frames	13.6%
Controls and Accessories	10.0%

correction factor. However, more verification cases are needed in order to validate this assumption and select the appropriate factor value.

4.3 Comparison with existing methods

4.3.1 Introduction

In order to further verify the accuracy of ATLAS, apart from considering existing engine designs, its results are compared against the trends that were observed in the existing preliminary weight methods in chapter 2. Since ATLAS is following a concept similar to the one used by the "component based" methods, which were proven to be more accurate than the "whole engine based" methods, the present study will only focus on those. However, the first of the two available methods, the Sagerser et al. method, performs a preliminary weight estimation by using existing design data and is not directly comparable to ATLAS. On the other hand, the NASA WATE method is similar to ATLAS in principle, but due to confidentiality reasons, the latest version of this method is not publicly available and thus a slightly older method was used.

4.3.2 Quantitative comparison

For simplicity reasons, only the selected 2-spool engine (CFM56-7B27) will be used in order to compare the preliminary weight estimation of the two methods, since the results were also presented in previous sections for each one of them. Summarising, both methods produce a geometry similar to the real engine and subsequently both provide an accurate whole engine weight estimate, with error below ±5% (Table 4.7).

Table 4.7

	Weight	**Difference**
CFM56-7B27	2405 kg	–
WATE	2289 kg	−4.8%
ATLAS	2285.5 kg	−4.97%

Even though ATLAS and WATE estimate engine weight using a similar approach, they use different assumptions and design processes. For instance, the weight of the components doesn't include the same parts in both codes, as is the case with the weight of support frames and engine structures, which is incorporated in the neighbouring components in WATE, while separate values are given for them in ATLAS. Therefore, in order to compare the weight breakdown of the two methods (Fig. 4.7), the component weight outputs were adjusted, where possible, in order to have a common reference.

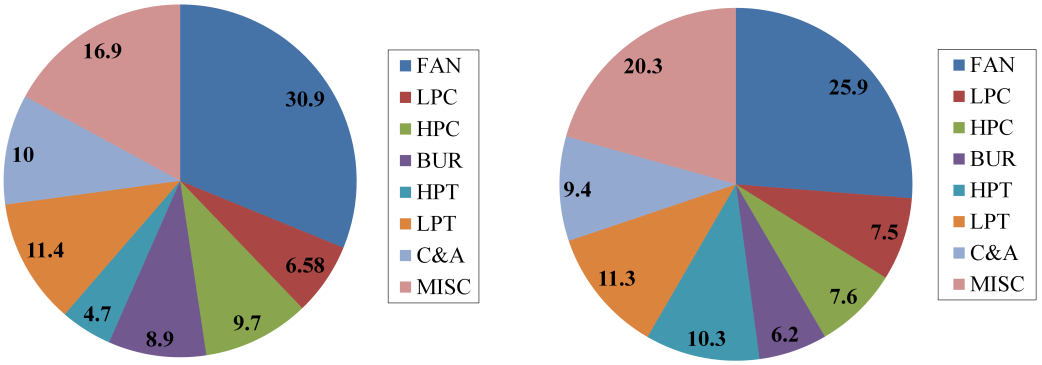

(a) ATLAS (b) WATE

Figure 4.7: CFM56-7B27 weight breakdown [%]

Figure 4.7 shows that both methods estimate roughly the same weight for the majority of the components, verifying thus the component weight prediction of ATLAS against an already validated method. However, there are also some differences in some components, with the HPT being the most characteristic case. The percentage of the HPT weight in WATE is almost double than the one estimated by ATLAS, attributed to the more detailed analysis of cooling in WATE and the inclusion of small parts and accessories that are not part of the HPT in ATLAS. Furthermore, the fan weight percentage is slightly lower in WATE, because the spinner weight is not included.

4.3.3 Qualitative comparison

In the method analysis section (2) the physics followed by NASA WATE were examined, using the cruise BPR and TET as variables. In the present section, a similar analysis will be performed with ATLAS to compare the weight prediction trends used by the two methods.

In the following paragraphs, the formulation of the performance model and the design inputs that were chosen are presented.

For consistency reasons, the engine performance model used in the present analysis is similar to the one used to evaluate the existing preliminary weight estimation methods in chapter 2. It represents a characteristic short-range, two-spool turbofan with a booster compressor engine and its main characteristics were presented in table 2.9.

Similarly to the WATE study, the cruise BPR and TET were selected as variables, based on their influence on engine weight. The former was varied from two to 30, aiming to present trends and physics at very high BPR engines, while the latter ranged between $1200\,K$ and $2000\,K$, capturing values for contemporary and future engines. More details about the present performance model can be found in the work of Giannakakis[53].

As presented in the previous chapter (3), in order to achieve a weight prediction based on the performance input, ATLAS requires additional design related

inputs and assumptions. The assumptions follow the guidelines suggested by gas turbine books[58;56] and are presented in table 4.8. On the other hand, the design inputs have CFM56-7B27 as a basis and were adjusted in order to be similar to the ones used by WATE. These are summarised for the main components in tables 4.9, 4.10, 4.11, 4.12 and 4.13.

Table 4.8: Basic preliminary design code assumptions

Parameter	Value
Fan inlet axial Mach	0.6
Fan inlet h/t	0.32
Fan inlet tip Mach number limit	1.6
Booster configuration	Constant hub
Booster inlet Mach number	0.5
HPC configuration	Constant tip
HPC inlet Mach number	0.5
HPT configuration	Constant mean
HPT inlet Mach number	0.1
HPT outlet Mach number	0.45
HPT AN^2	$30 \cdot 10^6$ $[rpm^2 m^2]$
HPT maximum loading coefficient	2.6
LPT configuration	Constant hub
LPT inlet Mach number	0.45
LPT outlet Mach number	0.40
LPT maximum loading coefficient	2.5

Table 4.9: FAN design inputs

Configuration	Constant tip
Inlet Mach number	0.7
Inlet hub to tip ratio	0.32
Rotor Aspect Ratio (AR)	2.2
Stator AR	2.8

Through use of the above mentioned performance and design inputs, the fan diameter and engine weight are estimated by ATLAS for the range of BPR and TET values (Fig. 4.8).

The trends emerging from this analysis are similar to the ones produced by NASA's WATE, signifying that these two approaches follow roughly the same

Table 4.10: Booster compressor design inputs

Configuration	Constant hub
Inlet Mach number	0.5
Inlet hub to tip ratio	Input from fan outlet
Rotor AR	2.0
Stator AR	1.2

Table 4.11: HPC design inputs

Configuration	Constant mean
Inlet Mach number	0.5
Inlet hub to tip ratio	0.725
Rotor AR	2.9
Stator AR	2.9

Table 4.12: HPT design inputs

Configuration	Constant mean
Inlet Mach number	0.1
Inlet hub to tip ratio	Input from combustor outlet
Rotor AR	1.88
Stator AR	1.3

Table 4.13: LPT design inputs

Configuration	Constant hub
Inlet Mach number	0.3
Inlet hub to tip ratio	Input from HPT outlet
Rotor AR	6.8
Stator AR	1.85

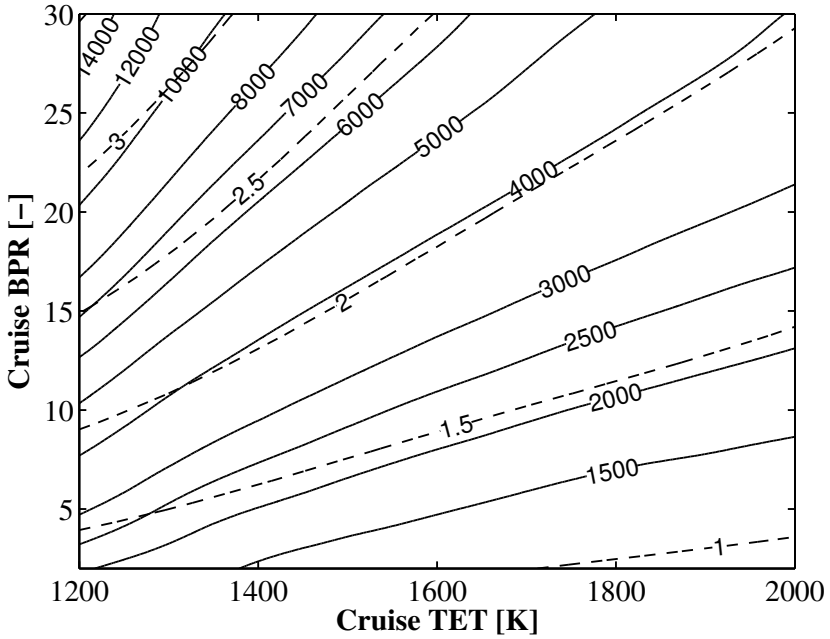

Figure 4.8: 2-spool boostered turbofan weight prediction $[kg]$.
Dashed lines: engine diameter $[m]$

physics. However, ATLAS and WATE present these similar trends by utilising different design methodologies for the same components, with different assumptions and required inputs. Therefore, there is a small difference at the inclination of the iso-weight and iso-diameter lines, but also a more significant difference at the absolute weight and fan diameter estimations. The most characteristic example of the diversity of design approaches by the two methods, which also has a great influence on the total engine weight, is the fan diameter, which is a direct result of WATE designing the fan at take-off, whereas ATLAS uses the top of climb as the fan design point.

Despite these inconsistencies between these methods, it can be said that ATLAS is capturing sufficiently the weight variations, when two of the most significant design values, the BPR and the TET, are varied.

4.4 Summary and Discussion

The present chapter showed that ATLAS can predict accurately the weight of existing engines, by testing it against two major turbofan engines, that integrate different design characteristics. Furthermore, when compared against a similar existing method (NASA WATE), showed matching weight breakdown values for CFM56-7B27, verifying that the component weight estimation methods provide valid results. Finally, ATLAS exhibited also realistic weight and diameter trends, when BPR and TET are varied.

The above results show that ATLAS is capable of accurate weight predictions, but the amount of cases tested was limited and should be further expanded. However, for the purposes of the present work, the above verification of the method was sufficient and it was not pursued further. This task will be included in the suggestions for further work, even though, due to unavailability of engine design data, component weights and parametric weight studies, the full validation of the method is a challenging mission. For this reason, cooperation with an OEM, that can provide component weight data, is recommended.

Furthermore, the disk shapes of the simulated engines are smaller or larger than expected in some components. The blade fixation, which is a function of the chord and not of the centrifugal load, was identified as the cause and its implementation would significantly improve the component weight estimation.

A sensitivity analysis on the component weight and their participation in the total engine weight will help identify the critical components for improvement and raise the method accuracy.

Finally, a sensitivity analysis as part of the future work, in order to evaluate the effect of design and performance parameters on engine weight, will shed some light on a remarkably unexplored area.

Chapter 5

Geared turbofan feasibility analysis

5.1 Introduction

In contemporary two-spool configurations, as was shown in the previous chapters, the rotational speed of the low pressure shaft is restricted by the fan geometry, aiming to provide acceptable compressibility losses and mechanical stresses[58]. Therefore, in this DDTF configuration, the LPT is directly coupled with the fan, resulting in increased stage count for a given power output. The rotational speed limitation affects also, but to a smaller extent, the booster compressor, which is connected at the LP shaft as well. This limitation is considered to result not only in direct increase of the weight and length of the engine, but also indirect, since the sizes of the support structures and the shafts are also modified to accommodate the bigger components[95].

Furthermore, the ACARE performance targets point towards even higher fan diameters, rotating at slower speeds due to aerodynamic and mechanical integrity restrictions. This will further increase the LPT stages and therefore the weight for the DDTF configuration[53], dramatically impacting the installed performance and negating all potential benefits. An appealing proposed solution to this problem is the GTF configuration, aiming to achieve higher fan diameters with limited

weight increase by decoupling the fan from the LPT and booster through the introduction of a gearbox.

The feasibility of this configuration depends on the installed performance that is a function of the SFC, weight and drag of the engine. In this context, even though the optimum GTF configuration may be heavier than the DDTF, the desirable weight benefit by reducing the LPT and booster stages is reduced by the weight increase associated with the gearbox and its accessories. Moreover, the GTF effect on fan and LPT efficiency also need to be taken into account, since they can vary significantly from a similar DDTF.

The present study presents the LPT performance, aerodynamics and mechanical integrity benefits and challenges arising at high and very high BPR engines. Design improvements and the GTF novel configuration are examined as options to raise the LP shaft rotational speed downstream of the fan.

Focusing on a short range 2-spool turbofan engine, the examined configurations are evaluated and the design space is explored by considering the aerodynamics, mechanical integrity and installed performance of the engine.

5.2 Engine model

The 2-spool boostered turbofan engine, analysed for the verification purposes of ATLAS, is the engine model that will be used in the present study and will be referred to as baseline in the following sections. The thermodynamic performance of the engine is kept the same for consistency, but the design inputs are expanded to introduce a gearbox between the fan and the booster in the GTF configuration. The gear ratio is not fixed, but the fan, booster and LPT are permitted to rotate at their maximum allowable speed according to the design choices and selected limits. Furthermore, contrary to the common practice, due to tool restrictions, it is assumed the fan diameter does not change when the gearbox is introduced.

In order to improve the clarity of the results and effectively illustrate the changes in engine performance and design with the introduction of a gearbox, only a selection of BPR and TET combinations are examined. Therefore, the present

study considers engines with BPR values of 4, 10, 14 and 18, which are considered to cover "modern", "immediate future" and "distant future" engines. For each one of these BPRs, three TET values (1400, 1600 and 1800 K) corresponding to "low", "medium" and "high" are also examined.

It is assumed that all the examined cases have the same thrust requirements and the FPR is optimised to achieve minimum SFC values.

The LP shaft rotational speed at the DDTF is dictated by the fan diameter and since its design and performance parameters are kept constant for the two engine configurations (DDTF and GTF), both of them have identical fan design and weight for given BPR and TET values. Similarly, the gas generator components (HPC, combustor and HPT are not modified with the introduction of the gearbox.

In order to minimise the variables, the velocities at the inlet and outlet of the LPT are kept constant for all BPR and TET combinations. During an engine design process, these will be adjusted to achieve better performance, even though in most cases higher Mach number values are not desirable due to associated losses and reduced power output per stage.

5.3 Performance and aerodynamics

5.3.1 Baseline configuration

In the previous chapter (Sec. 4.3.3), it was shown that for the DDTF configuration, the increase in BPR results also in bigger fan diameters restricting the LPT rotational speed. This speed decrease, apart from increased stage count, due to lower temperature drop per stage for a given stage loading, results also in modified stage efficiency, since the flow coefficient also varies.

Figure 5.1 presents the variation in stage efficiency for the DDTF configuration at the penultimate LPT stage, because at the engine model the last stage loading is reduced to satisfy the assigned outlet velocity angle. As expected, the flow coefficient increases with increasing BPR, as a result of decreasing blade

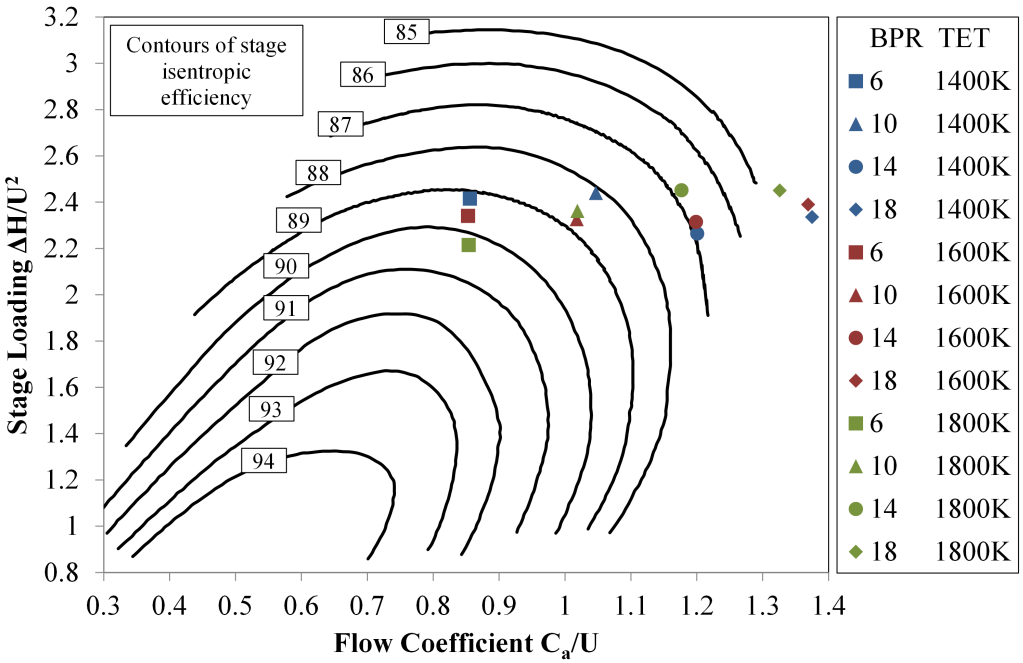

Figure 5.1: DDTF Smith chart

speed, resulting in turn in a significant stage isentropic efficiency drop. The TET variations have a small effect on the positioning of the engines on the Smith chart, since the stage loading is set to achieve the same target value in all designs.

As a solution to this problem, Kurzke[96] suggests that an efficiency target can be maintained, simply by increasing the number of stages. However, this approach is expected to move the points on figure 5.1 parallel to the y axis with small changes in flow coefficient. Therefore, at low BPR values the above assumption is valid and almost any stage isentropic efficiency target can be achieved. However, at higher BPR ratios, the engines lie on the right hand side of the Smith chart and is not possible to achieve high efficiency values if only the loading is modified.

The stage isentropic efficiency drop observed in this case is considered prohibitive at higher BPR values, but could be restricted with an increase in LPT blade speed and subsequent decrease of the flow coefficient. Since blade speed is a function of diameter and rotational speed, modifying either one of them could lead to the desired result.

5.3.2 LPT outlet tip diameter adjustment

In order to achieve higher blade speed, the modified LPT outlet tip diameter option is explored in this section. Considering that the last stages of the turbine are influenced more by the rotational speed restriction and for consistency purposes, the inlet dimensions were kept unaltered.

Therefore, following the engine design approach, a LPT stage efficiency target was set at 0.89 (close to the optimum value) and the LPT outlet tip diameter was adjusted to achieve it, as presented in figure 5.2. However, considering that in turbofan engines the LPT outlet diameter is usually restricted by the bypass duct inner diameter, a set of more "realistic" isentropic stage efficiencies for each engine were also calculated with this restriction (Fig. 5.3).

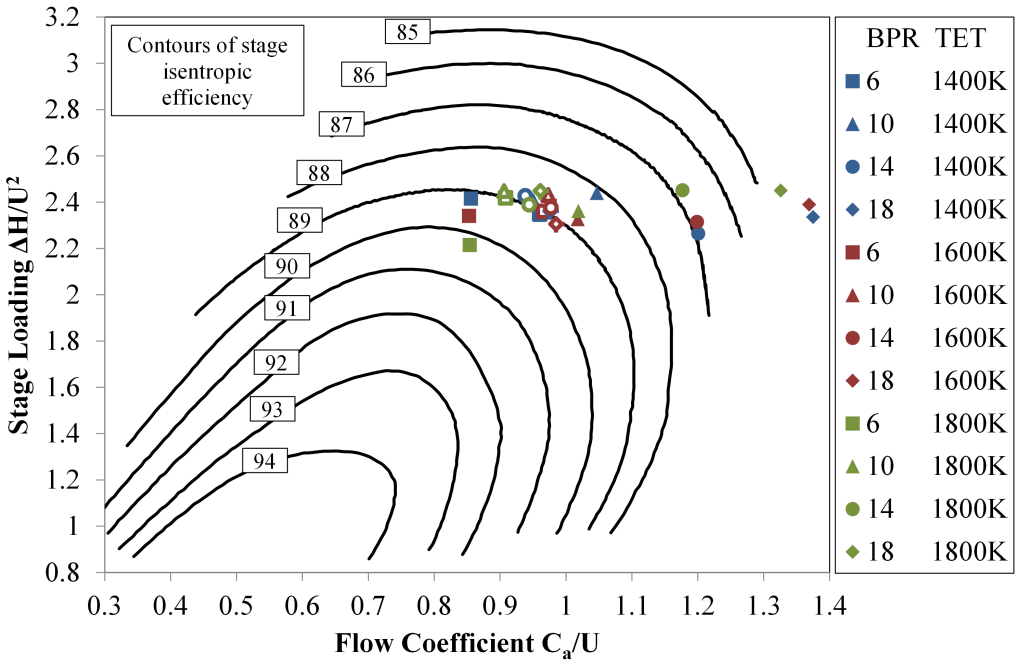

Figure 5.2: DDTF Smith chart. LPT outlet tip diameter increase for 0.89 stage isentropic efficiency (points with no fill)

For the lowest BPR engines that were examined (6), the LPT outlet diameter change dispositions the points on the Smith chart to lower stage isentropic efficiency values for both diameter adjustment variants, indicating that a diameter modification is not required in this case. On the other hand, at higher BPR

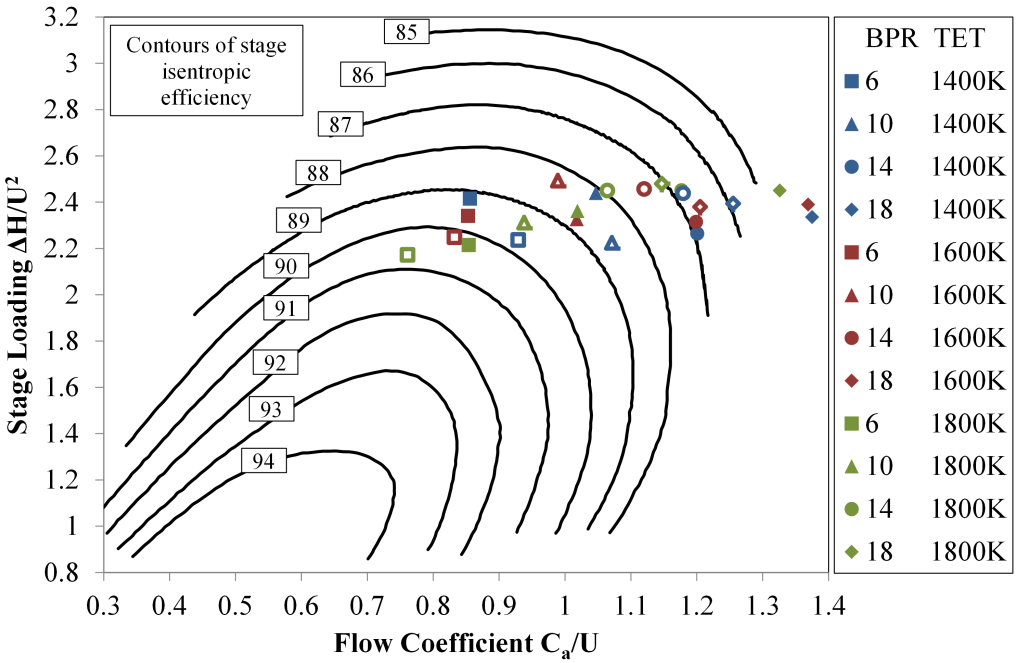

Figure 5.3: DDTF Smith chart. LPT outlet tip diameter increase (points with no fill)

values, the flow coefficient drops, improving thus the stage isentropic efficiency. However, at the bypass duct constrained case, the flow coefficient decrease is small and fails to achieve the expected high stage isentropic efficiency values for modern and novel engines.

In order to highlight the limitations of diameter adjustment, the LPT outlet tip diameter is presented in figure 5.4 for both examined variants. In line with what was observed on the Smith chart, in order to maintain an efficiency target, the LPT outlet tip diameter (dashed lines) has to increase as the BPR increases for a given TET, forming an almost linear correlation. Furthermore, as the TET increases, the required diameter is lower, since the fan diameter also drops, as shown in the previous chapter, allowing thus for higher rotational speed. Interestingly, at higher BPR values, the required diameter adjustment is higher for lower TET values, following also the fan tip diameter variations of figure 4.8.

The dashed lines that represent the LPT outlet tip diameter, when restricted by the bypass duct inner diameter, are similar to the efficiency target lines, but with a different slope. Therefore, the lines for the two variants cross, indicating

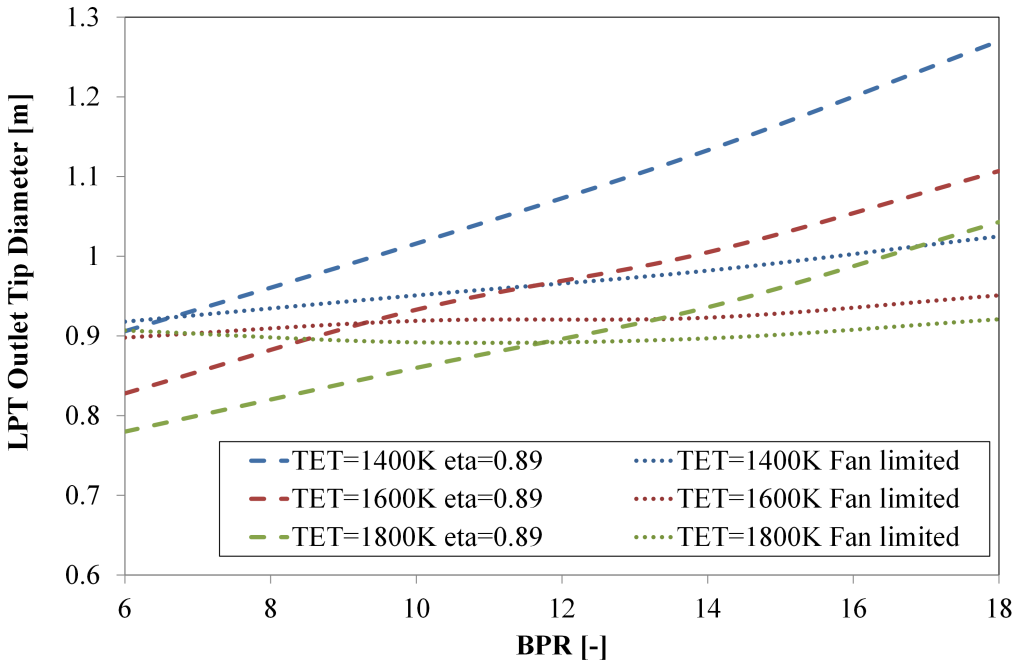

Figure 5.4: LPT tip diameter

the technology limit for the given efficiency target. The diameter adjustment option is not viable for low TET (1400), even for the modern engines at the lowest examined BPR value. On the other hand, the increase of TET allows this option to be used for higher BPRs, but it still requires extreme temperature values in order to achieve the target stage isentropic efficiency values.

Considering that the future engines aim for higher BPR values, it is evident that the allowable LPT outlet tip diameter increase is not sufficient in order to maintain high LPT stage efficiency values at high BPR values.

The bypass inner diameter that was used is not considered a "hard" limit by engine designers, but the LPT maximum diameter can slightly exceed this value. At high BPR values, the required diameter increase is significant and this allowance is not sufficient, but could be sufficient at lower values. However, despite the blade speed improvement potential, the "interaction" with the bypass duct is causing either an increase of velocity due to reduction in area in case the outer diameter is kept unchanged, or a turn of the flow and increased bypass duct outer diameter. Both these cases involve undesirable losses, with the latter also introducing increased drag and challenges in nacelle aerodynamics and in-

stallation under the aircraft wing. The feasibility of this option relies mainly on absolute dimension numbers and it was not considered in the present study, since the focus is mainly on examining trends .

In case a tip diameter increase at the LPT outlet is feasible and considered, the increase in stresses due to higher centrifugal load needs to be taken into account. This forces a weight penalty due to the requirement for heavier disks and stiffer blades that potentially can negate any benefit this design choice might have.

Along with the increase of the LPT outlet diameter, an increase of the inlet diameter is also desirable to raise the blade speed of the front stages as well. In most cases this requires a S shaped duct between the upstream component and the LPT, introducing losses, weight and complexity. However, the reduction in stages and the overall LPT efficiency improvement can still outweigh the incurred penalties. This approach is similar to the outlet diameter adjustment and was not examined in detail.

5.3.3 Rotational speed adjustment

Having established that the LPT outlet diameter adjustment is not always feasible or sufficient to achieve the required stage isentropic efficiency at the LPT, it is evident that the other parameter in blade speed needs to be modified when the BPR increases. As mentioned above, one of the enabling technologies that increases the LPT rotational speed is the introduction of a gearbox at the LP shaft (Fig. 5.5).

Figure 5.6 presents the percentage difference in rotational speed between the baseline engine and its geared version, where the turbine rotates at its maximum allowable speed. The rotation speed increase correlates almost linearly with BPR for a given TET and as expected, at higher BPRs the rotational speed increase is bigger, attributed to the restricted LPT rotational speed due to fan limitations at the DDTF configuration.

Furthermore, at low BPR values the benefit is almost similar for all TET values, but there is a significant difference between the lines at the right side

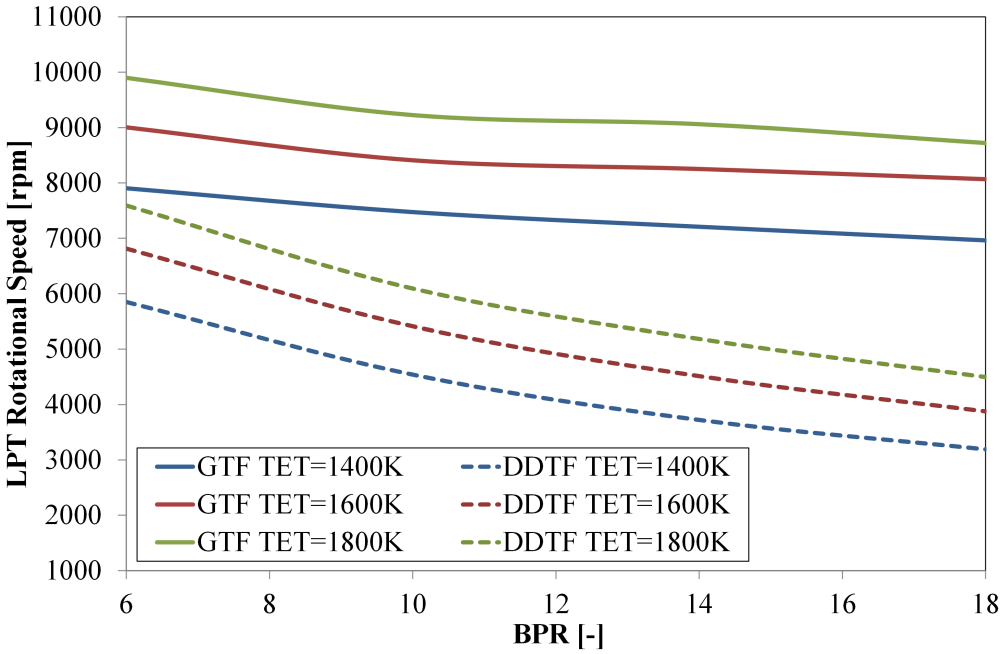

Figure 5.5: LPT rotational speed for the GTF and DDTF configurations

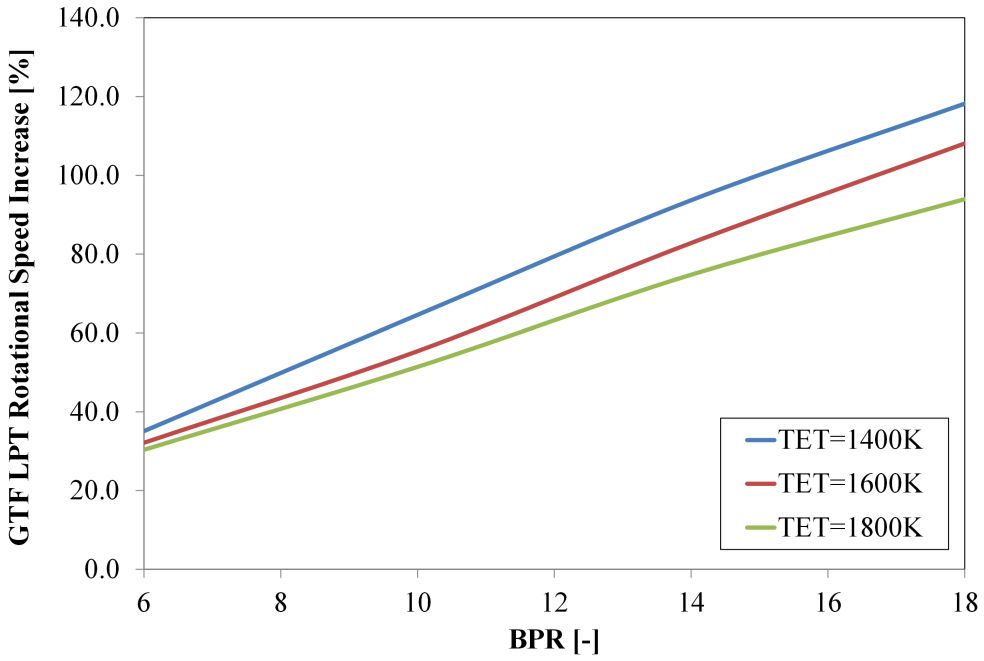

Figure 5.6: GTF LPT rotational speed percentage difference from DDTF

of the plot. This is merely a reflection of the fan tip diameter (Fig. 4.8) that constrains the rotational speed at the DDTF configuration and is more dependent on TET at high BPRs. Higher TET values imply also a smaller core, which in turn for a given BPR defines a smaller fan tip diameter that allows higher rotational speed at the LP shaft.

This remarkable increase in LPT rotational speed, achieved by introducing a gearbox, is also depicted in figure 5.7, which illustrates the change in LPT stage isentropic efficiency between the DDTF and GTF configurations. Due to this increase, the flow coefficient was reduced for all cases improving thus the isentropic efficiency. More importantly, due to similar LPT outlet parameters for all the examined cases, the flow coefficients assume similar values and the efficiency value is mostly determined by the stage loading, which depends on the number of stages.

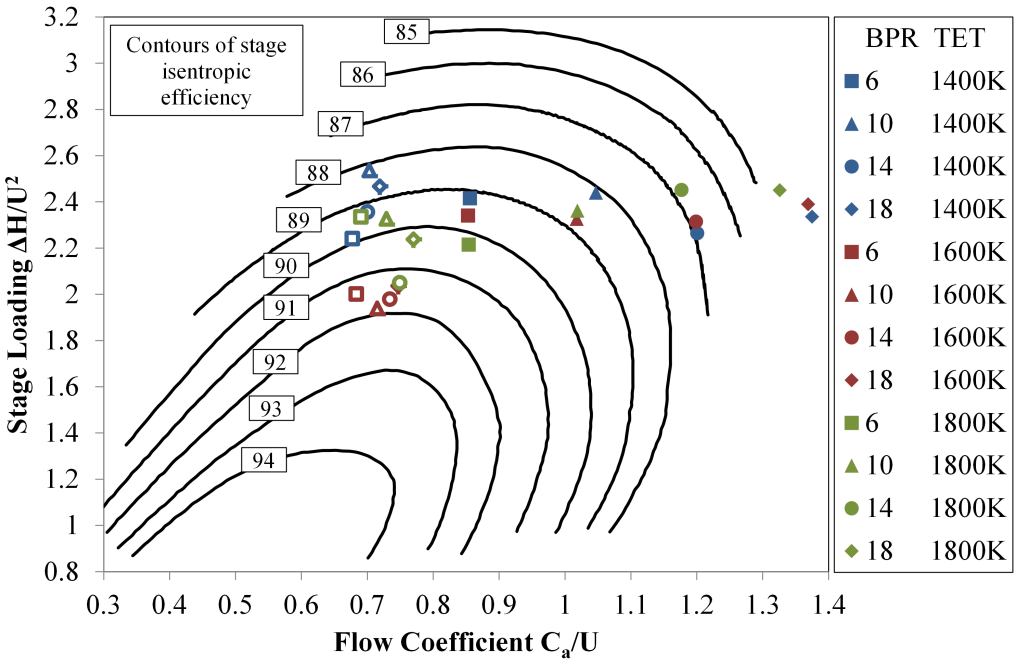

Figure 5.7: DDTF (filled points) comparison with GTF (no fill points) Smith chart.

Therefore, it is evident that the GTF configuration enables higher LPT stage isentropic efficiency values for high BPR engines than the ones achieved with the LPT outlet diameter adjustment. Furthermore, the design space is now shifted

to the left of the optimum line on the Smith chart, to the area where usually HPT designs are found, a behaviour also observed and confirmed in other similar studies[97].

Apart from benefiting the LPT efficiency, the introduction of a gearbox can also allow the reduction of the fan rotational speed and enable the use of bigger fan diameters with higher BPRs and improved propulsive efficiency. Most likely, this would also increase the engine weight, since apart from the heavier fan, heavier support frame, bearings and nacelle are required. As a result, the trade-off between SFC, drag and weight should be examined in this case.

Due to the absence of a loss model in the fan model and the complexity of the calculation, this option was not examined in the present study. Therefore, as will be shown in the next paragraphs, the gear ratio of the gearbox is slightly lower than the one used in only available GTF engine.

5.4 Mechanical integrity

The LPT rotational speed increase achieved with the GTF configuration is not only affecting the engine performance and aerodynamics, but also the mechanical integrity, size and weight of the engine components.

The component that is affected most by changing to a GTF configuration is the LPT turbine, since in the adopted engine model it is assumed to rotate at its optimal speed, which was restricted by the fan at the DDTF case. The higher rotational speed increases the centrifugal load at the blades and therefore increases the stresses on the disks as well. This blade and disk stress increase has an adverse effect on the size and weight of most LPT parts.

Since the LPT outlet diameter increase was proven inadequate at high BPRs from the performance and aerodynamics point of view, it will not be examined in the present section.

5.4.1 LPT mechanical integrity and weight

In the selected engine model, the LPT rotational speed is restricted by the product of outlet area and the square of rotational speed. This empirical parameter, commonly known as AN^2, is associated with blade and disk stresses[58], with the high values corresponding to highly mechanically loaded turbines.

However, as shown above, at the DDTF configuration this is not the limiting factor, as the LPT rotational speed is dictated by the fan diameter. On the other hand, at the GTF configuration, where the LPT is allowed to rotate at its maximum allowable speed, the assumed AN^2 limit of $30E6\, rpm^2 \cdot m^2$ is always reached and therefore the blade centrifugal load is higher. Figure 5.8 confirms, by using AN^2 at the last stage as the most characteristic value, that in all DDTF examined cases, AN^2 is lower than the GTF limit, with values matching the ones quoted by similar studies[96]. As expected, the stresses drop with increasing BPR, but rise with increasing TET, following a trend identical to the LPT rotational speed (Fig. 5.5).

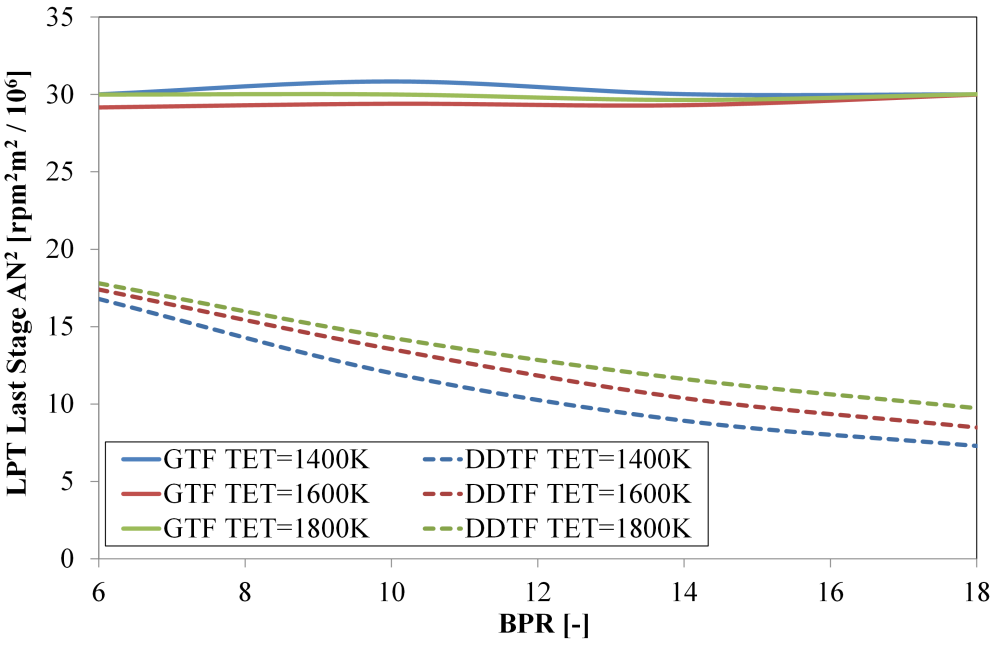

Figure 5.8: LPT last stage AN^2

AN^2 though is only an empirical parameter, used primarily at the early design

phases and gives a rough estimation of the turbine stress level. On the contrary, the disk rim stress(Equation 3.58) takes also into account the flowpath diameter and the blade height and chord, providing a more accurate estimation of the stress level, but the required inputs do not allow its use at very early design phases. Figure 5.9 shows that the disk rim stress for the DDTF follows a similar trend as the AN^2, indicating that any of those could be used. On the other hand, the lines at the GTF variant don't remain constant, as is the case with AN^2, a difference attributed mainly to the flowpath diameter, which is also responsible for the bigger distance between the iso-TET lines in both cases.

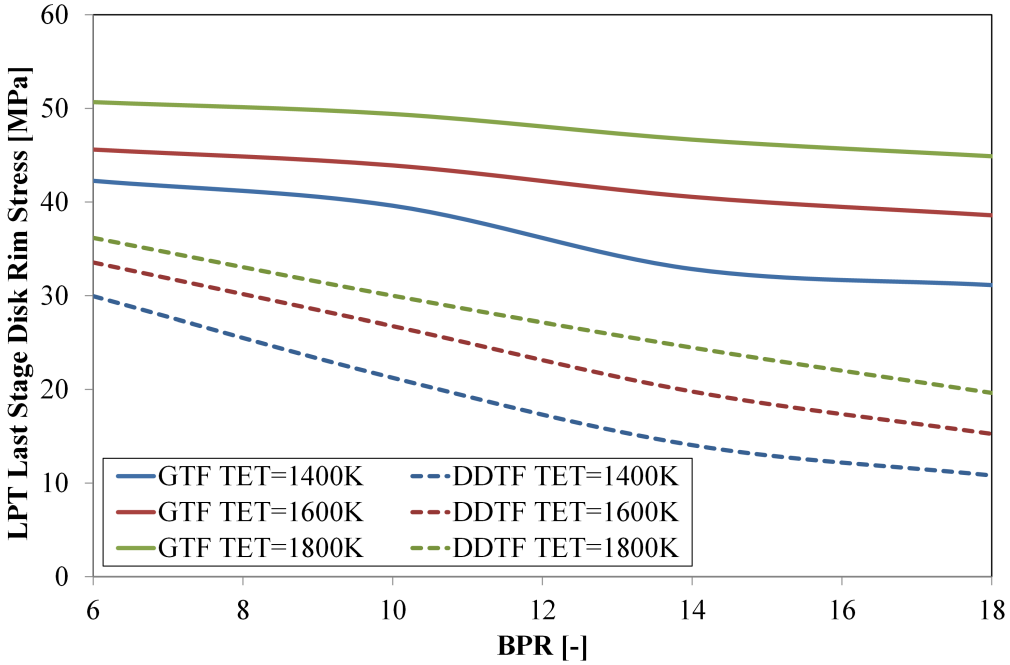

Figure 5.9: LPT last stage disk rim stress

The increased stress levels at the GTF configuration are associated, as expected, with increased LPT disk weight, as presented in figure 5.10, which shows the average LPT disk weight for the DDTF and the GTF engines.

However, in the used engine model, this weight penalty is less than the weight benefit due to LPT stage reduction when a gearbox is used. This is shown by the LPT weight difference between the two configurations (Fig. 5.11), which increases greatly with increasing bypass ratio, where the biggest stage decrease

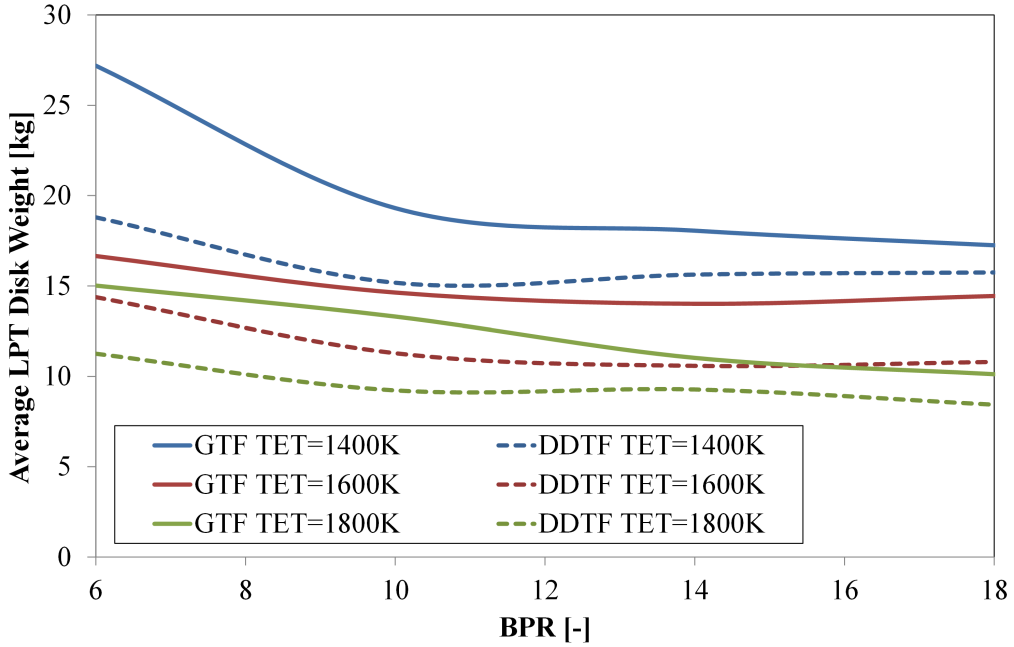

Figure 5.10: LPT average disk weight

is observed (Fig. 5.12).

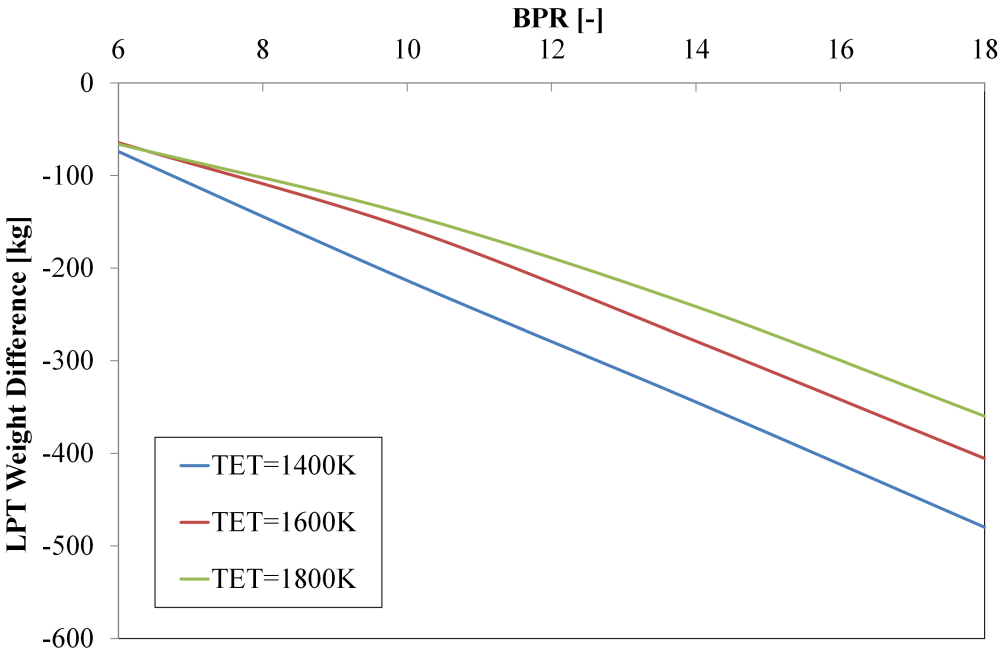

Figure 5.11: DDTF and GTF LPT weight difference

As a conclusion, the weight increase of the LPT disks, which are a significant

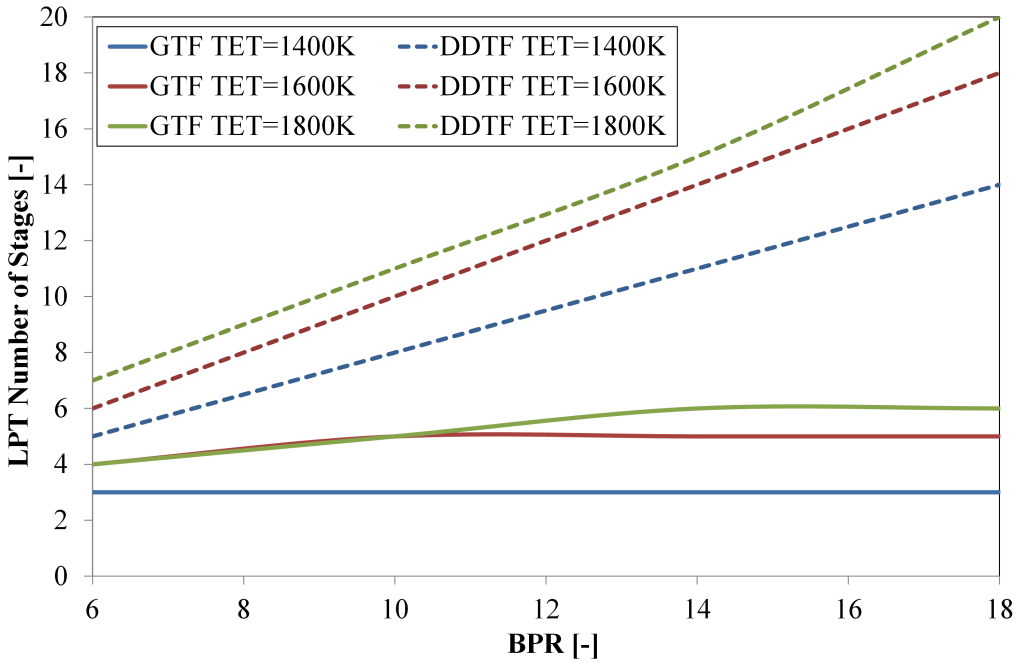

Figure 5.12: LPT number of stages

portion of the LPT total weight, when the LPT rotational speed is increased by using a gearbox, is outweighed by the reduced number of stages for the current engine model and weight estimation method. However, a more detailed mechanical integrity assessment of blades may reveal that their weight is also increased, due to the high stresses, reducing the LPT weight benefit. Furthermore, the increased loads may have an adverse effect on the frames and shafts weight, resulting in larger overall engine weight.

5.5 Shafts and frames weight

Apart from the LPT turbine weight, other components such as the booster compressor, the shafts and the supporting frames are affected by the change in rotational speed in the LP shaft.

As presented in chapter 3, the efficiency of the compressors and fans is imported from a performance code and is affected by the design related parameters, such as the rotational speed. Therefore, due to the absence of a high fidelity efficiency model for the compressors in the weight estimation method, that could

quantify more accurately the benefits at the booster compressor, the weight analysis on this component could be misleading and will not be presented in this section.

The LP shaft weight, since the gas generator is identical, is presented in figure 5.13 for both DDTF and GTF configurations. Considering that the LPT power output is the same for these, the higher rotational speed at the LP shaft should result in smaller shaft diameter and therefore to lower weight for the GTF engine, according to equation 3.84. However, in the used engine model, the rotational speed has a small contribution to the LP shaft weight, with the shaft length due to the stage reduction being responsible for the weight difference between the two configurations (Fig. 5.14). This point needs to be revisited as soon as the shaft sizing method is improved, as proposed in the future work section, or if a hollow inner shaft assumption is followed to verify that it is still valid.

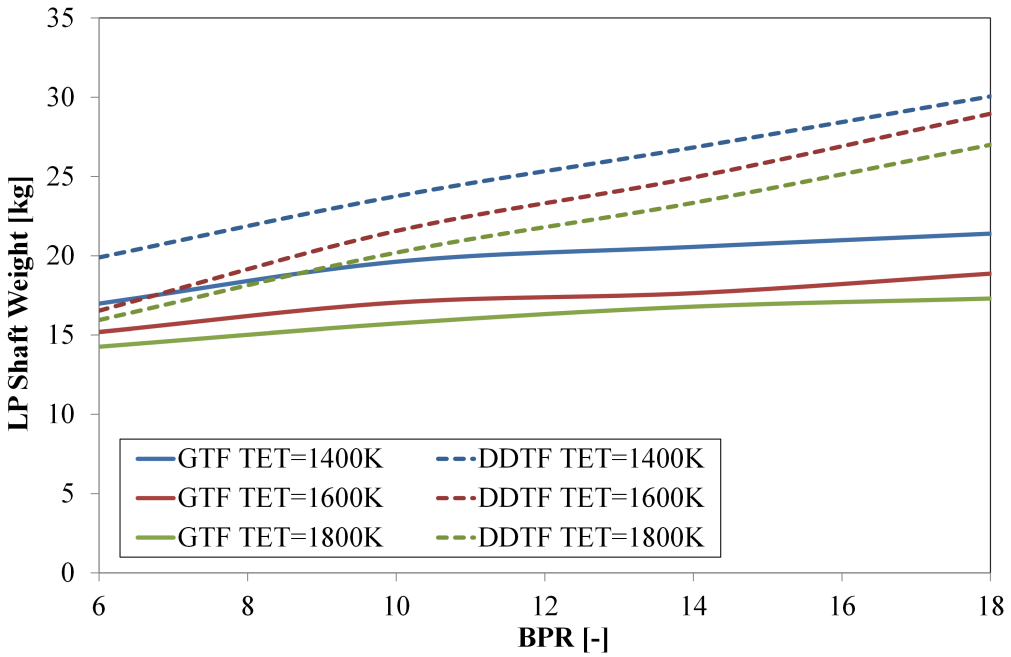

Figure 5.13: LP shaft weight

Contrary to the shaft weight estimation method, the frame method used is an empirical correlation, with the frame diameter being the only input variable. Therefore, it shows only a small weight change at the GTF configuration (Fig.

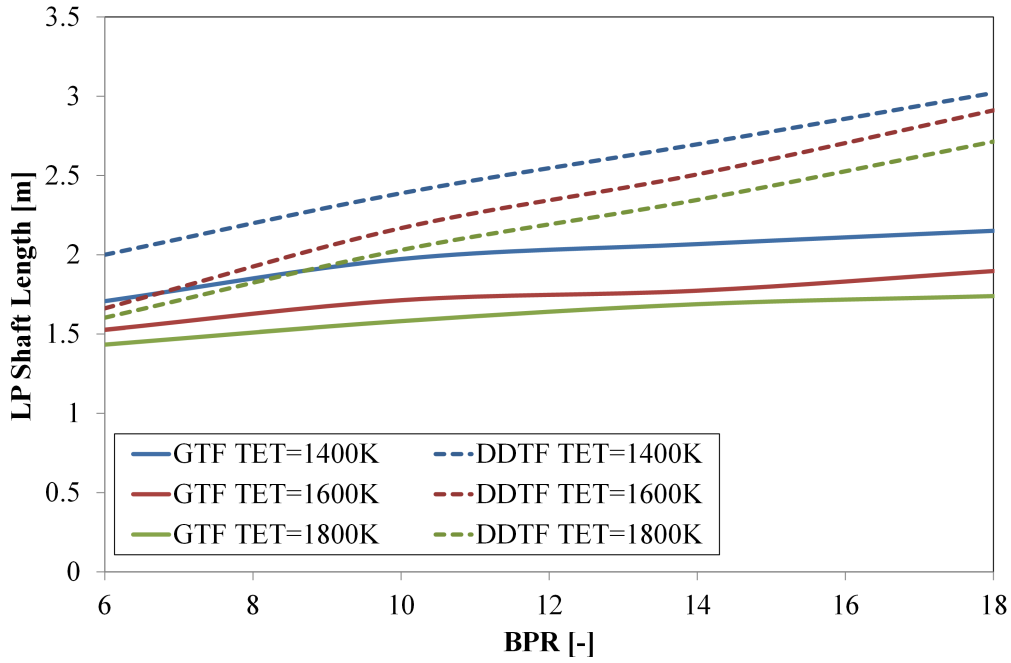

Figure 5.14: LP shaft length

5.15), attributed to the LPT outlet pressure adjustment that affects the component diameter.

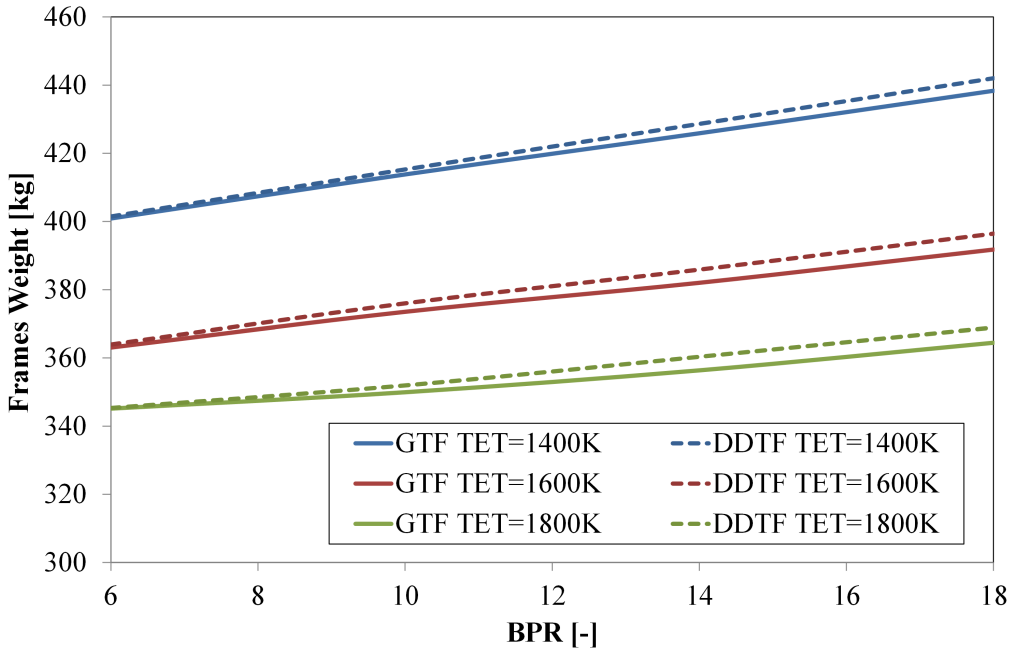

Figure 5.15: Sum of frames weight

The smaller size GTF engine, due to the lighter and shorter LPT, would be expected to require smaller support frames, despite the increased stresses in some components. However, the introduction of the gearbox calls for an extra housing to accommodate it and all its accessories, such as the oil system.

The complexity of the frame weight calculation, due to the variety of designs, and the absence of solid empirical correlations that also account for geared concepts, prohibit the detailed analysis of the frame weight trends.

Overall, the shaft and frame weight variations, in the present study, are small when compared with the weight decrease due to the LPT stage reduction. However, more detailed design and weight estimation methods are required for these components.

5.5.1 Gearbox weight

In the previous sections it was established that the use of a gearbox is not only necessary to achieve acceptable LPT efficiency in high BPR ratios, but also contributes towards reduced LPT weight. However, the gearbox and its accessories are introducing a weight penalty, which reduces the potential benefit due to weight reduction. Even if the total engine weight for the GTF is higher than the DDTF, the design could still be feasible if the installed performance is considered.

The gearbox weight for the GTF engine cases is presented in figure 5.16. Even though, it is rising with increasing BPR for all TET values, the higher TET engines require a heavier gearbox at low BPR values, a trend that is reversed at high BPRs, where the low TET engines have heavier gearboxes.

The gearbox weight estimation method (3.3.10) uses higher order equations and therefore understanding the influence of each of the three input parameters, in order to explain the gearbox weight trends, is not a straightforward task. Therefore, the LPT torque and the gearbox gear ratio are presented in figures 5.17 and 5.18 respectively as a function of BPR for the three examined TET values. The rotational speed, which is the third input parameter, has been already presented (Fig. 5.5) and shows a slightly falling trend as BPR rises, contrary to

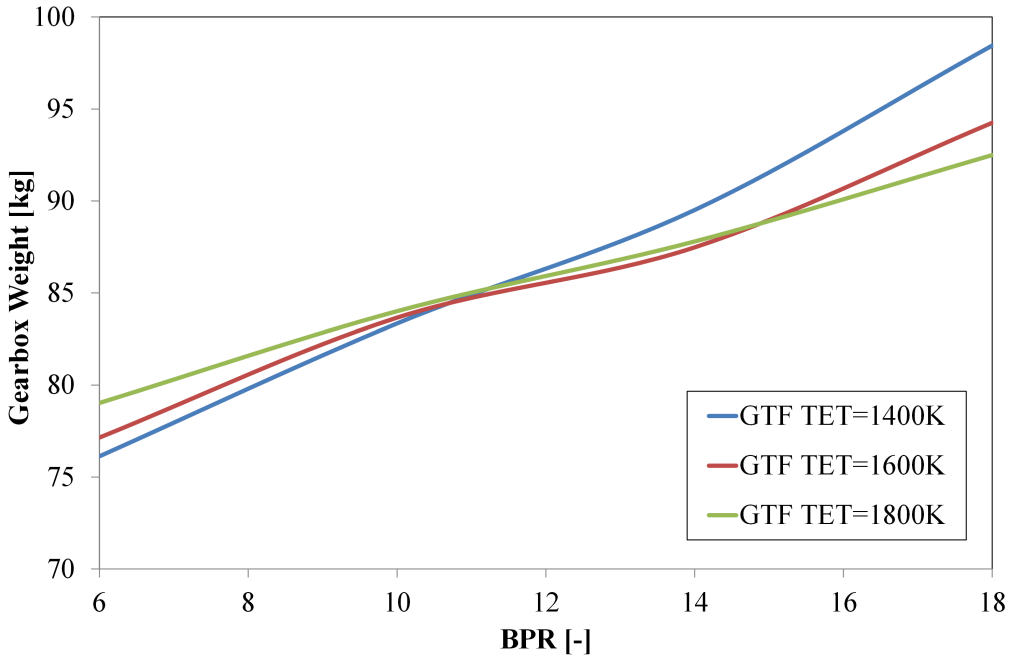

Figure 5.16: Gearbox weight

the rising trend observed for the TET.

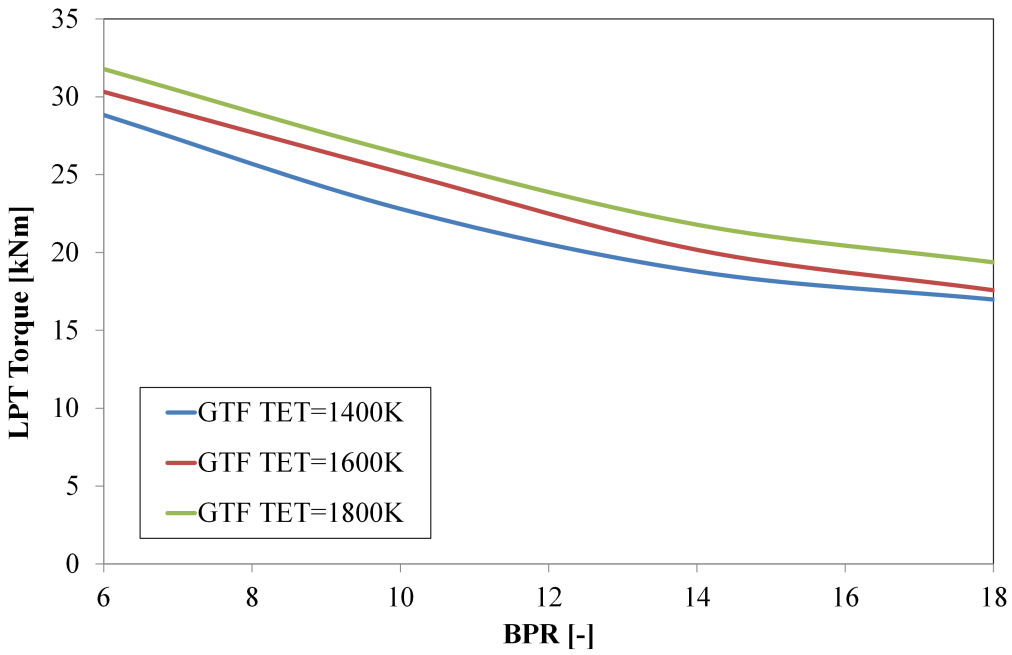

Figure 5.17: LPT torque

The LPT torque has a trend similar to the rotational speed, but the gear

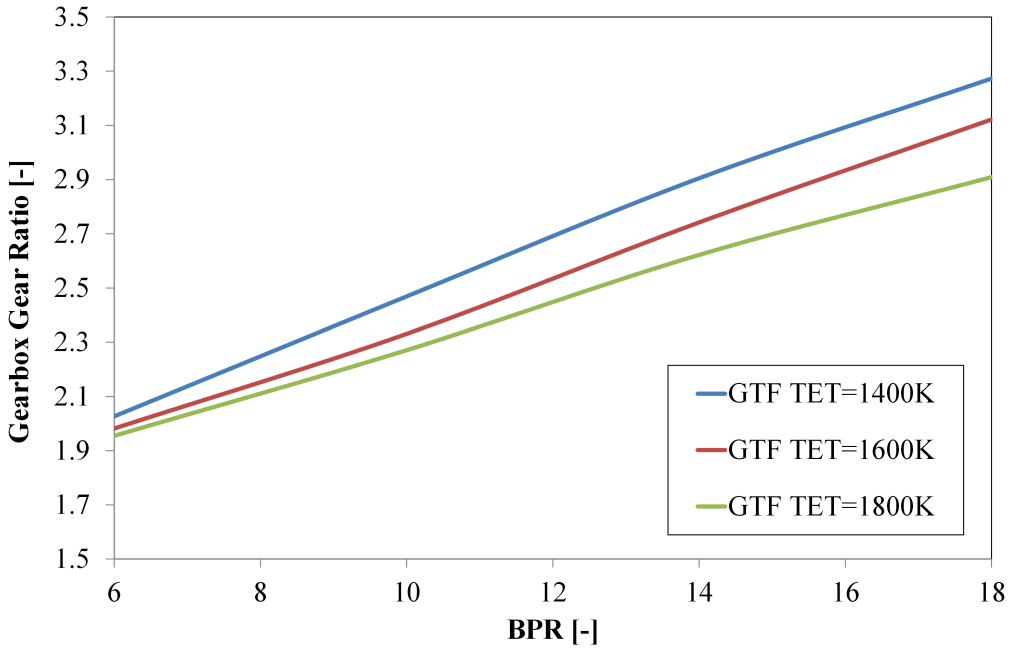

Figure 5.18: Gearbox gear ratio

ratio increases almost linearly with BPR. Furthermore, contrary to the other two variables, the gear ratio is higher at lower TET values, following the rotational speed increase between the DDTF and GTF configurations (Fig. 5.6).

Therefore, the gearbox weight for the chosen engine is primarily influenced by the gear ratio, since they both show rising trends with increasing BPR. The phenomenon that the low TET engines have heavier gearboxes at low BPR values, shows that at that area of the chart the other two parameters play a bigger role in the calculation of gearbox weight.

The estimated gearbox weight, along with its accessories, has to be compared with the weight benefit to define the feasibility of the GTF configuration. Figure 5.19 presents the total engine weight for both configurations, including the gearbox weight, but not its accessories due to lack of a calculation method or public data. In all examined cases, the weight reduction achieved by increasing the LPT rotational speed is greater than the weight of the gearbox. The weight benefit is greater at higher BPR values, proportional to the rotational speed increase (Fig. 5.6), contrary to the TET having a minimal influence on it.

However, in order to reach a verdict about the feasibility of the GTF con-

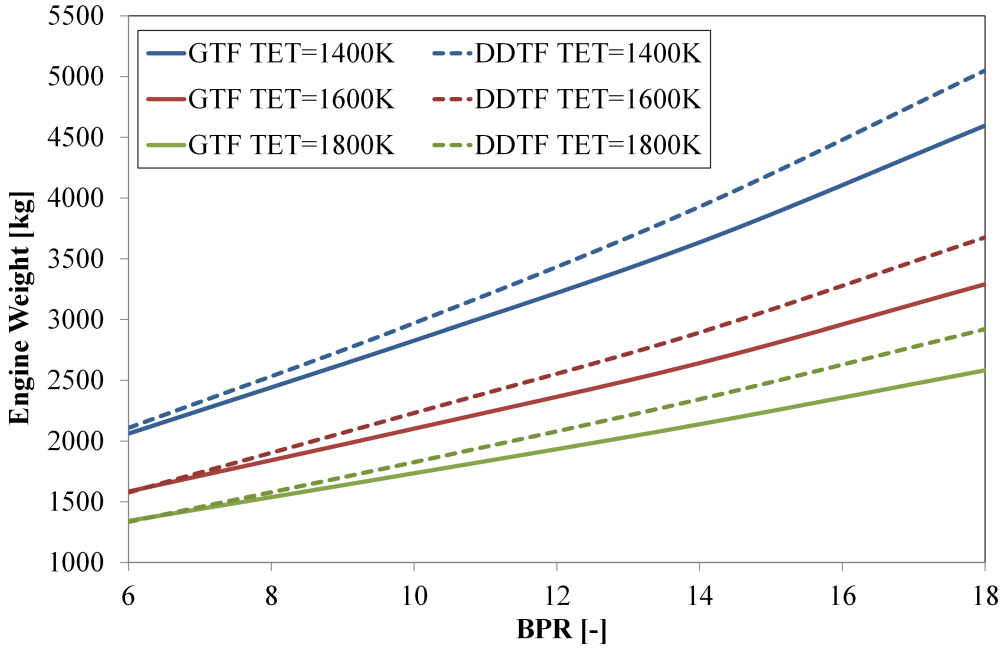

Figure 5.19: DDTF and GTF total engine weight

figurations, the weight penalty of components that don't have a detailed weight estimation method or have a method that wasn't designed for such engines has to be taken into account. These primarily include the gearbox accessories, that are not included in the study, and the frames, that are based on an empirical calculation, but contribute to the gearbox support and fixation in the engine. Therefore, it is only safe to say that the GTF configuration is feasible if these weight penalties don't exceed the weight benefit. Since the benefit is small at lower BPR values, care should be taken into that area of the plot, where it is more likely that the introduction of the gearbox is not beneficial.

5.5.2 Installed performance

The weight reduction benefit of the geared turbofan is reflected at the installed performance of the engine and more specifically at the installed SFC parameter. This is estimated by also taking into account also the nacelle weight and the engine drag, both functions of the engine outer dimensions.

However, instead of using the installed SFC, the installed engine performance

is evaluated using the range factor (K_{range}), as proposed by Walsh and Fletcher[58] and used in an earlier study by Giannakakis[53]. It is defined as the ratio of the installed engine (WT_{eng}) and fuel weight (WT_f) to the engine cruise thrust (FN_{cr}) reduced by the nacelle drag (Dr_{nac}) (Equation 5.1. Lower values of the range factor correspond to more fuel efficient engines.

$$K_{range} = \frac{WT_{eng} + WT_f}{FN_{cr} - Dr_{nac}} \tag{5.1}$$

The weight of the fuel is calculated by equation 5.2 as a function of the cruise thrust (FN_{cr}), the cruise SFC (SFC_{cr}), the aircraft range ($Range$) and the flight velocity (V_{cr})[58]. All these input parameters are calculated during the performance simulation, apart from the aircraft range that is selected accordingly.

$$WT_f = FN_{cr} \cdot SFC_{cr} \cdot \frac{Range}{V_{cr}} \tag{5.2}$$

The nacelle drag in equation 5.1 can be estimated as the sum of the cowl (Dr_{ca}) and afterbody drag (Dr_{af}), according to equations 5.3 to 5.5[58]. This formulation was also used in the studies of Jackson[23] and Giannakakis[53].

$$Dr_{nac} = Dr_{ca} + Dr_{af} \tag{5.3}$$

$$D_{ca} = 0.5 \cdot k_i \cdot \rho_{nac} \cdot V_0^2 \cdot C_{D,ca} \cdot \left[\pi \cdot \left(\frac{l}{D}\right)_{ca} \cdot D_{ca}^2\right] \tag{5.4}$$

$$D_{af} = 0.5 \cdot k_i \cdot \rho_{nac} \cdot V_{bp}^2 \cdot C_{D,af} \cdot (\pi \cdot l_{af} \cdot D_{af}) \tag{5.5}$$

According to Jackson[23] the interference drag factor (k_i) can be taken equal to 1.2 and Giannakakis[53] assumes a drag coefficient (C_D) of 0.002. The nacelle equivalent density (ρ_{nac}) is set at 24.88 $^{kg}/_{m^2}$[23] and the cowl length to diameter ratio is assumed to be 1.5, representing a typical engine. Finally, the bypass (V_{bp}) and the free stream (V_0) jet velocities are calculated at the engine performance simulation phase, whereas all the geometric calculations are outputs of the

design and weight estimation method (Fig. 3.24). The inputs for the installed performance calculations are summarised in table 5.1.

Table 5.1: Installed performance calculation inputs

Range	3000 km
Drag coefficient (C_D)	0.002
Interference drag factor (k_i)	1.2
Nacelle density (ρ_{nac})	24.88 $^{kg}/_{m^2}$
Cowl $^{l}/_{D}$	1.5

The range factor for the DDTF configuration, based on the engine model described in the previous sections is presented in figure 5.20. Contrary to the BPR limits that were used in the analysis so far, in this case, engines with BPR values of 2 and 4 were also examined in order to better define the optimum installed performance regions.

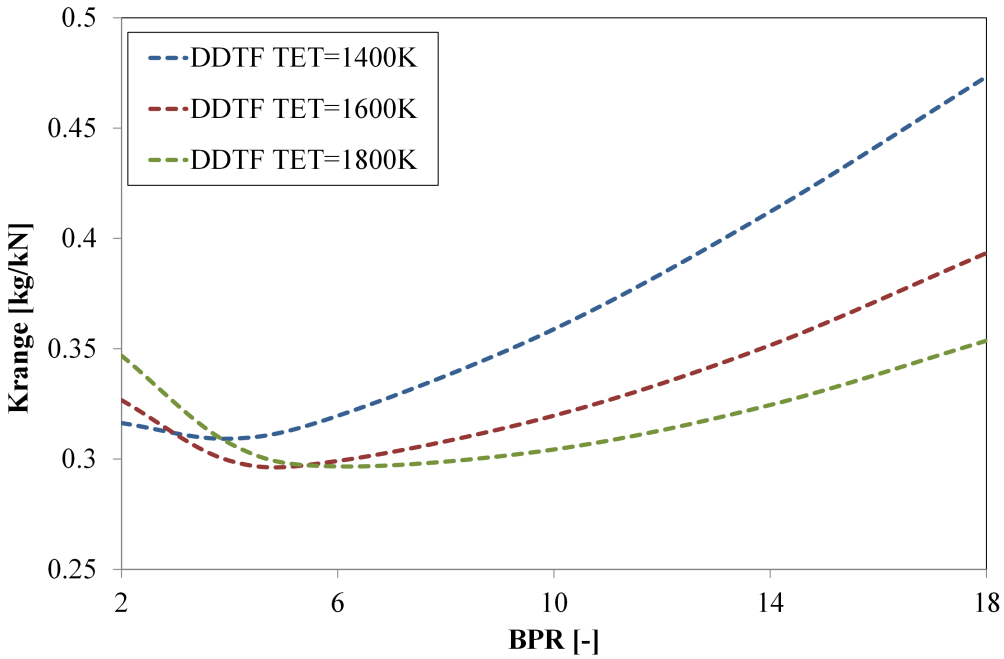

Figure 5.20: DDTF installed performance

In line with similar studies[53], the range factor becomes optimum at a certain BPR value for a given TET. This optimum BPR increases with increasing TET, providing also lower range factor value and thus more fuel efficient engines. According to Giannakakis[53], this is attributed to the variation of engine diameter

with BPR and TET, assuming that the optimum SFC, drag and engine weight trade-off point corresponds to a given fan diameter value.

The existence of an optimum point is also justified if the cruise SFC, fan diameter and engine weight plots are considered, where the falling SFC (Fig. 5.21), with increasing BPR, is dominant at low BPR values, but is outweighed by the rising fan diameter (Fig. 5.22) and engine weight (Fig. 5.19) at higher BPRs.

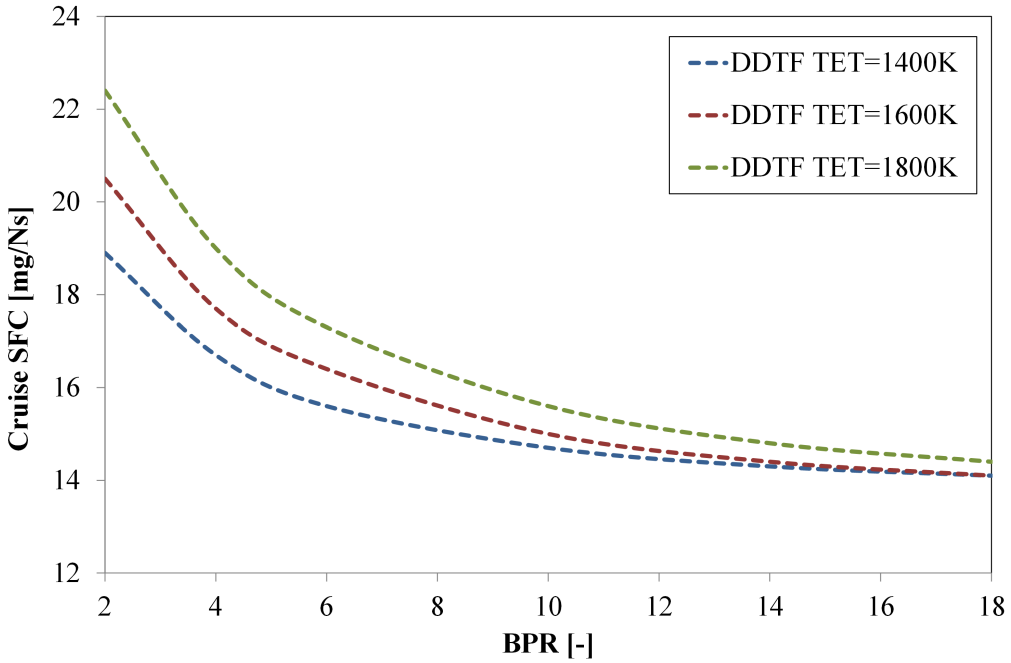

Figure 5.21: DDTF cruise SFC

Interestingly, in figure 5.20, the line having a TET value of 1600 K, corresponding to the CFM56-7B27 engine, which was the baseline of this analysis, has its optimum Krange for a BPR value of about five. This is matching the CFM56-7B27 design value, verifying that the installed performance calculation is representative of real engines.

Taking into account that CFM56-7B27 was designed about 20 years ago, it is evident that technology since then has advanced and the input values used in the range factor calculation are not representative of a future engine concept. Therefore, in order to provide a more realistic baseline concept for comparison

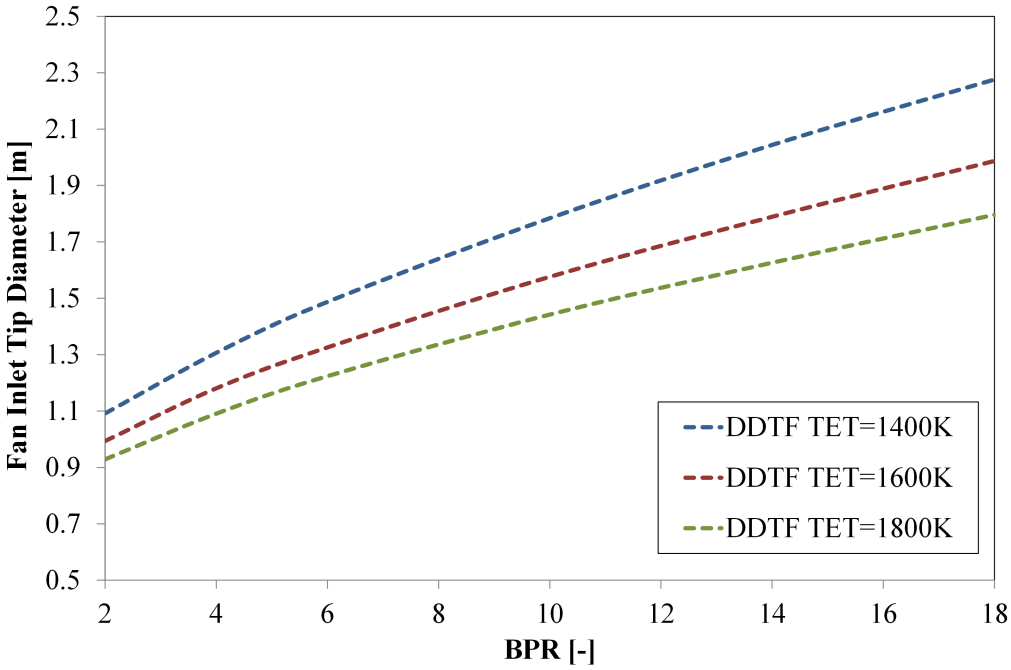

Figure 5.22: DDTF fan tip diameter

with the GTF concept, based on publicly available sources[98;95;99;100], the inputs for the range factor calculation were updated to reflect the technology advancements (Table 5.2) and describe a reduced weight and drag engine.

Table 5.2: Reduced weight and drag performance calculation inputs

Range	3000 km
Drag coefficient (C_D)	0.001
Interference drag factor (k_i)	1.2
Nacelle density (ρ_{nac})	20.0 $^{kg}/_{m^2}$
Cowl $^{l}/_{D}$	1.0
Fan weight	-50%
Other components weight	-15%

Since the GTF configuration applies only to current and future engines, the range factor for these cases will be also calculated with the updated values. Figure 5.23 presents the advanced technology range factor as a function of BPR with the TET as parameter, for both DDTF and GTF configurations.

As expected, the lower drag and weight technology results in improved installed performance and lower range factor values for the DDTF engines. Furthermore, the optimum BPR value has now moved to a higher BPR value(about

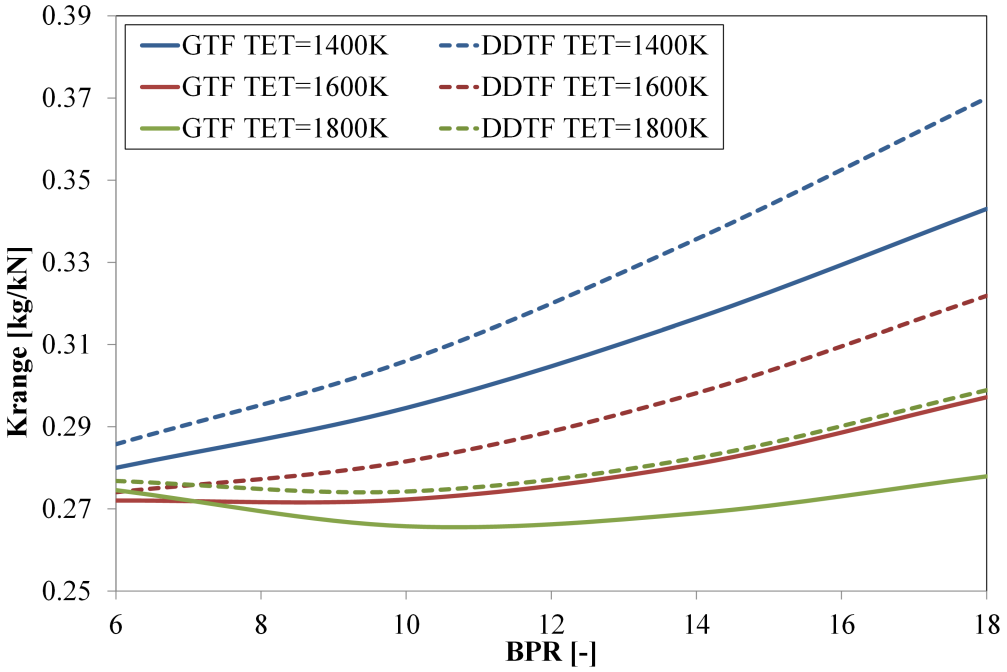

Figure 5.23: Advanced technology installed performance

9) for a given TET, since the engines now are lighter and therefore, the negative influence of engine weight appears at higher BPR values.

The effect of reduced engine weight is also clear at the GTF configuration, since for the selected engine model the fan diameter and the cruise SFC are not modified. Relative to the DDTF configuration, the GTF architecture results in a further range factor reduction, coupled with a shift of the BPR optimum to values higher than 10. The GTF benefit is higher the higher the BPR, as the reduction of LPT stages outweighs the additional gearbox weight.

The shift of the optimal BPR between the GTF and DDTF configurations indicates that the comparison of these engine architectures at iso-thermodynamic cycle, as done by other studies[96], can be misleading and doesn't reveal the full potential of the GTF arrangement. A fair evaluation should compare the two engine architectures using their respective optimal BPR, as these would be the BPRs chosen during the preliminary design.

It also becomes evident that the GTF benefit would decrease, if the aircraft manufacturer limited the engine diameter to a value lower than the GTF optimum (Fig. 5.24). In that case, the BPR would decrease, reducing the range factor

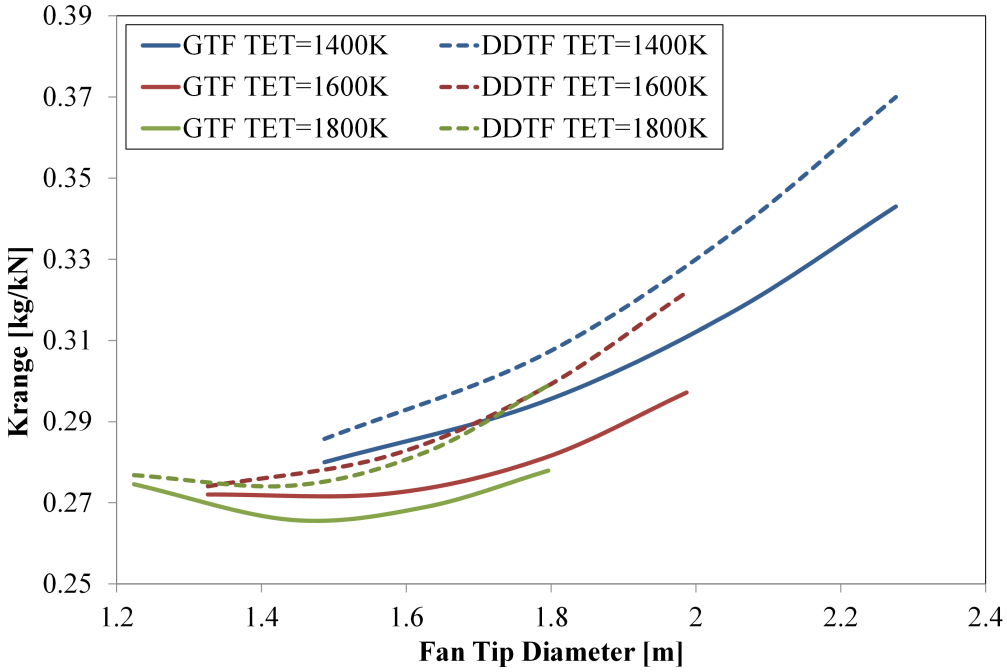

Figure 5.24: Installed performance as a function of diameter

difference between the two architectures.

5.6 Summary and Discussion

The present chapter illustrated an attempt to answer the question about the feasibility of a GTF concept. As shown, this question concerns not only the reduced amount of LPT stages and the installed performance benefit, but also achieving acceptable LPT efficiency values.

The increase of BPR, which is inevitable to achieve the installed performance optimum, has a detrimental effect on the LPT rotational speed at the DDTF configuration. The LPT diameter increase was presented as a solution that can restore part of the rotational speed loss, in order to avoid introducing a gearbox, which imposes a weight penalty and raises the complexity of the engine. However, at high fan diameters, where the rotational speed decrease is higher, this solutions is not feasible due to geometry and losses restrictions and only the GTF configuration can achieve an acceptable LPT efficiency. Furthermore, the adjustment of number of LPT stages, which is suggested by other studies, is also

not providing the desired LPT isentropic efficiency at high BPR.

On the other hand, the increase of the LPT rotational speed with the introduction of a gearbox, results in increased centrifugal load and thus bigger component sizes. However, as shown, this increase in size is insignificant when compared with the weight reduction achieved through the use of fewer LPT stages, but care should be taken regarding the available space for the bigger components. Similarly, the variations in the weight of frames and shafts is also considered small in the present study, but more accurate design and weight estimation methods are required. Therefore, even though the LPT stage reduction is expected to dominate the weight variation, when a DDTF engine is converted to a GTF, the adjustment of the fan rotational speed, not included in the engine model, should also provide a small weight benefit, due to reduced centrifugal loads.

Despite using only an empirical correlation to estimate the gearbox weight, this approach was validated against the only existing gearbox design and provides realistic results throughout the studied engine range. However, since the fan rotational speed is not adjusted at the GTF concept, the estimated gear ratio and therefore the gearbox weight are lower than expected. This problem was mitigated by introducing a gear ratio correction factor of 1.5. Therefore, as a conclusion, in order to achieve a better gearbox weight estimate, the fan efficiency prediction that will enable the accurate prediction of the gear ratio has to be implemented in ATLAS.

In all examined cases, the weight reduction in a GTF configuration exceeded the gearbox weight penalty, suggesting that the GTF configuration in a two spool engine results always in weight benefit. However, due to lack of public data or an estimation method, the weight of the gearbox accessories, which are considered to add a significant weight penalty, was excluded from the present study. Therefore, it is only safe to say that in order to have a beneficial conversion to a GTF from a DDTF, the weight of the accessories should not exceed the difference between the weight of the LPTs in the two cases, considering a fixed fan geometry. The variations in weight for components that don't use a detailed design method and might not be realistic, such as the shafts, frames and controls and accessories

should also be taken into account.

Finally, the installed performance study revealed that there is a trade-off between SFC, drag and engine weight and thus the installed SFC has an optimum. Since the engine model kept the SFC and fan diameter constant, the weight reduction, either due to technology advancements or to the introduction of the gearbox, is pushing this optimum to higher BPR values with a simultaneous improvement in installed performance. Therefore, the comparison of the DDTF and GTF configurations can be misleading, if done on the same engine performance basis and only the optimum design points should be considered to realise the full potential of novel arrangements. However, a comparison on the same performance basis is desirable when restrictions are imposed on the engine parameters.

The above conclusions, however, were drawn based only on a two spool engine model on a short range mission. In order to generalise them for all engines and missions, several more design cases could be considered, but priority should be given to a three shaft engine and a long mission.

Moreover, the assumptions and input parameters used in the engine model could be varied to study the dependency of the GTF feasibility on performance and design choices.

Furthermore, if the proposed design methodology improvements are implemented in ATLAS, the above plots should be updated, but the final conclusions are not expected to change significantly. The only exception, as mentioned above, is the introduction of the fan and compressor efficiency model and the coupling of ATLAS with a performance code that should provide more realistic results and possibly a clearer picture on the design limits of the GTF configuration.

Chapter 6

Conclusions & Future work

The goal of this project was to provide an insight into the existing aero preliminary weight estimation methods and their range of application. Additionally, to supply a new "component based" method for use in aero engine conceptual and optimisation studies. Moreover, the influence of weight on novel engine configurations needed to be understood, in order to better define their design envelope.

In the present chapter, the main points of this work are summarised and its contribution is highlighted. Furthermore, suggestions for future work are also included.

6.1 Summary & Conclusions

6.1.1 Existing preliminary weight estimation methods

Chapter 2 offered a thorough analysis of the existing preliminary weight estimation methods, focusing on the input variables used and the restrictions imposed by their authors. Furthermore, a quantitative and qualitative analysis was provided for almost every one of them.

The existing preliminary weight estimation methods were categorised in two major groups, with the "whole engine based" methods providing only weight estimations for the whole engine, whereas the "component based" methods perform an engine component weight prediction to reach the same goal.

The former group mainly consists of simple correlations and equations that have no more than four input variables. They were conceived using data from old existing engines, restrict their application range to values unrealistic for modern aero engines and involve uncertainties about the input variables. Therefore, they cannot be reliably used to extrapolate to future engines and are unsuitable for use in novel aero engine optimisation studies.

On the contrary, the "component based" methods perform a weight estimation for each engine component, usually achieved through a preliminary design process. Even though this requires a fair amount of inputs and assumptions, and could prove complex and time consuming, these methods are considered more accurate, capture better the weight trends and are able to model novel configurations.

Since engine optimisation and conceptual studies involve several runs to identify the optimum engine, the increased calculation speed of the "component based" methods can be mitigated by using a hybrid method. This involves a multivariate curve fitting technique, such as neural networks, to create one or more simple equations, that use a fraction of the "component based" method inputs and perform the weight estimation significantly faster.

The quantitative analysis showed that all methods exceed the target error of $\pm 10\%$. Furthermore, the qualitative analysis revealed that care should be taken when a weight estimation is used, since not all of them follow the same principles. Considering that fan diameter and BPR are the most representative variables for engine weight, only WATE manages to provide a realistic evaluation of their impact.

Summarising the main conclusions:

- Even though most of the existing preliminary weight estimation methods claim that they fall within $\pm 10\%$ error, none achieves that target for existing turbofan engines.

- Not all of the existing preliminary weight estimation methods follow the same physics and therefore care should be taken to use them when appropriate.

- Only NASA WATE is able to capture the variation of engine weight with fan diameter and BPR, which are the most closely linked variables to it.
- Through use of curve fitting techniques, a hybrid method can be developed to mitigate the calculation speed problem of "component based" methods.

6.1.2 New "component based" approach methodology

Realising the restrictions of the existing preliminary weight estimation methods, a new "component based" method was created using or adapting existing component design methods. It was developed in a modular fashion in order to maintain flexibility and extensibility and enable the weight estimation of a wide variety of configurations, focusing also on accuracy, reduced complexity and increased computational speed. The software implementation of this method is called ATLAS.

ATLAS was verified against two major existing engines, covering a wide variety of designs. It provided similar layouts in both cases, but also whole engine weight estimations with error less than 10% for the examined cases. Furthermore, it was compared against NASA WATE, resulting in similar trends and component weights as percentage of the total engine weight, for a two spool turbofan engine.

The main conclusion is that ATLAS combines flexibility, extensibility and accuracy and is able to provide accurate preliminary weight estimations over a wide variety of aero engines.

6.1.3 Geared turbofan feasibility analysis

One of the most promising novel engine configurations is the GTF, which decouples the fan from the rest of the LP shaft by using a gearbox. The main benefit of this modification is the increase of the LPT rotational speed, that is restricted by the fan in DDTF configurations. This problem is aggravated by the need for bigger and slower rotating fans in order to achieve better efficiency and lower emissions and noise.

As was shown in chapter 5, the GTF configuration has an impact not only on engine weight, but also on component performance and mechanical integrity.

Due to the reduction of LPT rotational speed with increasing fan diameter, the LPT flow coefficient increases resulting in unacceptable low stage isentropic efficiency values, since the air velocity is fixed and the stage loading is assigned a target value. The increase of the LPT diameter was studied as an alternative, with acceptable results at low BPR values, but the interaction with the bypass duct, restricts its use in high BPRs. Furthermore, the air velocity decrease is expected to have a positive effect on stage isentropic efficiency, but this was not studied, because it is expected to increase the flow area and thus the component size, but also drop the power output per stage, resulting in more stages. On the other hand, the introduction of a gearbox is the only examined solution that drops the flow coefficient to acceptable levels, through the increase of rotational speed, giving the opportunity to achieve high isentropic efficiency values.

On the other hand, the GTF imposes higher stress loads on the LPT components, especially on the disks, increasing thus their size. However, when compared with the weight decrease due to reduction of LPT stages, the effect of the disks is minimal and does not restrict the GTF application. Care should be taken though, that there is enough space to accommodate the bigger parts. Similarly, the weight variations of frames and shafts were considered, but also in this case, they are outweighed by the LPT stage decrease weight benefit. Nevertheless, more detailed design and weight methods for frames and shafts are required to verify or reject this conclusion.

For the examined two spool engine model, over the range of TET and BPR, the GTF configuration resulted in lower engine weight. However, due to lack of public data and methodologies, the present analysis didn't include the weight of the gearbox accessories. Therefore, it can be said that, for a fixed fan geometry, the introduction of a gearbox will result in a weight decrease, if this additional weight doesn't exceed the calculated weight margin between the DDTF and GTF configurations. However, even if the GTF engine is heavier, it would still be a feasible solution, if the installed SFC is lower.

On the other hand, the introduction of the gearbox, usually results also in a slower rotating fan with increased diameters, associated with reduced SFC,

which was not considered in this study. As expected, this imposes a direct weight penalty, due to the fan size, but also an indirect one, due to the heavier frames to support the bigger component. Therefore, also in this instance, the installed SFC is required to decide the engine feasibility.

Finally, the installed performance of the examined two spool engine was also studied to understand the trade-off between engine weight, drag and SFC. Due to the first two showing a rising trend, with increasing BPR, whereas the SFC shows a falling one, the installed performance has an optimum for a given TET value.

Considering that the baseline engine was developed about 20 years ago, weight and performance improvements were introduced based on public data. This approach improved the range factor values, but also shifted the optimum to a higher BPR, signifying that for a better installed performance the BPR increases. The same behaviour, but with even better results for the installed fuel consumption is shown by the GTF configuration, which also moves the optimum to an even higher BPR value. Therefore, for the examined engine model, the GTF configuration has superior installed performance due to the reduced weight, which is not compromised by the increased drag at the bigger fan diameter of the higher optimum BPR value.

The conclusions regarding the GTF feasibility study are listed below. Since the frames, shafts and accessories lack a detailed design method and the compressors and fans don't include a loss model, the conclusions that use these components are only valid for the given engine model and assumptions.

- The LPT diameter, air velocity and number of stages adjustments in a DDTF engine are not sufficient and a gearbox is required, especially in high BPRs, in order to achieve acceptable LPT efficiency.

- For the examined engine model, the weight benefit when a gearbox is introduced, comes primarily from the reduction of LPT stages.

- The increased stress loads, due to the rotational speed increase, affect the weight of the components, but this is insignificant when compared to the

total engine weight benefit of a GTF configuration.

- In this study, the feasibility of the GTF configuration depends on the weight of the gearbox, that should not exceed the LPT weight benefit. It was showed that for the two spool engine, at the examined BPR and TET ranges, there is always a benefit, but the auxiliaries, that were not estimated, should also be taken into account to reach the final verdict. However, a potentially larger fan with the introduction of the gearbox, which was not considered in this study, results in a weight penalty, but provides also improved SFC and therefore the GTF needs to be evaluated based on the installed performance.

- The installed performance of the two spool engine in a short range aircraft improves with the introduction of a gearbox, but the optimum point lies at higher BPR values. Therefore, for a given thrust requirement, it is misleading to compare the two configurations based on the same thermodynamic cycle, as was done in other studies, but the installed performance optimum engines should be considered. This is only desirable when restrictions, such as the aircraft ground clearance, are applied on the engine parameters and the installed performance optimum cannot be achieved.

6.2 Project contribution

The present work contributes to the following areas, which to the author's knowledge are not addressed in the literature:

- This work is the first to provide an extensive literature survey of the existing preliminary weight estimation methods, which were thoroughly analysed quantitatively and qualitatively, in order evaluate their accuracy and their ability to follow variations of the major engine parameters.

- The new "component based" preliminary weight estimation method (ATLAS) that was developed as part of this work is a valuable contribution to

the Center for Propulsion. Even though it follows the principles of NASA WATE, it employs more robust component design methods and can be expanded to allow for the weight estimation of novel engines.

- Very high BPR values were considered at DDTF configurations, revealing that the adjustments of LPT number of stages or LPT diameter are not sufficient, if high stage isentropic efficiency values are targeted. On the other hand, this is possible if the LPT rotational speed is modified, with the GTF configuration being a possible design solution.

- The introduction of a gearbox in a DDTF engine results in overall weight reduction, for a fixed fan geometry, since the smaller number of LPT stages, outweighs the heavier components due to increased stresses. For the examined case study, this is true even after introducing the weight of the gearbox, but the feasibility of the GTF arragement is dependent on the trade-off between the total estimated weight decrease and the gearbox accessories weight that is not estimated. However, a larger fan, associated with the GTF configuration imposes a weight penalty, but also a performance benefit and should be evaluated based on the installed performance.

- For a given thrust requirement, the comparison of DDTF and GTF engines is not realistic considering the same thermodynamic cycle, but in order to realise the full potential of the GTF their installed performance optima should be compared. The same cycle is only considered if the optimum cycle cannot be utilised due to restrictions on design parameters, with the aircraft ground clearance being a typical case.

6.3 Future work

Even though the present work reached several conclusions, there are several aspects of it that could be further explored or improved. These are listed below:

1. The $\pm 10\%$ error limit for the preliminary weight estimation methods was

adopted in this project since it is widely used by the existing methods. However, this should be verified with a sensitivity study considering the effect of engine weight on the installed performance and in the engine optimisation framework.

2. Based on available data from existing engines, the existing preliminary weight estimation methods can be recalibrated in order to raise their accuracy and lift some of their restrictions, as was already done by Doulgeris[54] on the Gerend and Roundhill method.

3. Despite providing accurate weight estimations, ATLAS is considered by no means finalised and there are several areas of improvement as listed below:

   - Improve the fidelity of efficiency estimation in compressor and fan design. The currently estimated efficiency value by the performance calculation should be recalculated in ATLAS, respecting turbomachinery restrictions. This is also an essential step towards the coupling of ATLAS with a performance code in a feedback loop, that will redefine the cycle parameters, raising the accuracy of both.
   - New components, including a propeller, an intercooler, a recuperator and a contra-rotating turbine, could be included in ATLAS to enable the weight estimation of novel configurations.
   - The weight of the gearbox accessories should be estimated in ATLAS, since it is a critical component for the weight estimation of a GTF engine.
   - The optimisation process to define the volume of the disks is currently the slowest process in ATLAS. This could be improved by implementing faster optimisation methods or redefining the problem to reduce the unknown variables, but without compromising the weight estimation accuracy.
   - The disk shapes of the simulated engines are smaller or larger than expected in some components. The blade fixation, which is a function

of the chord and not of the centrifugal load, was identified as the cause and its implementation would significantly improve the component weight estimation.

- The empirical weight estimation method of the frames was based on old data and should be updated. Ideally, it could be substituted by a detailed frame design method that will also yield weight. This should also include the bearings and their housings.
- The preliminary weight estimation of controls and accessories is based on a rough empirical rule and a more detailed process for fuel, oil, control and starting systems is required. Furthermore, the weight of the accessory gearbox, which is currently part of the controls and accessories, needs to be evaluated.
- The estimation of shaft thickness is done considering only the transmitted power and torque. Ideally, shaft bending and rotor dynamics should also be part of the calculation process. Furthermore, the assumption of a solid inner shaft is not realistic and a methodology to estimate the minimum weight shaft, by modifying the inner diameter, can be developed. However, this approach may increase the weight of other engine components that are affected by the outer diameter of the shafts, such as the disks.
- A more accurate modelling of the turbine cooling is required in order to estimate the passages that reduce the blade volume. Alternatively, an empirical correlation can be used.
- The hub and tip calculations at the fans, compressors and turbines are currently informative only. These should be integrated into the design process and new limits should be set for critical hub and tip parameters.
- Apart from temperature, other criteria, such as stress, cost and life, have to be included in the material selection process for all parts.

- Introduce the blade taper ratio at all blades for more accurate preliminary weight estimations. Even though the taper ratio is not expected to have a big effect on individual blade weight accuracy, this will affect the spacing of the components at the hub area and thus their total length.
- Since the adopted nacelle weight estimation is method is empirical, an analytic design method should be developed. This should also include thrust reversers, since they also contribute to nacelle weight.
- Only single stage fans are currently supported by ATLAS, but that needs to be modified to cover multi-stage fans for low BPR values.
- The estimation of the space to chord ratio used in ATLAS was developed considered primarily compressor blades. It is currently used for fans as well in ATLAS, but it has to be verified against existing fan designs.
- The turbine rotational speed limits should be expanded to include not only mechanical integrity restrictions, but also aerodynamic as well.

4. The verification of ATLAS examined only two major turbofans and should be expanded to include a wider variety of engines with different characteristics, expanding thus the applicability of the method.

5. Since component weights are not publicly available, it is proposed to approach an OEM to acquire them. This will greatly improve the accuracy and the credibility of ATLAS, but will also enable the development of more accurate empirical correlations. Also, a sensitivity analysis on the component weight participation in the total engine weight will help identify the critical components for improvement and raise the method accuracy.

6. ATLAS is capable of illustrating the effect of performance or design variables on engine weight. However, the key parameters that influence weight have not been defined and should be performed on existing and novel en-

gine arrangements. Potentially, a "whole engine based" method can be generated for use at the conceptual design phase.

7. The calculation time of ATLAS can be further reduced by introducing a hybrid method. ATLAS results over a design space can be used in a neural network or other curve fitting method to generate multivariate correlations for specific engine types, that can be used in engine optimisation studies.

8. The GTF feasibility analysis used a two spool engine on a short range mission to draw its conclusions and therefore has limited applicability. This can be expanded to include more engines and mission profiles, but priority should be given to a two spool engine on a long mission and a three shaft engine, covering thus a wide spectrum of existing turbofans.

9. ATLAS could be combined with other methods or pieces of software in order to provide more detailed analysis on an engine, aircraft and mission basis. Apart from the coupling with a performance code that was mentioned above, the interaction with an aircraft weight and drag estimation method will result in more accurate installed performance values. Furthermore, both the above integration processes could be part of a greater TERA framework that will perform engine optimisation studies and design space exploration, considering also noise, cost and emissions restrictions.

10. The flexibility of ATLAS enables the study of existing and novel engine configurations, provided that the required component design methods are included. As mentioned above, by introducing a propeller, a contra-rotating turbine, an intercooler and a recuperator, turboprop, open-rotor, contra-rotating fan and intercooled and/or recuperated engines can be simulated. These should be studied in detail in order to define their limitations and their design envelope

References

[1] N. T. Birch. 2020 vision: The prospects for large civil aircraft propulsion. *The Aeronautical Journal*, 104(1038):347–352, August 2000.

[2] P. Butterwoth-Hayes. Europe reaches for aerospace dominance. *Aerospace America*, 42(8):36–40, August 2004.

[3] Advisory Council for Aeronautics in Europe (ACARE). European aeronautics – a vision for 2020. Technical report, January 2001.

[4] R. Gardner. Mapping the future. *Aerospace International*, 32(5):30–32, May 2005.

[5] J. J. Lee. Greener manufacturing, maintenance and disposal - towards the acare targets. *The Aeronautical Journal*, 110(1110):567–571, August 2006.

[6] J. E. Green. Civil aviation and the environmental challenge. *The Aeronautical Journal*, 107(1072):281–300, June 2003.

[7] S. Ogaji, P. Pilidis, and Sethi V. Advanced power plant selection: The TERA (Techno-economic Environmental Risk Analysis) framework. Number 2009-1115. ISABE, 2009.

[8] S. Bretschneider, S. Staudacher, and O. Arago. Architecture of a techno-economic and environmental risk assessment tool using a multi-modular build approach. In *ISABE 2007 Proceedings*, number ISABE-2007-1103. ISABE, 2007.

[9] K. Kyprianidis, T. Groensted, S.O.T. Ogaji, P. Pilidis, and R. Singh. Assessment of future aero engine designs with intercooled and recuperated cores. In *Proceedings of ASME Turbo Expo 2010*, number GT-2010-23621. ASME, 2010.

[10] J. J. Korsia. VITAL – European RnD programme for greener aero engines. In *ISABE 2007 Proceedings Proceedings*, number ISABE-2007-1118. ISABE, 2007.

[11] G. Wilfert, J. Sieber, A. Rolt, N. Baker, A. Touyeras, and S. Colantuoni. New environmental friendly aero engine core concepts. In *ISABE 2007 Proceedings*, number ISABE-2007-1120. ISABE, 2007.

[12] European Commission. DREAM – valiDation of Radical Engine Architecture systeMs, 2012. URL `http://ec.europa.eu/research/transport/projects/items/dream_en.htm`. Last accessed 19/6/2014.

[13] Gas turbine engineering group. *The TURBOMATCH scheme, User's manual*. Cranfield University, 2008.

[14] A. Bala, V. Sethi, E. Lo Gatto, V. Pachidis, and P. Pilidis. PROOSIS – A collaborative venture for gas turbine performance simulation using an object oriented programming schema. In *ISABE 2007 Proceedings*, number ISABE-2007-1357. ISABE, 2007.

[15] K. Kyprianidis, R. Colmenares Quintero, D. Pascovici, S. Ogaji, P. Pilidis, and A. Kalfas. EVA - A tool for EnViromental Assessment of novel propulsion cycles. In *Proceedings of ASME Turbo Expo 2008*, number GT-2008-50602, 2008.

[16] P. Laskaridis, P. Pilidis, and P. Kotsiopoulos. An integrated engine - aircraft performance platform for assesssing new technologies in aeronautics. In *ISABE 2005 Proceedings*, number ISABE-2005-1165. ISABE, 2005.

[17] C. Celis, B. Moss, and P. Pilidis. Emissions modelling for the optimisation of greener aircraft operations. In *Proceedings of ASME Turbo Expo 2009*. ASME, June 2009.

[18] European Commission. SILENCER – low-noise engines making europe a quieter place, 2012. URL `http://ec.europa.eu/research/transport/projects/items/_silencer____low_noise_engines_making_europe_a_quieter_place_en.htm`. Last accessed 19/6/2014.

[19] Dassault Systems. Isight and SEE overview, 2014. URL `http://www.3ds.com/products-services/simulia/portfolio/isight-simulia-execution-engine/overview/`. Last accessed 19/6/2014.

[20] P. Lolis, P. Giannakakis, Sethi V., A. J. B. Jackson, and P. Pilidis. Evaluation of aero gas turbine preliminary weight estimation methods. *The Aeronautical Journal*, 118(1204), June 2014.

[21] P. Lolis, B. Arumungam Shanmugasundaram, Sethi V., and P. Pilidis. An empirical aero gas turbine preliminary weight estimation method based on artificial neural networks. In *Proceedings of the 71st SAWE Conference*. Society of allied weight engineers (SAWE), 2012.

[22] P. Lolis, V. Sethi, A.J.B. Jackson, and P. Pilidis. Analysis of aero engine preliminary weight estimation methods used within a Techno-economic and Environmental Risk Analysis framework. In *Proccedings of the 24th International Cogress On Condition Monitoring and Diagnostics Engineering Management (COMADEM)*. COMADEM International, 2011.

[23] A. J. B. Jackson. *Optimisation of aero and industrial gas turbine design for the enviroment*. PhD thesis, Cranfield University, February 2009.

[24] L. T. Whitehead and J. Brown. A mechanical design for a lightweight turbo-jet engine and the variation of engine weight with size. Memorandum M.177, National gas turbine establishment, August 1953.

[25] W. A. Pennington. Choice of engines for aircraft. *Shell Aviation News*, pages 14–19, January 1959.

[26] A. Guha, D. Boylan, and P. Gallagher. Determination of optimum specific thrust for civil aero gas turbine engines: A multidisciplinary design synthesis and optimisation. *Proceedings of the Institution of Mechanical Engineers, Part G: Journal of Aerospace Engineering*, 227(3), 2012.

[27] C. Svoboda. Turbofan engine database as a preliminary design tool. *Aircraft design*, 3:17–31, 2000.

[28] D. P. Raymer. *Aircraft design: A conceptual approach.* AIAA, 1989.

[29] L. R. Jenkinson, P. Simpkin, and D. Rhodes. *Civil Jet Aircraft Design.* Butterwoth-Heinemann, 1999.

[30] M. Daly, editor. *Jane's aero-engines.* IHS Janes, 28th edition, September 2010.

[31] E. Torenbeek. *Synthesis of Subsonic Airplane Design.* Martinus Nijhoff publishers, 1975.

[32] J. Clavier. Aero gas turbine engine design project (AVIC). Ultra high bypass ratio (12-14) study. Master's thesis, Cranfield University, 2008.

[33] R. P. Gerend and J. P. Roundhill. Correlation of gas turbine engine weights and dimensions. In *Propulsion Joint Specialist Conference*, volume 669, pages 1–7. AIAA, 1970.

[34] M. W. Whellens. *Multidisciplinary optimization of aero-engines using genetic algorithms and preliminary design tools.* PhD thesis, Cranfield University, 2003.

[35] R. F. Colmenares Quintero. *Techno-economic and enviromental risk assessment of innovative propulsion systems for short-range civil aircraft.* PhD thesis, Cranfield University, April 2009.

[36] D. A. Sagerser, S. Lieblein, and R. P. Krebs. Empirical expressions for estimating length and weight of axial-flow components of VTOL powerplants. Technical Report TM X-2406, NASA, December 1971.

[37] R. J. Pera, E. Onat, G. W. Klees, and E. Tjonneland. A method to estimate weight and dimensions of aircraft gas turbine engines. volume 1: Method of analysis final report. Technical Report NASA-CR-135170, NASA, 1977.

[38] G. W. Klees and L. H. Fishbach. Aircraft engine weight estimation method. In *Proceedings of the thirty-seventh annual conference of the Society of Allied Weight Engineers*, number 1248. SAWE, May 1978.

[39] E. Onat and F. F. Tolle. An extension of engine weight estimation techniques to compute engine production cost. Technical Report N62269-78-C-0286, Naval Air Development Center, 1979.

[40] P. L. Hale. A method to estimate weight and dimensions of small aircraft propulsion gas turbine engines. Technical Report NASA-CR-168049, NASA – Garrett turbine engine company, 1982.

[41] M. T. Tong, I. Halliwell, and L. J. Ghosn. A computer code for gas turbine engine weight and disk life estimation. *Journal of Engineering for Gas Turbines and Power*, 126(2):265–270, Apr. 2004.

[42] M. T. Tong and B. A. Naylor. An object-oriented computer code for aircraft engine weight estimation. In *Proceedings of the ASME Turbo Expo*, volume 1, pages 1–7, 2008.

[43] V. Sanghi, K. Kumar, V. Sundararajan, and S. K. Sane. Preliminary estimation of engine gas-flow-path size and weight. *Journal of Propulsion and Power*, 14(2):208–214, Mar.-Apr. 1998.

[44] Gasturb. URL `http://www.gasturb.de/`. Last accessed 25/6/2014.

[45] J. E. Merriman. Turbofan engine weight (TEW I). Technical Report DAC-67265, Douglas aircraft Co., April 1969.

[46] E. C. Stevens. Engine weight and size estimating techniques. Technical Report SEG-TR-66-36, General Motors Corp., August 1966.

[47] W. H. Parker and G. G. Love. Presentation of turbine engine weight estimating techniques at wright patterson air force base. In *Proceedings of the third weight prediction workshop for advanced aerospace design projects*, October 1967.

[48] F. R. Holden. A statistical study of turbojet engine component weights. Technical Report AC-5310-A, Naval air development center, 1954.

[49] W. L. Macmillan. *Development of a module type computer program for the calculation of gas turbine off design performance.* PhD thesis, Cranfield University, 1974.

[50] V. Pachidis, P. Pilidis, L. Marinai, and I. Templalexis. Towards a full two dimensional gas turbine performance simulator. *The Aeronautical Journal*, 111(1121):433–442, 2007.

[51] P. Giannakakis, P. Laskaridis, and P. Pilidis. Effects of offtakes for aircraft secondary-power systems on jet engine efficiency. *Journal of Propulsion and Power*, 27(5), 2011.

[52] RTO applied vehicle technology panel (ATV) task group. Performance prediction and simulation of gas turbine engine operation. Technical Report RTO TR-AVT-036, NATO, 2007.

[53] P. Giannakakis. *Design space exploration and performance modelling of advanced turbofan and open-rotor engines.* PhD thesis, Cranfield University, 2013.

[54] G. Doulgeris. *Modelling and integration of advanced propulsion systems.* PhD thesis, Cranfield University, 2008.

[55] G. Doulgeris, T. Korakianitis, E. J. Avital, P. Pilidis, and P. Laskaridis. Effect of jet noise reduction on gas turbine engine efficiency. *Proceedings*

of the Institution of Mechanical Engineers, Part G: Journal of Aerospace Engineering, 227(9):1441–1445, 2013.

[56] H.I.H. Saravanamuttoo, G.F.C. Rogers, H. Cohen, and P.V. Straznicky. *Gas turbine theory*. Pearson Education, 6th edition, 2009.

[57] S. L. Dixon. *Fluid Mechanics and Thermodynamics of Turbomachinery*. Elsevier Butterworth-Heinemann, Amsterdam, 5th edition, 2005.

[58] P. P. Walsh and P. Fletcher. *Gas turbine performance*. Blackwell Science, 2nd edition, 2004.

[59] Y. A. Cengel and M. A. Boles. *Thermodynamics: An engineering approach*. Mc Graw Hill, 6th edition, 2007.

[60] D. F. Young, B. R. Munson, T. H. Okiishi, and W. W. Huebsch. *A brief introduction to fluid mechanics*. John Wiley and Sons, 4th edition edition, 2007.

[61] S.F. Smith. A simple correlation of turbine efficiency. *Journal of the Royal Aeronautical Society*, 69:467–470, 1965.

[62] D. G. Ainley and G. C. R. Mathieson. A method of performance estimation for axial-flow turbines. Technical Report 2974, Aeronautical Research Council, 1957.

[63] O. Zweifel. The spacing of turbomachine blading, especially with large angular deflection. *Brown Boveri Review*, 32(12), 1945.

[64] K.W. Ramsden. *A multimedia computational aid to gas turbine design teaching*. PhD thesis, Cranfield University, 1995.

[65] N.A. Cumpsty. *Compressor aerodynamics*. Pearson Education Singapore, 1989.

[66] C. De Boor. *A practical guide to splines*. Springer, 2001.

[67] A.B. McKenzie. *Axial Flow Fans and Compressors*. Ashgate, 1997.

[68] Rolls-Royce plc. *The jet engine*. Key Publishing, 2005.

[69] J. Kurzke. Aero-engine design: A state of the art. von Karman Institute for Fluid Dynamics Lecture Series, April 2003.

[70] R.A. Cookson and A.S. Haslam. *Mechanical design of turbomachinery*. Lecture notes. Cranfield University, 2009.

[71] M. L. Luchi, A. Poggialini, and F. Persiani. An interactive optimization procedure applied to the design of gas turbine discs. *Computers and Structures*, 11:629–637, 1980.

[72] S. C. Armand. Structural optimization methodology for rotating disks of aircraft engines. Technical Report NASA-TM-4693, NASA, 1995.

[73] M. C. Potter, J. L. Goldberg, and E. Aboufadel. *Advanced engineering mathematics*. Oxford University Press, 3rd edition, February 2005.

[74] T. M. Pollock and S. Tin. Nickel-based superalloys for advanced turbine engines: Chemistry, microstructure and properties. *Journal of Propulsion and Power*, 22(2):361–374, 2006.

[75] H. Deconinck, J. Periaux, and K. Giannakoglou. *Optimization methods and tools for multicriteria / multidisciplinary design*. Lecture Series 2004-2007. von Karman Istitute for Fluid Dynamics, 2004.

[76] P Spellucci. A SQP method for general nonlinear programs using only equality constrained subproblems. *Methematical Programming, Series B*, 82(3):413–448, August 1998.

[77] A. M. Mellor. *Design of modern turbine combustors*. Harcourt Brace Jovanovich Publishers, 1990.

[78] A. H. Lefebvre and D. R. Ballal. *Gas turbine combustion – Alternative fuels and emissions*. Taylor and Francis group, 2010.

[79] B.S. Mohammad and S.M. Jeng. Design procedures and a developed computer code for preliminary single annular combustor design. In *45th AIAA/ASME/SAE/ASEE Joint Propulsion Conference and Exhibit*, number AIAA 2009-5208. AIAA, August 2009.

[80] A. Klein. Characteristics of combustor diffusers. *Progress in Aerospace Sciences*, 31:171–271, 1995.

[81] L. R. Reneau, J. P. Johnston, and S. J. Kline. Performance and design of straight, two-dimensional diffusers. *Journal of Basic Engineering*, 89(1): 141–150, 1967.

[82] S. Chattopadhyay. *Pressure vessels design and practice*. Mechanical Engineering Series. CRC Press, Boca Raton, 2005.

[83] S. Bretschneider, F. Rothe, M.G. Rose, and S. Staudacher. Compressor casing preliminary design based on features. In *Proceedings of ASME Turbo Expo*, volume 5, pages 1–9. ASME, 2008.

[84] R. E. Chupp, R. C. Hendricks, S. B. Lattime, and B. M. Steinetz. Sealing in turbomachinery. Technical Report NASA/TM-2006-214341, NASA, 2006.

[85] S. H. Loewenthal. Design of power transmitting shafts. NASA Reference Publication 1123, NASA, July 1984.

[86] E. Onat and G. W. Klees. A method to estimate weight and dimensions of large and small gas turbine engines. Technical Report CR-159481, NASA, 1979.

[87] C. Kjelgaard. Gearing up for the GTF. *Aircraft Technology*, 105, 2010.

[88] R. J. Willis Jr. New equations and charts pick off lightest-weight gears. *Product Engineering*, 1963.

[89] The Flight Engineer. Pratt and Whitney PW1100G geared turbofan engine, 2013. URL `http://theflyingengineer.com/flightdeck/pw1100g-gtf/`. Last accessed 15/12/2013.

[90] K. Walker. Pratt and Whitney pursues higher GTF bypass ratios, 2013. URL http://atwonline.com/engines/pratt-whitney-pursues-higher-gtf-bypass-ratios. Last accessed 15/12/2013.

[91] Design-Engine. Pratt and Whitney geared turbofan engine - Changing the course of aviation, 2013. URL http://design-engine.com/pratt-whitneys-geared-turbofan-engine-changing-the-course-of-avaition/. Last accessed 15/12/2013.

[92] CFM International. CFM56-7B turbofan engine, 2013. URL http://www.cfmaeroengines.com/. Last accessed 15/12/2013.

[93] Federal aviation administration. Type certificate data sheet E00055EN. Technical Report E00055EN, U.S. department of transportation, 2003.

[94] UK Civil Aviation Authority. Civil type approval of RB211 TRENT 895-17, 892-17, 892b-17, 884-17, 884b-17, 877-17 and 875-15 engines. Technical Report 1051, October 2004.

[95] C. Riegler and C. Bichlmaier. The geared turbofan technology - opportunities, challenges and readiness status. Technical report, MTU Aero Engines GmbH, 2008.

[96] J. Kurzke. Fundamental differences between conventional and geared turbofans. In *Proceedings of ASME Turbo Expo 2009*, number GT2009-59745. ASME, June 2009.

[97] F.J. Malzacher, J. Gier, and F. Lippi. Aerodesign and testing of an aeromechanically highly loaded LP turbine. In *ASME Turbo Expo 2003. Power for Land, Sea and Air.* ASME, June 2003.

[98] Rolls Royce plc. Low density materials, 2014. URL http://www.rolls-royce.com/about/technology/material_tech/low_density_materials.jsp. Last accessed 15/6/2014.

[99] D. Riordan. Environmentaly friendly engine nacelle technology development., 2012. URL http://flygreen.info/wp-content/uploads/2012/10/bombardier_driordan_ppt_w2.pdf. Last accessed 15/6/2014.

[100] S. Lott. One giant leap, 2012. URL http://www.aero-mag.com/features/19/20121/1206/. Last accessed 15/6/2014.